Title
Reflective Cracking Study: Backcalculation of HVS Test Section Deflection Measurements

Authors
Lu, Qing
Jones, David
Harvey, John T

Publication Date
2008-10-01

Peer reviewed

November 2007
Research Report: UCPRC-RR-2007-08

Reflective Cracking Study: Backcalculation of HVS Test Section Deflection Measurements

Authors:
Q. Lu, D. Jones, and J. Harvey

Partnered Pavement Research Program (PPRC) Contract Strategic Plan Element 4.10:
Development of Improved Rehabilitation Designs for Reflective Cracking

PREPARED FOR:

California Department of Transportation
Division of Research and Innovation
Office of Roadway Research

PREPARED BY:

University of California
Pavement Research Center
UC Davis, UC Berkeley

DOCUMENT RETRIEVAL PAGE		Research Report: UCPRC-RR-2007-08
Title: Reflective Cracking Study: Backcalculation of HVS Test Section Deflection Measurements		
Authors: Q. Lu, D. Jones, and J. Harvey		
Prepared for: Caltrans	**FHWA No:** CA091073M	**Date**: November 2007
Contract No: 65A0172	**Client Reference No:** SPE 4.10	**Status:** Stage 6, Approved Version

Abstract:

This report is one in a series that describe the results of HVS testing and associated analyses on a full-scale experiment being performed at the Richmond Field Station (RFS) to validate Caltrans overlay strategies for the rehabilitation of cracked asphalt concrete. It describes the analysis of deflection data measured with a Falling Weight Deflectometer (FWD) throughout the study. The test forms part of Partnered Pavement Research Center Strategic Plan Element 4.10: "Development of Improved Rehabilitation Designs for Reflective Cracking."

Findings and observations based on the data collected during this HVS study include:

- Variation of material properties were recorded both between sections and within sections, and were mostly attributed to variation in the degree of recementation of recycled concrete particles in the base material.
- The asphalt concrete modulus was significantly affected by the pavement temperature, as expected. In general, lower modulus was obtained at high temperatures, and higher modulus at low temperatures.
- The modulus of the aggregate base was generally positively correlated with the moduli of the asphalt concrete and subgrade. Correlation between the asphalt concrete modulus and the base modulus was weaker in the untrafficked area and/or in the trafficked area before HVS testing. No significant correlation was found between the asphalt concrete modulus and the subgrade modulus.
- The load level of the FWD did not have a significant effect on the values of the backcalculated moduli.
- Aging of the asphalt concrete was apparent on five of the six sections. The stiffness of the base increased significantly with time after initial construction, primarily due to recementation of the recycled concrete particles. This increase continued after overlay construction in certain areas of the test road.
- Phase 2 HVS testing generally damaged the asphalt concrete layers in the trafficked area of each section.
- In the one to three year period after Phase 2 HVS testing, the modulus of the damaged asphalt concrete generally recovered to some extent on all sections.
- Seasonal effects on pavement stiffness were not detected from the limited data collected during this study.
- The asphalt concrete moduli backcalculated from the overlay sections match reasonably well with the moduli determined during laboratory frequency sweep tests on flexural beam specimens.
- There was a difference between the moduli backcalculated from FWD data and from the RSD data. Differences in test conditions and backcalculation assumptions of the two procedures contributed to this difference.

No recommendations as to the use of the modified binders in overlay mixes are made at this time. These recommendations will be included in the second-level analysis report, which will be prepared and submitted on completion of all HVS and laboratory testing.

Keywords:
Reflective cracking, overlay, modified binder, HVS test, FWD test, backcalculation, MB Road

Proposals for implementation:
None

Related documents:
UCPRC-RR-2005-03, UCPRC-RR-2006-04, UCPRC-RR-2006-05, UCPRC-RR-2006-06, UCPRC-RR-2006-07, UCPRC-2006-12

Q. Lu 1st Author	J Harvey Technical Review	D. Spinner Editor	J. Harvey Principal Investigator	M Samadian Caltrans Contract Manager

DISCLAIMER

The contents of this report reflect the views of the authors who are responsible for the facts and accuracy of the data presented herein. The contents do not necessarily reflect the official views or policies of the State of California or the Federal Highway Administration. This report does not constitute a standard, specification, or regulation.

PROJECT OBJECTIVES

The objective of this project is to develop improved rehabilitation designs for reflective cracking for California.

This objective will be met after completion of four tasks identified by the Caltrans/Industry Rubber Asphalt Concrete Task Group (RACTG):

1. Develop improved mechanistic models of reflective cracking in California
2. Calibrate and verify these models using laboratory and HVS testing
3. Evaluate the most effective strategies for reflective cracking
4. Provide recommendations for reflective cracking strategies

This document is one of a series addressing Tasks 2 and 3.

ACKNOWLEDGEMENTS

The University of California Pavement Research Center acknowledges the assistance of the Rubber Pavements Association, Valero Energy Corporation, and Paramount Petroleum which contributed funds and asphalt binders for the construction of the Heavy Vehicle Simulator test track discussed in this study.

REFLECTIVE CRACKING STUDY REPORTS

The reports prepared during the reflective cracking study document data from construction, Heavy Vehicle Simulator (HVS) tests, laboratory tests, and subsequent analyses. These include a series of first- and second-level analysis reports and two summary reports. On completion of the study this suite of documents will include:

1. Reflective Cracking Study: Summary of Construction Activities, Phase 1 HVS testing and Overlay Construction (UCPRC-RR-2005-03).
2. Reflective Cracking Study: First-level Report on the HVS Rutting Experiment (UCPRC-RR-2007-06).
3. Reflective Cracking Study: First-level Report on HVS Testing on Section 590RF — 90 mm MB4-G Overlay (UCPRC-RR-2006-04).
4. Reflective Cracking Study: First-level Report on HVS Testing on Section 589RF — 45 mm MB4-G Overlay (UCPRC-RR-2006-05).
5. Reflective Cracking Study: First-level Report on HVS Testing on Section 587RF — 45 mm RAC-G Overlay (UCPRC-RR-2006-06).
6. Reflective Cracking Study: First-level Report on HVS Testing on Section 588RF — 90 mm AR4000-D Overlay (UCPRC-RR-2006-07).
7. Reflective Cracking Study: First-level Report on HVS Testing on Section 586RF — 45 mm MB15-G Overlay (UCPRC-RR-2006-12).
8. Reflective Cracking Study: First-level Report on HVS Testing on Section 591RF — 45 mm MAC15TR-G Overlay (UCPRC-RR-2007-04).
9. Reflective Cracking Study: HVS Test Section Forensic Report (UCPRC-RR-2007-05).
10. Reflective Cracking Study: First-Level Report on Laboratory Fatigue Testing (UCPRC-RR-2006-08).
11. Reflective Cracking Study: First-Level Report on Laboratory Shear Testing (UCPRC-RR-2006-11).
12. Reflective Cracking Study: Backcalculation of HVS test section deflection measurements (UCPRC-RR-2007-08).
13. Reflective Cracking Study: Second-level Analysis Report (UCPRC-RR-2007-09).
14. Reflective Cracking Study: Summary Report (UCPRC-SR-2007-01). Detailed summary report.
15. Reflective Cracking Study: Summary Report (UCPRC-SR-2007-03). Four page summary report.

CONVERSION FACTORS

SI* (MODERN METRIC) CONVERSION FACTORS				
APPROXIMATE CONVERSIONS TO SI UNITS				
Symbol	**Convert From**	**Multiply By**	**Convert To**	**Symbol**
LENGTH				
in	inches	25.4	millimeters	mm
ft	feet	0.305	meters	m
AREA				
in^2	square inches	645.2	square millimeters	mm^2
ft^2	square feet	0.093	square meters	m2
VOLUME				
ft^3	cubic feet	0.028	cubic meters	m^3
MASS				
lb	pounds	0.454	kilograms	kg
TEMPERATURE (exact degrees)				
°F	Fahrenheit	5 (F-32)/9 or (F-32)/1.8	Celsius	C
FORCE and PRESSURE or STRESS				
lbf	poundforce	4.45	newtons	N
lbf/in^2	poundforce/square inch	6.89	kilopascals	kPa
APPROXIMATE CONVERSIONS FROM SI UNITS				
Symbol	**Convert From**	**Multiply By**	**Convert To**	**Symbol**
LENGTH				
mm	millimeters	0.039	inches	in
m	meters	3.28	feet	ft
AREA				
mm^2	square millimeters	0.0016	square inches	in^2
m^2	square meters	10.764	square feet	ft^2
VOLUME				
m^3	cubic meters	35.314	cubic feet	ft^3
MASS				
kg	kilograms	2.202	pounds	lb
TEMPERATURE (exact degrees)				
C	Celsius	1.8C+32	Fahrenheit	F
FORCE and PRESSURE or STRESS				
N	newtons	0.225	poundforce	lbf
kPa	kilopascals	0.145	poundforce/square inch	lbf/in^2

*SI is the symbol for the International System of Units. Appropriate rounding should be made to comply with Section 4 of ASTM E380. (Revised March 2003)

EXECUTIVE SUMMARY

This report is one in a series that describe the results of HVS testing and associated analyses on a full-scale experiment being performed at the Richmond Field Station (RFS) to validate Caltrans overlay strategies for the rehabilitation of cracked asphalt concrete. It describes the analysis of deflection data measured with a Falling Weight Deflectometer (FWD) after initial construction, before and after each HVS test in the first phase of testing on the original DGAC surface, before and after construction of the overlays, and before and after each HVS test on each overlay. FWD results are compared with Road Surface Deflectometer (RSD) measurements taken during each HVS test. The testing forms part of Partnered Pavement Research Center Strategic Plan Element 4.10: "Development of Improved Rehabilitation Designs for Reflective Cracking."

The objective of this project is to develop improved rehabilitation designs for reflective cracking for California. This objective will be met after completion of the following four tasks:

1. Develop improved mechanistic models of reflective cracking in California
2. Calibrate and verify these models using laboratory and HVS testing
3. Evaluate the most effective strategies for reflective cracking
4. Provide recommendations for reflective cracking strategies

This report is one of a series addressing Tasks 2 and 3. It consists of six main chapters. Chapter 2 provides an overview of the HVS the test program including experiment layout, loading sequence, instrumentation, and data collection. Chapter 3 summarizes backcalculation and analysis of the FWD data. Chapter 4 discusses aging, seasonal effects and stiffness recovery, and Chapter 5 provides a comparison of backcalculated and laboratory results. Chapter 6 contains a summary of the results together with conclusions and observations.

The underlying pavement was designed following standard Caltrans procedures and it incorporates a 410-mm (16 in) Class 2 aggregate base on subgrade with a 90-mm dense-graded asphalt concrete (DGAC) surface. Design thickness was based on a subgrade R-value of 5 and a Traffic Index of 7 (~121,000 equivalent standard axles, or ESALs). This structure was trafficked with the HVS in 2003 to induce fatigue cracking, then overlaid with six different treatments to assess their ability to limit reflective cracking. The treatments included:

- Half-thickness (45 mm [1.7 in]) MB4 gap-graded (MB4-G) overlay;
- Full-thickness (90 mm [3.5 in]) MB4 gap-graded (MB4-G) overlay;

- Half-thickness MB4 gap-graded overlay with minimum 15 percent recycled tire rubber (MB15-G);
- Half-thickness MAC15TR gap-graded overlay with minimum 15 percent recycled tire rubber (MAC15-G);
- Half-thickness rubberized asphalt concrete gap-graded overlay (RAC-G), included as a control for performance comparison purposes, and
- Full-thickness (90 mm) AR4000 dense-graded overlay (AR4000-D), included as a control for performance comparison purposes.

The thickness for the AR4000-D overlay was determined according to Caltrans Test Method 356. The other overlay thicknesses were either the same or half of the AR4000-D overlay thickness. Details on construction, the first phase of HVS trafficking, and second phase HVS trafficking on the overlays are provided in earlier reports. Laboratory fatigue and shear studies were conducted in parallel with HVS testing and are also discussed in separate first-level reports. Comparison of the laboratory and test section performance will be discussed in a second-level report once all the data from all of the studies has been collected and analyzed.

Findings and observations based on the data collected during this analysis include:

- Variation of material properties were recorded both between sections and within sections, which was mostly attributed to variation in the degree of recementation of recycled concrete particles in the aggregate base material. Base and subgrade were stiffest on Sections 567RF/586RF (MB15-G), and weakest on Sections 572RF/590RF (90 mm MB4-G).
- The asphalt concrete modulus was significantly affected by the pavement temperature, as expected. In general, lower modulus was obtained at high temperatures, and higher modulus at low temperatures.
- The modulus of the aggregate base was generally positively correlated with the moduli of the asphalt concrete and subgrade. Correlation between the asphalt concrete modulus and the base modulus was weaker in the untrafficked area and/or in the trafficked area before HVS testing, probably because of recementation of particles in the base after construction and subsequent destruction of the bonds during HVS trafficking. No significant correlation was found between the asphalt concrete modulus and the subgrade modulus.
- The load level of the FWD did not have a significant effect on the values of the backcalculated moduli.
- Aging of the asphalt concrete was apparent on all sections except Section 591RF (MAC15-G). A logarithm function appeared to fit the data well. The stiffness of the base increased significantly

with time after initial construction, primarily due to recementation of the recycled concrete particles. This increase continued after overlay construction in certain areas of the test road (e.g. in the vicinity of Sections 586RF [MB15-G] and 588RF [AR4000-D]), but not in other areas.

- Phase 2 HVS testing generally damaged the asphalt concrete layers in the trafficked area of each section. Minimal damage was measured on Section 586RF (MB15-G).
- In the one to three year period after Phase 2 HVS testing, the modulus of the damaged asphalt concrete generally recovered to some extent except for part of the control section overlaid with AR4000-D, where the asphalt concrete layer was severely cracked. Little change in the moduli of the base and subgrade was recorded on this subsection. The recovery rates of sections overlaid with RAC-G and MB4-G (45 mm) were similar, while that of the MB4-G (90 mm) overlay section was slightly higher.
- Seasonal effects on pavement stiffness were not detected from the limited data collected during this study.
- The asphalt concrete moduli backcalculated from the overlay sections match reasonably well with the moduli determined during laboratory frequency sweep tests on flexural beam specimens. However, the asphalt concrete moduli backcalculated from the underlying DGAC were significantly lower than those measured by the frequency sweep test in the laboratory.
- There was a difference between the moduli backcalculated from FWD data and from the RSD data. Differences in test conditions (temperature, load, and load frequency) and backcalculation assumptions of the two procedures contributed to this difference.

The following recommendations for using backcalculated data in other reflective cracking study analyses are suggested:

- All sections except Sections 573RF/591RF should be subdivided into two equal-length subsections (i.e. Stations 2 to 8, and Stations 8 to 14) to account for non-uniformity of material properties within test sections in pavement modeling and simulation. Sections 573RF/591RF can be treated as one uniform section.
- For pavement modeling and simulations of actual HVS test conditions, the asphalt concrete modulus backcalculated from both FWD and RSD testing should be used. The asphalt concrete modulus determined from laboratory frequency sweep test on flexural beams should be used for modeling and simulation of uniform sections.

No recommendations as to the use of modified binder mixes are made at this time. These recommendations will be included in the second-level analysis report, which will be prepared and submitted on completion of all HVS and laboratory testing and analysis.

TABLE OF CONTENTS

LIST OF TABLES

LIST OF FIGURES

1. INTRODUCTION

1.1. Objectives

The analysis presented in this report is part of Partnered Pavement Research Center Strategic Plan Element 4.10 (PPRC SPE 4.10) being undertaken for the California Department of Transportation (Caltrans) by the University of California Pavement Research Center (UCPRC). The objective of the study is to evaluate the reflective cracking performance of asphalt binder mixes used in overlays for rehabilitating cracked asphalt concrete pavements in California. The study includes mixes modified with rubber and polymers, and it will develop tests, analysis methods, and design procedures for mitigating reflective cracking in overlays. This work is part of a larger study on modified binder (MB) mixes being carried out under the guidance of the Caltrans Pavement Standards Team (PST) (1), which includes laboratory and accelerated pavement testing using the Heavy Vehicle Simulator (carried out by the UCPRC), and the construction and monitoring of field test sections (carried out by Caltrans).

1.2. Overall Project Organization

This UCPRC project is a comprehensive study, carried out in three phases, involving the following primary elements (2):

- Phase 1
  - The construction of a test pavement and subsequent overlays;
  - Six separate Heavy Vehicle Simulator (HVS) tests to crack the pavement structure;
  - Placing of six different overlays on the cracked pavement;
- Phase 2
  - Six HVS tests to assess the susceptibility of the overlays to high-temperature rutting (Phase 2a);
  - Six HVS tests to determine the low-temperature reflective cracking performance of the overlays (Phase 2b);
  - Laboratory shear and fatigue testing of the various hot-mix asphalts (Phase 2c);
  - Falling Weight Deflectometer (FWD) testing of the test pavement before and after construction and before and after each HVS test;
  - Forensic evaluation of each HVS test section;
- Phase 3
  - Performance modeling and simulation of the various mixes using models calibrated with data from the primary elements listed above.

Phase 1

In this phase, a conventional dense-graded asphalt concrete (DGAC) test pavement was constructed at the Richmond Field Station (RFS) in the summer of 2001. The pavement was divided into six cells, and within each cell a section of the pavement was trafficked with the HVS until the pavement failed by either fatigue (2.5 m/m^2 [0.76 ft/ft^2]) or rutting (12.5 mm [0.5 in], to limit the effects of excessive deformation in the overlay performance). This period of testing began in the fall of 2002 and was concluded in the spring of 2003. In June 2003 each test cell was overlaid with either conventional DGAC or asphalt concrete with modified binders as follows:

- Full-thickness (90 mm) AR4000 dense-graded (AR4000-D) overlay, included as a control for performance comparison purposes;
- Full-thickness (90 mm) MB4 gap-graded (MB4-G) overlay;
- Half-thickness (45 mm) rubberized asphalt concrete gap-graded overlay (RAC-G), included as a control for performance comparison purposes;
- Half-thickness (45 mm) MB4 gap-graded (MB4-G) overlay;
- Half-thickness (45 mm) MB4 gap-graded overlay with minimum 15 percent recycled tire rubber (MB15-G), and
- Half-thickness (45 mm) MAC15TR gap-graded overlay with minimum 15 percent recycled tire rubber.

The conventional overlay was designed using the current (2003) Caltrans overlay design process. The various modified overlays were either full (90 mm) or half thickness (45 mm). Mixes were designed by Caltrans. The overlays were constructed in one day.

Phase 2

Phase 2 included high-temperature rutting and low-temperature reflective cracking testing with the HVS as well as laboratory shear and fatigue testing. The rutting tests were started and completed in the fall of 2003. For these tests, the HVS was placed above a section of the underlying pavement that had not been trafficked during Phase 1. A reflective cracking test was conducted next on each overlay from the winter of 2003-2004 to the summer of 2007. For these tests, the HVS was positioned precisely on top of the sections of failed pavement from the Phase 1 HVS tests to investigate the extent and rate of crack propagation through the overlay.

In conjunction with Phase 2 HVS testing, a full suite of laboratory testing, including shear and fatigue testing, was carried out on field-mixed, field-compacted, field-mixed, laboratory-compacted, and laboratory-mixed, laboratory-compacted specimens.

Phase 3

Phase 3 entailed a second-level analysis carried out on completion of HVS and laboratory testing. This included extensive analysis and characterization of the mix fatigue and mix shear data, backcalculation of the FWD data, performance modeling of each HVS test, and a detailed series of pavement simulations carried out using the combined data.

An overview of the project timeline is shown in Figure 1.1.

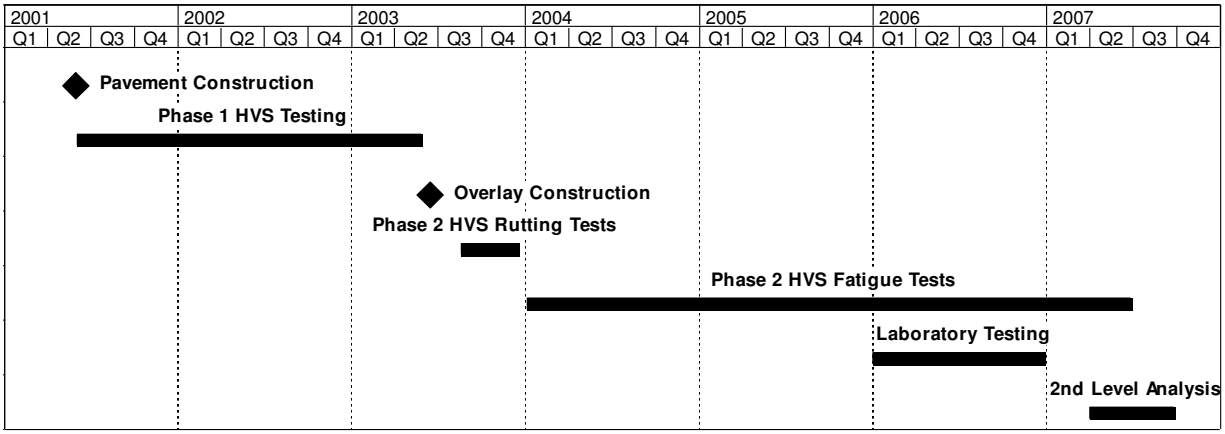

Figure 1.1: Timeline for the Reflective Cracking Study.

Reports

The reports prepared during the reflective cracking study document data from construction, HVS tests, laboratory tests, and subsequent analyses. These include a series of first- and second-level analysis reports and two summary reports. On completion of the study this suite of documents will include:

- One first-level report covering the initial pavement construction, the six initial HVS tests, and the overlay construction (Phase 1);
- One first-level report covering the six Phase 2 rutting tests (but offering no detailed explanations or conclusions on the performance of the pavements);
- Six first-level reports, each of which covers a single Phase 2 reflective cracking test (containing summaries and trends of the measured environmental conditions, pavement responses, and pavement performance but offering no detailed explanations or conclusions on the performance of the pavement);
- One first-level report covering laboratory shear testing;
- One first-level report covering laboratory fatigue testing;
- One report summarizing the HVS test section forensic investigation;
- One report summarizing Falling Weight Deflectometer (FWD) results and analysis;

- One second-level analysis report detailing characterization of shear and fatigue data, pavement modeling analysis, comparisons of the various overlays, and simulations using various scenarios (Phase 3), and
- One four-page summary report capturing the conclusions and one longer, more detailed summary report that covers the findings and conclusions from the research conducted by the UCPRC.

Reports are prepared as soon as a specific HVS or laboratory test is complete. Additional findings from forensic investigations and later analysis are covered in the forensic, second-level analysis, and summary reports.

1.3. Structure and Content of This Report

This report summarizes analysis of the Falling Weight Deflectometer (FWD) measurements taken over the course of the study and is organized as follows:

- Chapter 2 contains a description of the HVS test program including experiment layout, loading sequence, instrumentation, and data collection;
- Chapter 3 presents a summary and discussion of the FWD backcalculation analysis;
- Chapter 4 discusses aging, seasonal effects, and stiffness recovery;
- Chapter 5 provides a comparison of backcalculated and laboratory results, and
- Chapter 6 contains a summary of the results together with conclusions and observations.

The purpose of the report covers several aspects, including:

- Characterization of the HVS sections with Falling Weight Deflectometer (FWD). Although the test sections were designed and built to be homogeneous, some variations in material properties and layer thickness were measured. With the actual layer thickness (measured by Dynamic Cone Penetrometer [DCP], coring, or trenching) as input, moduli backcalculated from FWD data provided accurate characterization of material properties at selected points on the sections, and therefore, reduced errors in performance comparison of the different overlay materials.
- Comparison of trafficked and untrafficked stiffness change. In analyzing stiffness change of the trafficked areas, FWD testing was used to detect the potential trend of stiffness recovery due to healing and other factors. In analyzing stiffness change of the untrafficked areas, FWD testing was used to characterize effects due to binder aging, recementation of aggregate particles, consolidation of subgrade, and other potential influences.

- Accounting for seasonal changes. The Richmond Field Station experiences seasonal variation in climate. Changes in precipitation and water table depth affect the moisture content of pavement layers and therefore the material properties.
- Providing inputs for simulations. Material properties characterized by FWD tests are closer to actual field conditions than those measured with laboratory tests. With these material properties as inputs, the simulation of pavement damage process in pavement design software (e.g., *CalME*) is more rational and accurate.

1.4. Measurement Units

Metric units have always been used in the design and layout of HVS test tracks, and for all the measurements, data storage, analysis, and reporting at the eight HVS facilities worldwide (as well as all other international accelerated pavement testing facilities). Continued use of the metric system facilitates consistency in analysis, reporting, and data sharing.

In this report, metric and English units are provided in the Executive Summary, Chapters 1 and 2, and the Conclusion. In keeping with convention, only metric units are used in Chapters 3, 4 and 5. A conversion table is provided on Page iv at the beginning of this report.

2. HEAVY VEHICLE SIMULATOR TEST DETAILS

2.1. Phase 2 Experiment Layout

Twelve test sections (six rutting and six reflective cracking) were constructed as part of the second phase of the study, as follows (Figure 2.1):

1. Sections 580RF and 586RF: Half-thickness (45 mm) MB4 gap-graded overlay with minimum 15 percent recycled tire rubber (referred to as "MB15-G" in this report);
2. Sections 581RF and 587RF: Half-thickness (45 mm) rubberized asphalt concrete gap-graded (RAC-G) overlay;
3. Sections 582RF and 588RF: Full-thickness (90 mm) AR4000 dense-graded asphalt concrete overlay (designed using CTM356 and referred to as "AR4000-D"AR4000-D"-D in this report);
4. Sections 583RF and 589RF: Half-thickness (45 mm) MB4 gap-graded overlay (referred to as "45 mm MB4-G" in this report);
5. Sections 584RF and 590RF: Full-thickness (90 mm) MB4 gap-graded overlay (referred to as "90 mm MB4-G" in this report), and
6. Sections 585RF and 591RF: Half-thickness (45 mm) MAC15TR gap-graded overlay with minimum 15 percent recycled tire rubber (referred to as "MAC15-G" in this report).

2.2. Test Section Layout

The general test section layout for each section is shown in Figure 2.2. Station numbers refer to fixed points on the test section and are used for measurements and as a reference for discussing performance.

2.3. Underlying Pavement Design

The pavement for the first phase of HVS trafficking was designed according to the Caltrans Highway Design Manual Chapter 600 using the computer program *NEWCON90.* Design thickness was based on a tested subgrade R-value of 5 and a Traffic Index of 7 (~121,000 ESALs) (3).

The pavement design for the test road and the as-built pavement structure for each section (580RF through 591RF) are illustrated in Figure 2.2. As built thicknesses were determined from cores removed from the edge of the sections.

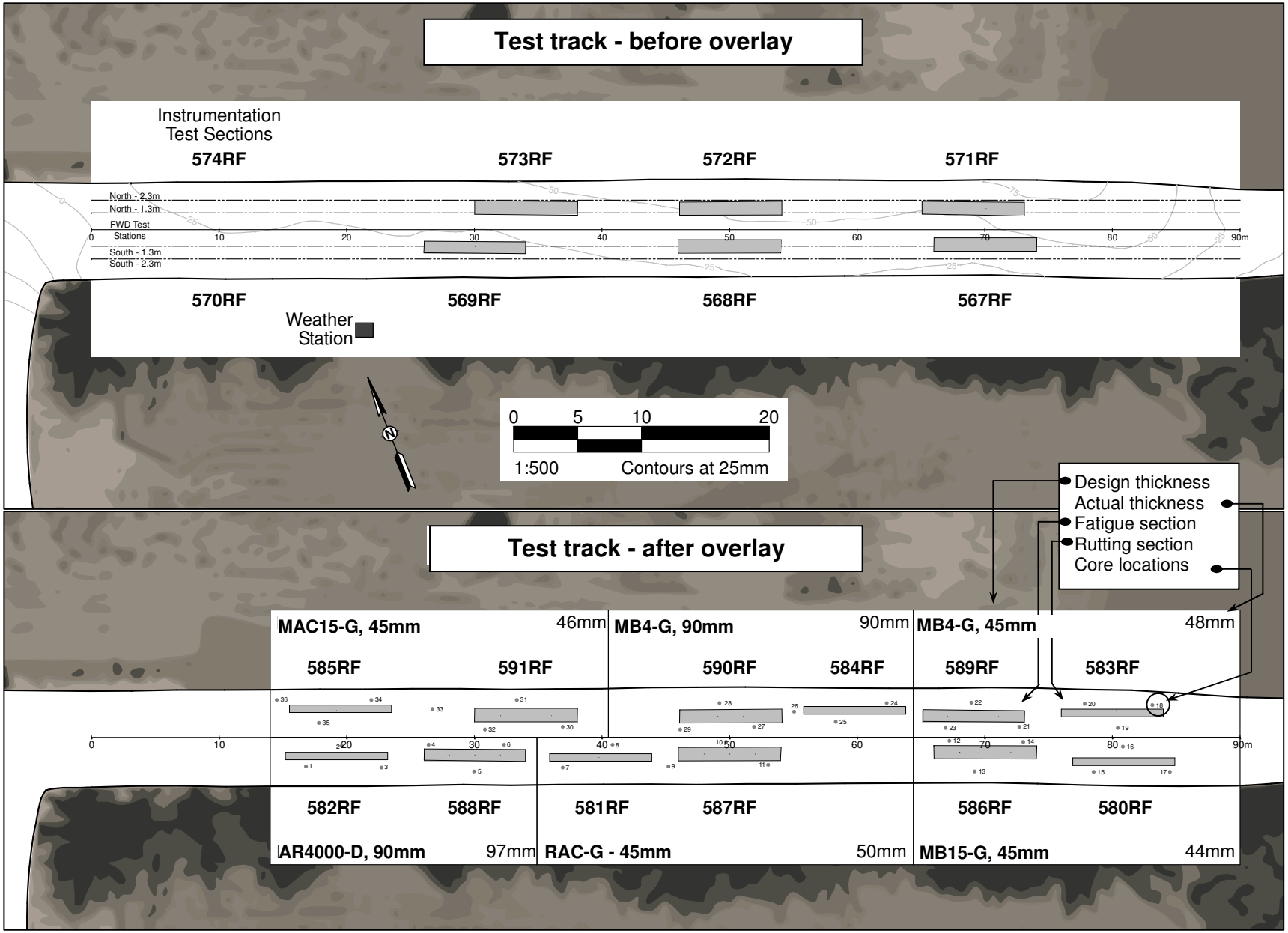

Figure 2.1: Layout of Reflective Cracking Study project.

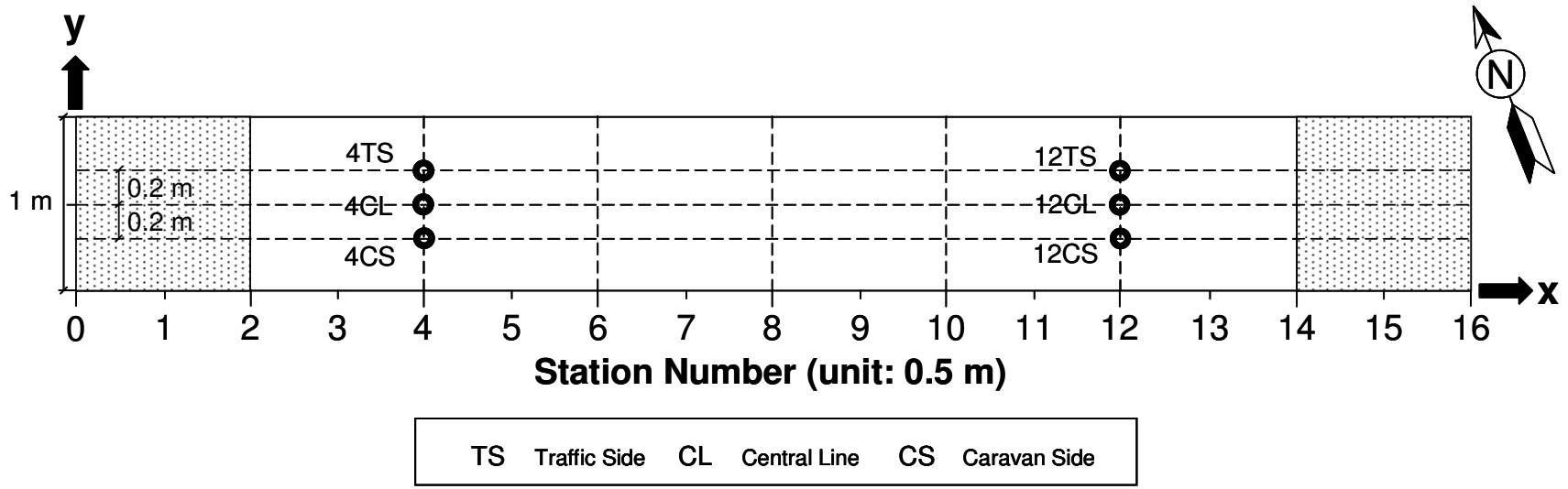

Figure 2.2: Test section layout.

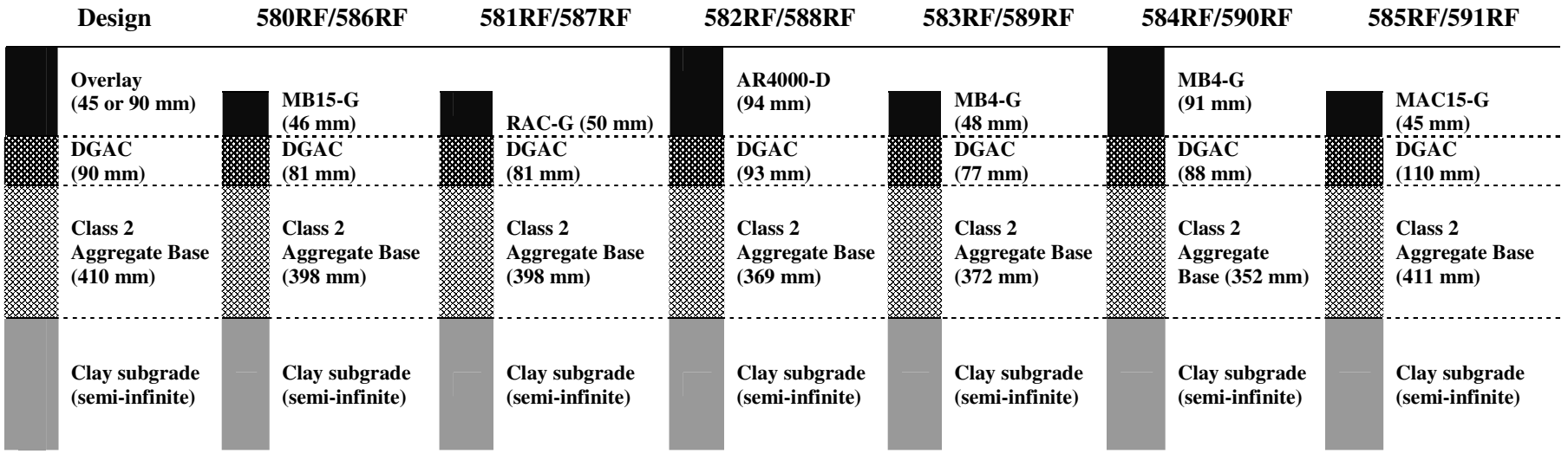

Figure 2.3: Pavement design for reflective cracking experiment (design and actual).

The existing subgrade was ripped and reworked to a depth of 200 mm (8 in) so that the optimum moisture content and the maximum wet density met the specification per Caltrans Test Method CTM 216. The average maximum wet density of the subgrade was 2,180 kg/m^3 (136 pcf). The average relative compaction of the subgrade was 97 percent (3).

The aggregate base was constructed to meet the Caltrans compaction requirements for aggregate base Class 2 using CTM 231 nuclear density testing. The maximum wet density of the base determined according to CTM 216 was 2,200 kg/m^3 (137 pcf). The average relative compaction was 98 percent.

The DGAC layer consisted of a dense-graded asphalt concrete (DGAC) with AR-4000 binder and aggregate gradation limits following Caltrans 19-mm (0.75 in) maximum size coarse gradation (3). The target asphalt content was 5.0 percent by mass of aggregate, while actual contents varied between 4.34 and 5.69 percent. Nuclear density measurements and extracted cores were used to determine a preliminary as-built mean air-void content of 9.1 percent with a standard deviation of 1.8 percent. The air-void content after traffic compaction and additional air-void contents from cores taken outside the trafficked area will be determined on completion of trafficking of all sections and will be reported in the second-level analysis report.

2.4. Summary of HVS Testing on the Underlying Layer

Phase 1 HVS trafficking took place between December 21, 2001, and March 25, 2003, and is summarized in Table 2.1.

Table 2.1: Summary of HVS Testing on the Underlying DGAC Layer

Section	Start Date	End Date	Repetitions	Wheel Load (kN)	Wheel	Tire Pressure (kPa)	Direction
567RF	12/21/01	01/07/02	78,500	60 (13,500 lb)	Dual	720 (104 psi)	Bi
568RF	01/14/02	02/12/02	377,556				
569RF	03/25/03	04/11/03	217,116				
571RF	07/12/02	10/02/02	1,101,553				
572RF	01/23/03	03/12/03	537,074				
573RF	03/19/02	07/08/02	983,982				

Figure 2.4 presents the final cracking patterns and average maximum rut depth for the middle six meters of each trafficked section after Phase 1 HVS testing. Cracking on all of the sections exceeded the 2.5 m/m^2 failure criteria, while all but one of the sections (569RF) exceeded the 12.5 mm rutting criteria. Analysis of the Phase 1 HVS testing is discussed in detail in a separate report (3) and is not covered in this report.

567RF 78,500 repetitions	568RF 377,556 repetitions	569RF 217,116 repetitions	571RF 1,101,553 repetitions	572RF 537,074 repetitions	573RF 983,982RF
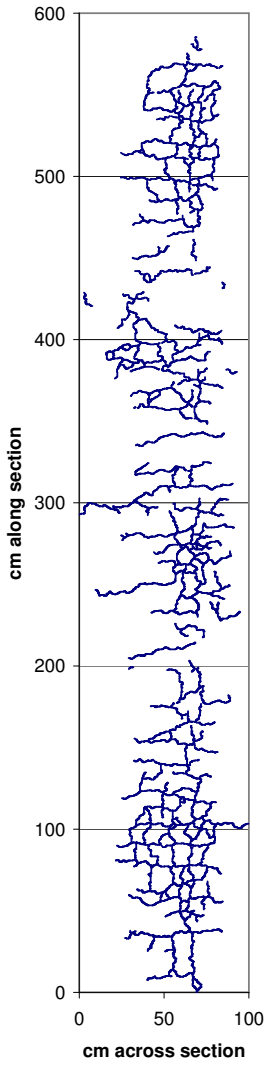	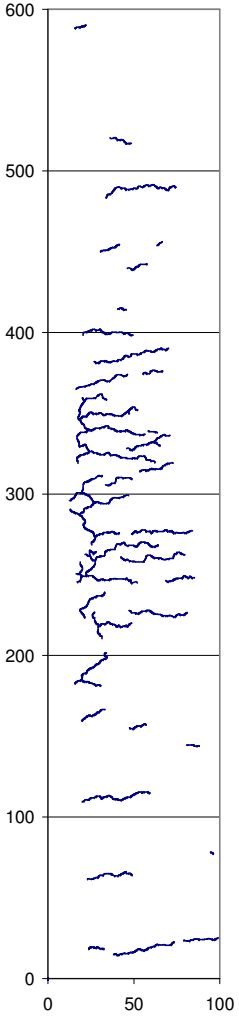	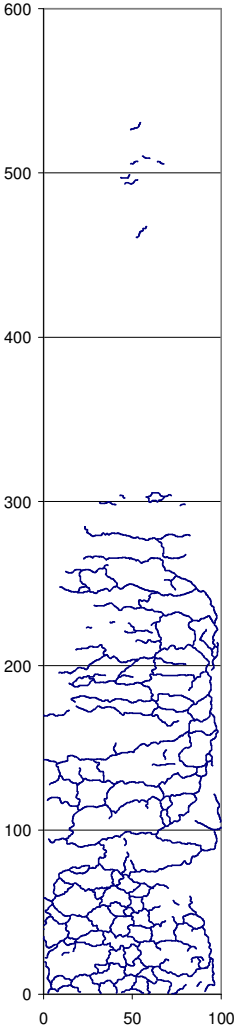	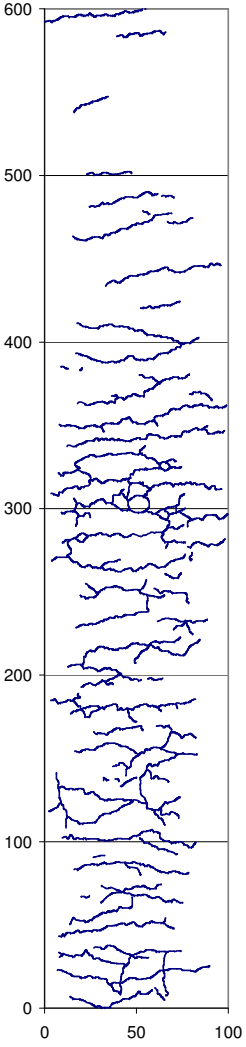	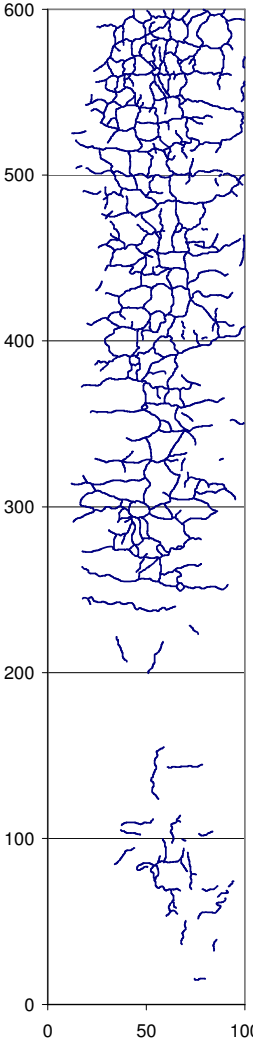	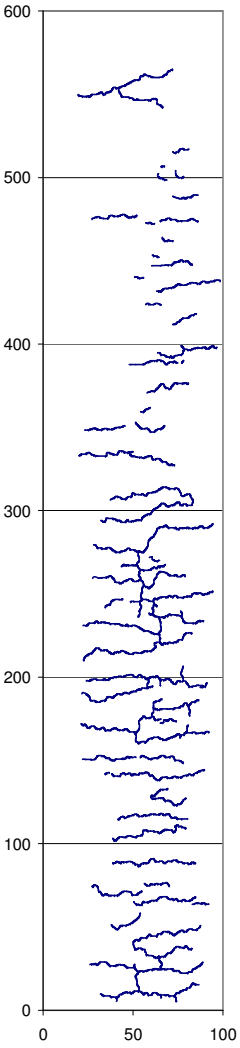
Average Maximum Rut Depths					
15.7 mm (0.62 in)	**13.9 mm (0.55 in)**	**6.3 mm (0.25 in)**	**14.3 mm (0.56 in)**	**16.4 mm (0.65 in)**	**14.6 mm (0.57 in)**

Figure 2.4: Cracking patterns and rut depths on Sections 567RF through 573RF after Phase 1.

2.5. Overlay Design

The overlay thickness for the experiment was determined according to Caltrans Test Method CTM 356 using Falling Weight Deflectometer data from the Phase 1 experiment.

Laboratory testing was carried out by Caltrans and UCPRC on samples collected during construction to determine actual binder properties, binder content, aggregate gradation, and air-void content (4,5). The binders met requirements, based on testing performed by Caltrans. The average ignition-extracted binder contents of the various layers, corrected for aggregate ignition and compared to the design binder content, are listed in Table 2.2. For each section, actual binder contents were higher than design contents. It is not clear whether this is a function of the test or contractor error.

Table 2.2: Design versus Actual Binder Contents

Section	Mix	Binder Content (%)	
		Design	Actual
580RF and 586RF	MB15-G	7.1	7.52
581RF and 587RF	RAC-G	8.0	8.49
582RF and 588RF	AR4000-D	5.0	6.13
583RF and 589RF	MB4-G (45 mm)	7.2	7.77
584RF and 590RF	MB4-G (90 mm)	7.2	7.77
585RF and 591RF	MAC15-G	7.4	7.55

The aggregate gradations for the dense- and gap-graded mixes generally met Caltrans specifications for 19.0 mm (0.75 in.) maximum size coarse and gap gradations respectively, with specifics for each section detailed below. Gradations are illustrated in Figure 2.5 (AR4000-D) and Figure 2.6 (modified binders).

- 580RF and 586RF: Material passing the 6.35 mm (1/4 in), 9.5 mm (3/8 mm), 12.5 mm (1/2 in), and 19.0 mm (3/4 in) sieves was on the lower envelope limit (Figure 2.6).
- 581RF and 587RF: Material passing the 0.3 mm (#50), 0.6 mm (#30), and 2.36 mm (#8) sieves was on the lower envelope limit (Figure 2.6).
- 582RF and 588RF: Material passing the 0.6 mm (#30), 2.36 mm (#8), and 4.75 mm (#4) sieves was on the upper envelope limit (Figure 2.5).
- 583RF and 589RF: Material passing the 6.35 mm (1/4 in) and 9.5 mm (3/8 in) sieves was on the lower envelope limit (Figure 2.6).
- 584RF and 590RF: Material passing the 6.35 mm (1/4 in) and 9.5 mm (3/8 in) sieves was on the lower envelope limit (Figure 2.6).
- 585RF and 591RF: Material passing the 0.6 mm (#30), 9.5 mm (3/8 in), 12.5 mm (1/2 in), and 19.0 mm (3/4 in) sieves was on the upper envelope limit, while material passing the 2.36 mm (#8), 4.75 mm (#4), and 6.35 mm (1/4 in) sieves was outside the upper limit (Figure 2.6).

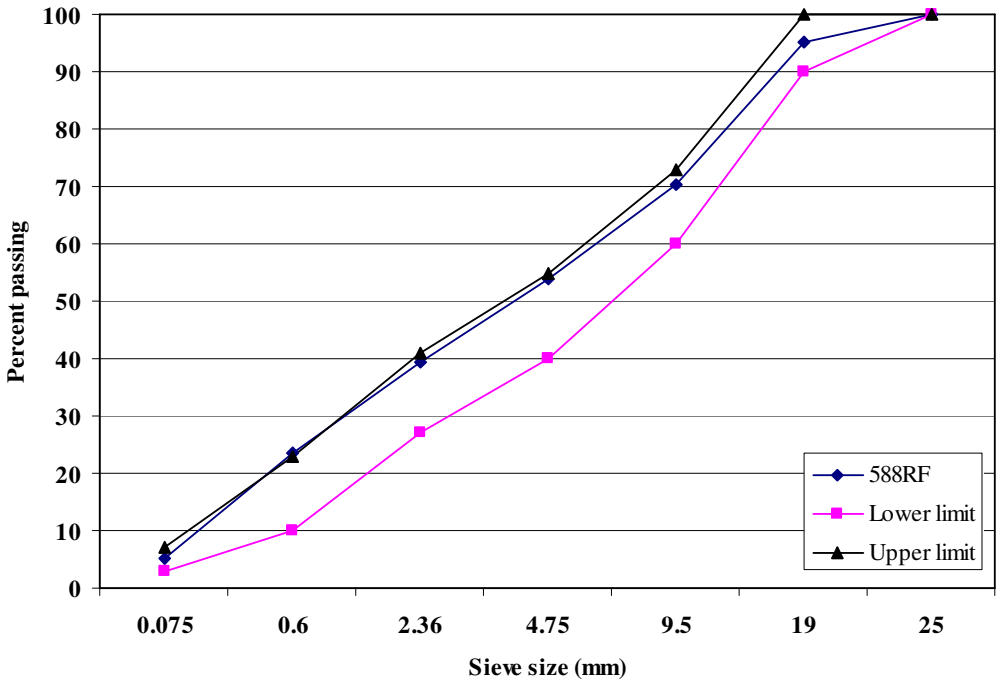

Figure 2.5: Gradation for AR4000-D overlay.

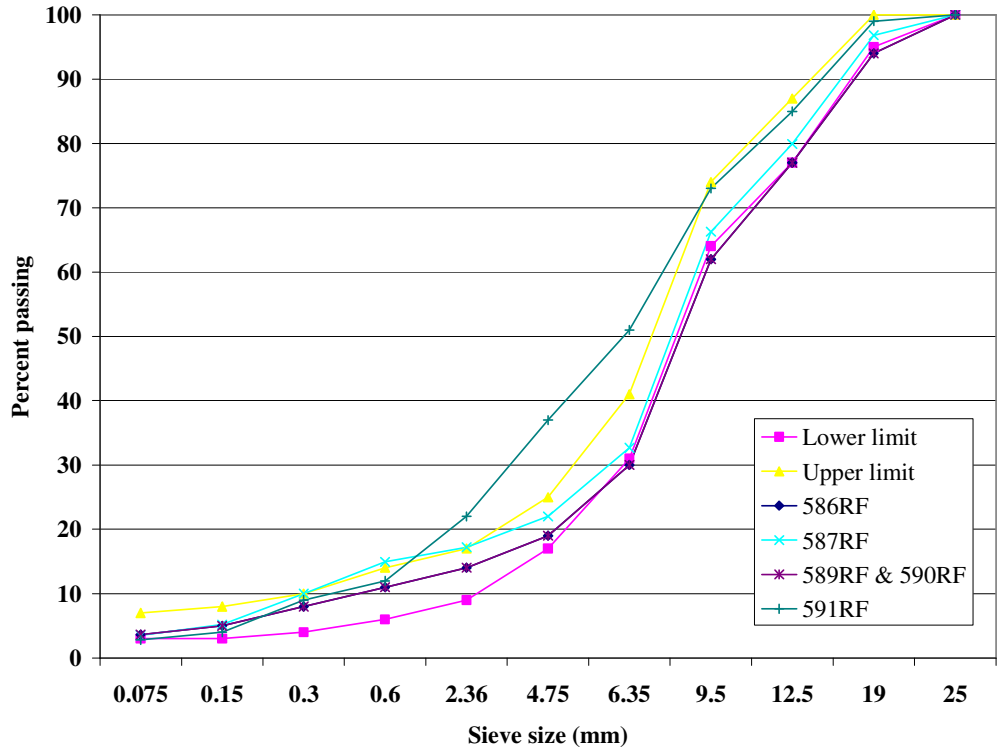

Figure 2.6: Gradation for modified binder overlays.

The preliminary as-built air-void contents for each section, based on cores taken outside of the HVS sections prior to HVS testing are listed in Table 2.3.

Table 2.3: Air-Void Contents

Section	Mix	Air-Void Content (%)	
		Average for Section	Standard Deviation
580RF and 586RF	MB15-G	5.1	1.7
581RF and 587RF	RAC-G	8.8	1.3
582RF and 588RF	AR4000-D	7.1	1.5
583RF and 589RF	MB4-G (45 mm)	6.5	0.6
584RF and 590RF	MB4-G (90 mm)	6.5	0.6
585RF and 591RF	MAC15-G	4.9	1.0

2.6. Summary of Phase 2 HVS Testing

Phase 2 HVS testing is discussed in a series of first-level analysis reports (6-11) and a forensic investigation report (12).

2.6.1 Test Section Failure Criteria

Failure criteria for HVS testing were set as follows:

- Rutting study:
  - Maximum surface rut depth of 12.5 mm (0.5 in) or more
- Reflective Cracking study:
  - Cracking density of 2.5 m/m^2 (0.76 ft/ft^2) or more, and/or
  - Average maximum surface rut depth of 12.5 mm (0.5 in) or more.

2.6.2 Environmental Conditions

In the rutting study, the pavement surface temperature was maintained at 50°C±4°C (122°F±7°F) in order to assess the susceptibility of the mixes to early rutting under typical pavement temperatures. In the reflective cracking study, the pavement surface temperature was maintained at 20°C±4°C (68°F±7°F) for the first one million repetitions to minimize rutting in the asphalt concrete and to accelerate fatigue damage. Thereafter, the pavement surface temperature was reduced to 15°C±4°C (59°F±7°F) to further accelerate fatigue damage. A temperature control chamber (13) was used to maintain the test temperatures.

The pavement surface of a test section received no direct rainfall during the actual HVS test as it was protected by the temperature control chamber. The sections were tested during both wet and dry seasons and hence water infiltration into the pavement from the side drains and through the raised groundwater table was possible at certain stages of the testing.

2.6.3 Test Duration

HVS trafficking on each section was initiated and completed as shown in Table 2.4.

Table 2.4: Test Duration for Phase 2 HVS Testing

Phase	Section	Mix	Start Date	Finish Date	Repetitions
Rutting	580RF	MB15-G	09/29/03	10/01/03	2,000
	581RF	RAC-G	09/15/03	09/19/03	7,600
	582RF	AR4000-D	09/04/03	09/09/03	18,564
	583RF	MB4-G (45 mm)	12/08/03	12/16/03	15,000
	584RF	MB4-G (90 mm)	11/13/03	11/26/03	34,800
	585RF	MAC15-G	10/10/03	10/20/03	3,000
Reflective cracking	586RF	MB15-G	05/25/06	11/21/06	2,492,387
	587RF	RAC-G	03/15/05	10/10/05	2,024,793
	588RF	AR4000-D	11/02/05	04/11/06	1,410,000
	589RF	MB4-G (45 mm)	06/23/04	02/08/05	2,086,004
	590RF	MB4-G (90 mm)	01/13/04	06/16/04	1,981,365
	591RF	MAC15-G	01/10/07	06/25/07	2,554,335

2.6.4 Loading Program

The HVS loading program for each section is summarized in Table 2.5. Test configurations were as follows:

- In the rutting tests, all trafficking was carried out with a dual-wheel configuration, using radial truck tires (Goodyear G159 - 11R22.5- steel belt radial) inflated to a pressure of 720 kPa (104 psi), in a channelized, unidirectional loading mode.
- In the reflective cracking tests, all trafficking was carried out with a dual-wheel configuration, using radial truck tires (Goodyear G159 - 11R22.5- steel belt radial) inflated to a pressure of 720 kPa, in a bidirectional loading mode. Lateral wander over the one-meter width of the test section was programmed to simulate traffic wander on a typical highway lane.

Table 2.5: Summary of HVS Loading Program

Phase	Section	Start Repetition	Total Repetitions	Wheel load (kN [lb])		ESALs	Traffic Index
				Planned	Actual*		
Rutting	580RF	Full test	2,000	40 (8,000)	60 (13,500)	11,000	N/A
	581RF		7,600			42,000	N/A
	582RF		18,564			102,000	N/A
	583RF		15,000			83,000	N/A
	584RF		34,800			191,000	N/A
	585RF		3,000			17,000	N/A

* The loading program differs from the original test plan due to an incorrect hydraulic control system setup on loads less than 65 kN in the Phase 1 experiment. The loading pattern from the Phase 1 experiment was thus retained to facilitate comparisons of performance between all tests in the Reflective Cracking Study.

Table 2.5: Summary of Load History (cont.)

Phase	Section	Start Repetition	Total Repetitions	Wheel Load (kN)		ESALs	Traffic Index
				Planned	Actual*		
Reflective cracking	586RF (MB15-G)	0 215,000 410,000 1,000,001	2,492,387	40 60 80 100	60 90 80 100	88 million	15
	587RF (RAC-G)	0 215,000 410,000 1,000,001	2,024,793	40 60 80 100	60 90 80 100	66 million	15
	588RF (AR4000-D)	0 215,000 410,000 1,000,001	1,410,000	40 60 80 100	60 90 80 100	37 million	14
	589RF (45 mm MB4-G)	0 215,000 407,197 1,002,000	2,086,004	40 60 80 100	60 90 80 100	69 million	15
	590RF** (90 mm MB4-G)	0 1,071,004 1,439,898 1,629,058	1,981,365	40 60 80 100	60 90 80 100	37 million	14
	591RF (MAC15-G)	0 215,000 410,000 1,000,001	2,554,335	40 60 80 100	60 90 80 100	91 million	15

* The loading program differs from the original test plan due to an incorrect hydraulic control system setup on loads less than 65 kN in the Phase 1 experiment. The loading pattern from the Phase 1 experiment was thus retained to facilitate comparisons of performance between all tests in the Reflective Cracking Study.

** 590RF was the first HVS test on the overlays, and the 60 kN loading pattern was retained for an extended period to prevent excessive initial deformation (rutting) of the newly constructed overlay.

40 kN = 8,000 lb 60 kN = 13,500 lb 80 kN = 18,000 lb 90 kN = 20,200 lb 100 kN = 22,500 lb

2.7. Phase 2 Test Results

The final crack densities and average maximum rut depths for each section on completion of Phase 2 HVS testing are listed in Table 2.6. The final cracking patterns are presented in Figure 2.7.

Table 2.6: Summary of Phase 2 HVS Test Results

Section	Overlay	Crack Density (m/m^2 [ft/ft^2])	Average Maximum Rut (mm [in])
586RF	MB15-G	No cracking	4.6 (0.18)
587RF	RAC-G	3.6 (1.10)	18.2 (0.72)
588RF	AR4000-D	9.1 (2.77)	15.9 (0.63)
589RF	45 mm MB4-G	1.5 (0.47)	37.2 (1.46)
590RF	90 mm MB4-G	No cracking	12.7 (0.50)
591RF	MAC15-G	No cracking	1.7 (0.07)

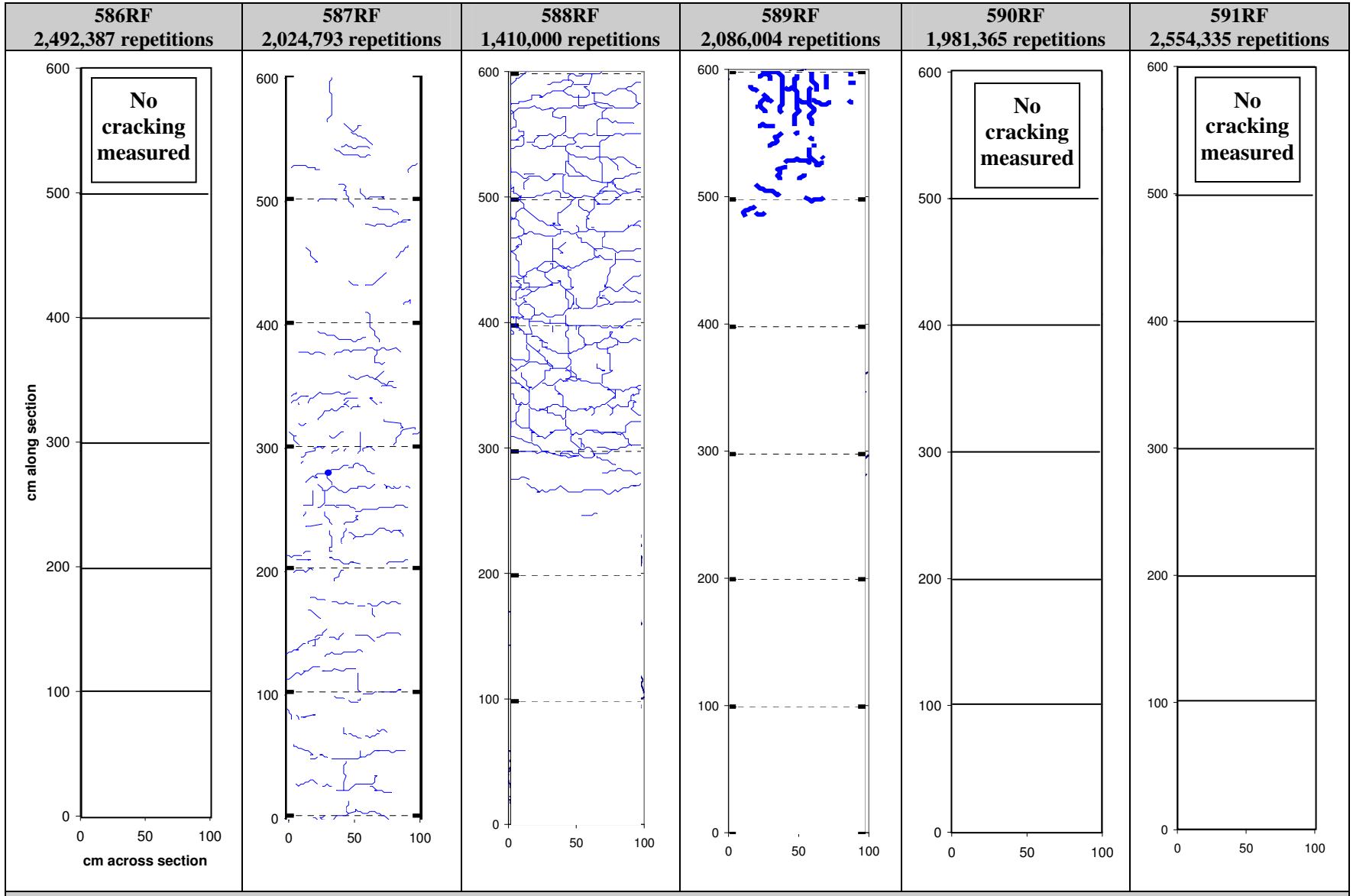

Figure 2.7: Cracking patterns and rut depths on Sections 586RF through 591RF after Phase 2 testing.

2.8. Summary of FWD Testing

The University of California Pavement Research Center's Heavy Weight Deflectometer (Dynatest Model 8082 HWD), referred to as FWD in this report, was used to measure deflection at regular intervals throughout the experiment. Measurements were taken over the entire test track, in both trafficked and untrafficked areas, and before and after HVS testing, to monitor changes in stiffness of the asphalt concrete, aggregate base, and subgrade over time.

The FWD generates a transient, impulse-type load of 25–30 milliseconds duration, at any desired (peak) load level between 27 kN and 245 kN (6,000 and 55,000 lbf.), thereby approximating the effect of a 50 to 80 km/h (30 to 50 mph) moving wheel load. Three load levels were applied on the various sections and each load level was applied once. Target loads for the pavement sections were 30 kN, 40 kN, and 50 kN. The UCPRC FWD is configured with a segmented 300-mm diameter load plate and eight deflection sensors. The sensor locations are shown in Table 2.7.

Table 2.7: FWD Sensor Locations

Sensor Number	Distance from center of load plate (mm)
1	0
2	210
3	315
4	475
5	630
6	925
7	1,535
8	1,985

Deflection measurements on the original test track were carried out along the centerline and at 1.3 m (4.3 ft) and 2.3 m (8.3 ft) offsets either side of the centerline (Figures 2.1 and 2.8). After the overlays were placed, deflections were measured on the offsets only. Centerline measurements were not possible due to unevenness of the surface resulting from the differences in thickness of the overlays. Deflections were not measured on the Phase 2 rutting experiments due to the unevenness caused by deformation.

A summary of the FWD measurement schedule over the duration of the study is provided in Table 2.8 through Table 2.14.

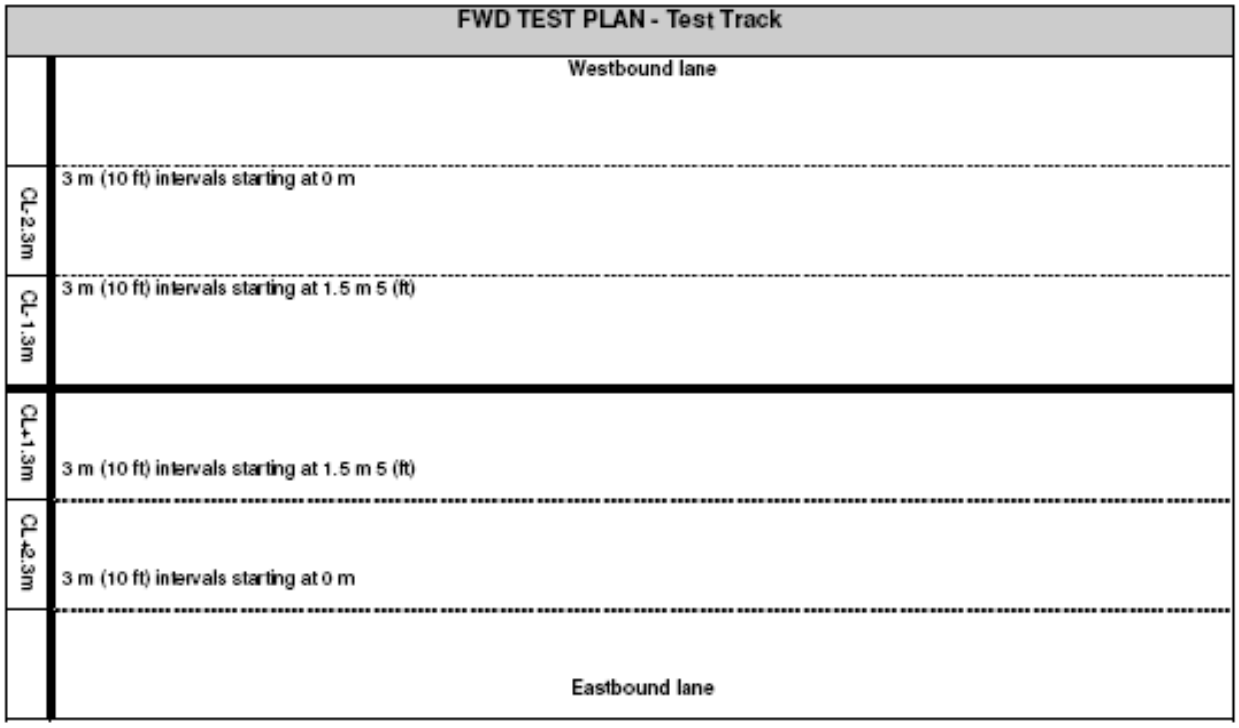

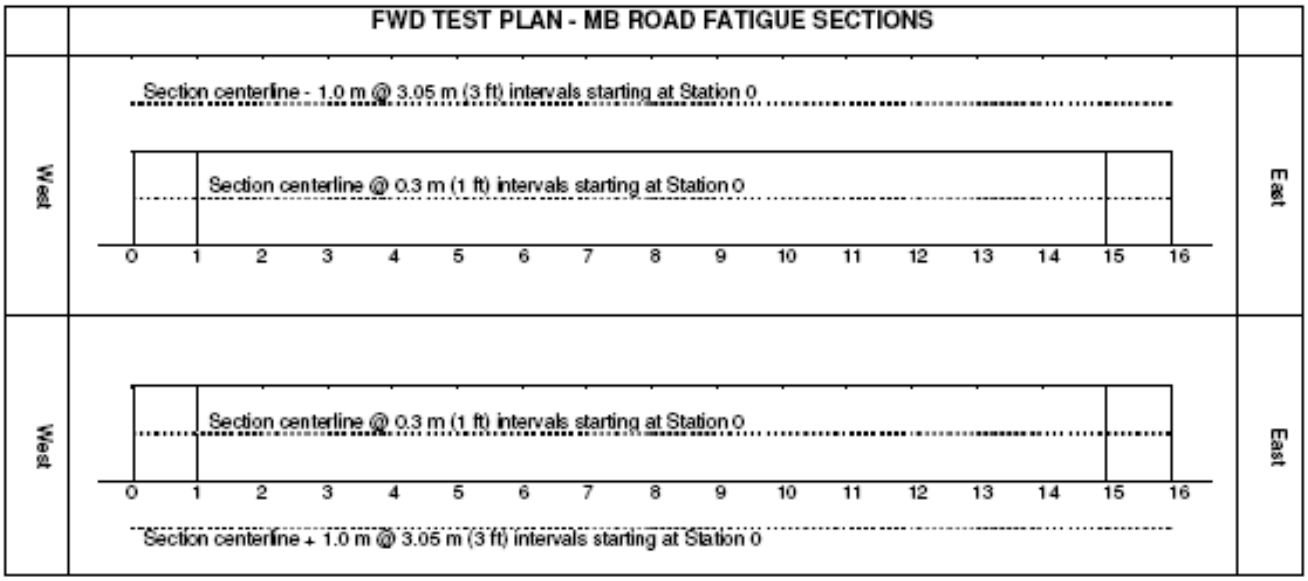

Figure 2.8: FWD test plans (test track and HVS trafficked section).

Table 2.8: List of FWD Tests by Lines on Underlying Sections

Section ID (From FWD Datalogger)	Date	Test Time		Number of Test Points	Interval (m)	Transverse Location	Average Surface Temp. (°C)
		Start	End				
MBACCL	10/03/01	07:30	07:56	27	3.05	Center	17.4
MBACN13	10/03/01	09:04	09:31	27	3.05	North 1.3	19.6
MBACN23	10/03/01	09:35	10:00	27	3.05	North 2.3	20.5
MBACS13	10/03/01	08:01	08:30	29	3.05	South 1.3	17.5
MBACS23	10/03/01	08:34	08:59	27	3.05	South 2.3	17.6
MBACCL11	10/11/01	13:39	14:10	27	3.05	Center	30.4
MBACN131	10/11/01	14:47	15:15	27	3.05	North 1.3	29.9
MBACN231	10/11/01	15:18	15:45	27	3.05	North 2.3	30.6
MBACS131	10/11/01	14:15	14:42	28	3.05	South 1.3	28.6
MBACCL2	10/25/01	13:21	13:51	26	3.05	Center	32.2
MBACN132	10/25/01	12:55	13:18	26	3.05	North 1.3	32.8
MBACN232	10/25/01	12:29	12:52	27	3.05	North 2.3	32.2
MBACS132	10/25/01	13:54	14:39	26	3.05	South 1.3	32.7
MBACS232	10/25/01	14:50	15:18	27	3.05	South 2.3	30.5
MBACN133	11/07/01	16:02	16:27	27	3.05	North 1.3	22.2
MBACN233	11/07/01	16:31	16:54	27	3.05	North 2.3	21.0
MBACS133	11/07/01	17:00	17:24	27	3.05	South 1.3	18.4
MBACS233	11/07/01	17:27	17:51	27	3.05	South 2.3	16.9
MBACCL4	12/14/01	11:45	11:53	10	3.05	Center	11.1
MBACN134	12/14/01	11:55	12:19	28	3.05	North 1.3	11.8
MBACN234	12/14/01	12:22	12:46	27	3.05	North 2.3	12.9
MBACS134	12/14/01	11:35	11:43	9	3.05	South 1.3	11.3
MBACS234	12/14/01	11:24	11:31	8	3.05	South 2.3	12.3
MBACCL5	01/08/02	13:31	13:58	27	3.05	Center	17.7
MBACN135	01/08/02	14:10	14:39	28	3.05	North 1.3	17.1
MBACS135	01/08/02	12:05	13:10	27	3.05	South 1.3	18.1
MBACS235	01/08/02	11:07	11:42	27	3.05	South 2.3	16.3
MBACN235	01/09/02	09:05	09:35	27	3.05	North 2.3	13.4
MBACCL6	02/13/02	13:11	13:51	27	3.05	Center	15.0
MBACN136	02/13/02	14:09	14:46	27	3.05	North 1.3	14.3
MBACN236	02/13/02	15:03	15:35	27	3.05	North 2.3	13.8
MBACN236B	02/13/02	15:03	15:35	27	3.05	North 2.3	13.8
MBACS136	02/13/02	12:22	13:02	27	3.05	South 1.3	15.3
MBACS236	02/13/02	11:33	12:07	27	3.05	South 2.3	14.0
MBAECL7	10/07/02	15:19	15:49	28	3.05	Center	37.4
MBAEN137	10/07/02	14:38	15:08	29	3.05	North 1.3	39.9
MBAEN237	10/07/02	13:34	14:30	29	3.05	North 2.3	37.7
MBAES137	10/07/02	15:57	16:30	29	3.05	South 1.3	33.9
MBAES237	10/07/02	16:41	17:13	28	3.05	South 2.3	29.4
MBBACCL7	01/02/03	10:58	11:28	27	3.05	Center	13.3
MBBAN137	01/02/03	10:20	10:49	27	3.05	North 1.3	13.2
MBBAN237	01/02/03	09:40	10:11	27	3.05	North 2.3	12.3
MBBAS137	01/02/03	13:35	14:05	27	3.05	South 1.3	15.5
MBBAS237	01/02/03	14:20	14:49	27	3.05	South 2.3	15.3
MBAGCL7	05/19/03	13:25	13:53	28	3.05	Center	42.2
MBAGN137	05/19/03	10:34	11:10	27	3.05	North 1.3	33.8
MBAGN237	05/19/03	09:50	10:24	27	3.05	North 2.3	29.9
MBAGS137	05/19/03	13:58	14:31	29	3.05	South 1.3	43.0
MBAGS237	05/19/03	14:41	15:17	27	3.05	South 2.3	43.1

Table 2.9: FWD Tests on Sections 567RF and 586RF (MB15-G)

Section ID	Test Date	Test Time		Number of Test Points	Interval (m)	Transverse Location	Surface Temp. (ºC)
		Start	End				
567RF	01/10/2002	12:10	12:37	28	0.3	Center	19
	02/14/2002	11:46	12:14	27	0.3	Center	16
	10/10/2002	15:06	15:33	28	0.3	Center	21
	01/08/2003	14:04	14:29	29	0.3	Center	18
	05/19/2003	09:09	09:41	29	0.3	Center	23
	06/10/2003	11:07	11:20	15	0.9	Side	25
	06/10/2003	16:29	16:45	15	0.9	Side	29
586RF MB15-G	06/24/2003	15:58	16:40	27	0.3	Center	40
	06/25/2003	07:40	8:14	29	0.3	Center	22
	12/23/2003	10:24	10:50	28	0.3	Center	13
	12/30/2003	10:47	11:07	26	0.3	Center	13
	03/23/2004	10:12	10:35	29	0.3	Center	19
	04/28/2006	15:00	15:32	25	0.3	Center	28
	04/28/2006	15:35	15:43	9	0.9	Side	25
	04/28/2006	16:45	17:10	18	0.3	Center	23
	04/28/2006	17:19	17:28	10	0.9	Center	23
	04/28/2006	17:32	17:45	10	0.9	Side	22
	12/40/2006	09:25	10:10	27	0.3	Center	7
	12/13/2006	15:32	17:00	28	0.3	Center	15
	12/15/2006	12:37	12:49	10	0.9	Side	13
	12/17/2006	09:56	10:09	10	0.9	Side	7

Table 2.10: FWD Tests on Sections 568RF and 587RF (RAC-G)

Section ID	Test Date	Test Time		Number of Test Points	Interval (m)	Transverse Location	Surface Temp. (ºC)
		Start	End				
568RF	01/10/2002	11:17	11:42	28	0.3	Center	18
	02/14/2002	11:19	11:42	28	0.3	Center	18
	10/10/2002	14:34	15:02	28	0.3	Center	21
	01/08/2003	10:37	11:13	29	0.3	Center	18
	05/16/2003	09:06	09:33	26	0.3	Center	22
	06/10/2003	10:50	11:03	15	0.9	Side	31
	06/10/2003	16:12	16:26	15	0.9	Side	26
587RF RAC-G	06/24/2003	15:19	15:54	27	0.3	Center	42
	06/25/2003	07:10	07:37	28	0.3	Center	21
	12/23/2003	09:30	10:11	24	0.3	Center	12
	12/30/2003	10:18	10:40	26	0.3	Center	12
	03/23/2004	09:46	10:09	28	0.3	Center	22
	02/18/2005	10:53	11:15	27	0.3	Center	19
	02/18/2005	11:24	11:32	10	0.9	Side	17
	02/24/2005	05:30	05:38	10	0.9	Side	13
	02/24/2005	05:43	06:09	30	0.3	Center	14
	10/19/2005	07:30	07:53	27	0.3	Center	17
	10/19/2005	08:35	08:55	27	0.3	Side	17
	10/19/2005	15:14	15:36	31	0.3	Center	23
	10/19/2005	16:04	16:22	27	0.3	Side	20
	12/04/2006	08:40	09:23	27	0.3	Center	6
	12/12/2006	16:00	16:29	27	0.3	Center	14
	12/15/2006	12:16	12:28	10	0.9	Side	14
	12/17/2006	09:43	09:55	10	0.9	Side	15

Table 2.11: FWD Tests on Sections 569RF and 588RF (AR4000-D)

Section ID	Test Date	Test Time		Number of Test Points	Interval (m)	Transverse Location	Surface Temp. (ºC)
		Start	End				
569RF	01/10/2002	10:03	10:31	28	0.3	Center	13
	02/14/2002	10:48	11:11	28	0.3	Center	14
	10/10/2002	13:59	14:26	28	0.3	Center	23
	01/08/2003	13:20	14:01	30	0.3	Center	18
	03/28/2003	13:18	14:06	36	0.3	Center	32
	04/04/2003	10:51	11:50	39	0.3	Center	20
	04/11/2003	11:10	12:02	35	0.3	Center	22
	05/16/2003	08:29	09:03	28	0.3	Center	20
	06/10/2003	10:23	10:43	15	0.9	Side	24
	06/10/2003	15:52	16:09	15	0.9	Side	30
588RF AR4000-D	06/24/2003	14:41	15:12	28	0.3	Center	41
	06/25/2003	06:38	07:06	28	0.3	Center	19
	12/19/2003	11:10	11:56	23	0.3	Center	15
	12/30/2003	09:38	10:05	30	0.3	Center	10
	03/23/2004	09:15	09:41	29	0.3	Center	18
	10/19/2005	06:55	07:20	28	0.3	Center	16
	10/19/2005	14:38	15:09	31	0.3	Center	27
	10/19/2005	08:04	08:27	27	0.3	Side	17
	10/19/2005	15:41	16:01	27	0.3	Side	21
	04/28/2006	12:50	13:20	23	0.3	Center	25
	04/28/2006	15:47	16:26	25	0.3	Center	28
	04/28/2006	13:23	13:33	10	0.9	Side	28
	04/28/2006	16:28	16:38	9	0.9	Side	28
	12/04/2006	07:55	08:38	27	0.3	Center	5
	12/12/2006	15:30	15:58	27	0.3	Center	15
	12/14/2006	14:48	15:20	10	0.9	Side	17
	12/16/2006	14:38	14:52	10	0.9	Side	12

Table 2.12: FWD Tests on Sections 571RF and 589RF (45 mm MB4-G)

Section ID	Test Date	Test Time		Number of Test Points	Interval (m)	Transverse Location	Surface Temp. (ºC)
		Start	End				
571RF	01/10/2002	15:11	15:37	28	0.3	Center	19
	02/14/2002	15:38	16:02	27	0.3	Center	18
	10/10/2002	11:25	11:52	28	0.3	Center	20
	01/08/2003	09:57	10:21	28	0.3	Center	15
	05/16/2003	11:30	11:57	28	0.3	Center	30
	06/10/2003	11:57	12:11	15	0.9	Side	27
	06/10/2003	17:41	18:00	15	0.9	Side	28
589RF 45 mm MB4-G	06/24/2003	17:49	18:20	29	0.3	Center	36
	06/25/2003	09:51	10:20	28	0.3	Center	32
	12/19/2003	16:40	17:12	12	0.3	Center	14
	12/22/2003	15:18	15:50	22	0.3	Center	19
	12/30/2003	14:11	14:36	28	0.3	Center	15
	03/22/2004	08:42	09:05	27	0.3	Center	17
	06/17/2004	11:01	11:31	32	0.3	Center	27
	06/17/2004	13:08	13:19	11	0.9	Side	34
	06/21/2004	10:10	10:35	30	0.3	Center	28
	06/21/2004	10:54	11:02	10	0.9	Side	31
	02/18/2005	11:41	11:52	11	0.9	Side	18
	02/18/2005	12:31	12:42	11	0.9	Center	20
	02/23/2005	07:53	08:18	30	0.3	Side	11
	02/24/2005	05:05	05:30	23	0.3	Center	13
	12/15/2006	10:51	11:11	10	0.9	Side	13
	12/15/2006	11:17	11:57	25	0.3	Center	13
	12/17/2006	08:42	09:37	30	0.3	Center	6
	12/17/2006	08:28	08:40	10	0.9	Side	4

Table 2.13: FWD Tests on Sections 572RF and 590RF (90 mm MB4-G)

Section ID	Test Date	Test Time		Number of Test Points	Interval (m)	Transverse Location	Surface Temp. (ºC)
		Start	End				
572RF	01/10/2002	14:32	15:00	28	0.3	Center	21
	02/14/2002	15:10	15:36	26	0.3	Center	18
	10/10/2002	10:22	10:49	28	0.3	Center	20
	01/08/2003	09:21	09:49	29	0.3	Center	12
	02/04/2003	09:28	10:16	31	0.3	Center	10
	02/04/2003	13:22	14:04	35	0.3	Center	23
	02/21/2003	10:56	11:37	35	0.3	Center	23
	02/28/2003	11:23	12:27	39	0.3	Center	22
	03/12/2003	13:11	13:40	26	0.3	Center	29
	05/16/2003	10:59	11:27	28	0.3	Center	30
	06/10/2003	11:42	11:55	15	0.9	Side	28
	06/10/2003	17:14	17:31	15	0.9	Side	29
590RF 90 mm MB4-G	06/24/2003	17:20	17:45	26	0.3	Center	38
	06/25/2003	09:10	09:42	29	0.3	Center	30
	01/05/2004	08:54	09:21	29	0.3	Center	6
	03/22/2004	10:54	11:00	4	0.3	Center	22
	03/22/2004	11:17	11:38	30	0.3	Center	23
	03/22/2004	13:14	13:37	14	0.9	Side	23
	06/16/2004	16:27	16:54	30	0.3	Center	27
	06/16/2004	17:00	17:09	10	0.9	Side	27
	06/21/2004	09:36	10:08	30	0.3	Center	24
	06/21/2004	10:42	10:51	10	0.9	Side	32
	12/13/2006	10:17	11:34	28	0.3	Center	16
	12/15/2006	10:05	10:32	10	0.9	Side	13
	12/16/2006	13:48	14:23	28	0.3	Center	14
	12/17/2006	08:05	08:19	10	0.9	Side	2

Table 2.14: FWD Tests on Sections 573RF and 591RF (MAC15-G)

Section ID	Test Date	Test Time		Number of Test Points	Interval (m)	Transverse Location	Surface Temp. (ºC)
		Start	End				
573RF	01/10/2002	13:57	14:26	28	0.3	Center	21
	02/14/2002	14:41	15:07	27	0.3	Center	22
	07/19/2002	11:00	11:22	28	0.3	Center	27
	10/10/2002	09:25	09:53	28	0.3	Center	20
	01/08/2003	08:50	09:17	28	0.3	Center	10
	05/16/2003	10:24	10:56	30	0.3	Center	26
	06/10/2003	11:24	11:37	15	0.9	Side	28
	06/10/2003	16:51	17:05	15	0.9	Side	30
591RF MAC15-G	06/24/2003	16:46	17:15	27	0.3	Center	39
	06/25/2003	08:25	09:06	30	0.3	Center	26
	12/22/2003	13:53	14:54	27	0.3	Center	17
	12/30/2003	14:44	15:13	30	0.3	Center	16
	12/13/2006	09:39	10:15	28	0.3	Center	15
	12/15/2006	09:43	10:04	10	0.9	Side	11
	12/16/2006	13:11	13:44	27	0.3	Center	15
	12/17/2006	07:47	08:05	10	0.9	Side	1
	06/27/2007	15:24	16:04	35	0.3	Center	31
	06/27/2007	16:16	16:40	12	0.9	Side	31
	06/28/2007	10:39	11:10	35	0.3	Center	26
	06/28/2007	11:30	11:42	12	0.9	Side	28
	06/29/2007	07:23	08:16	36	0.3	Center	19
	06/29/2007	09:58	10:11	12	0.9	Side	25

3. DEFLECTION ANALYSIS

3.1. Backcalculation Methods Used

The backcalculation program *Calback* (April 2007 version) was used to calculate the modulus of the pavement layers from Falling Weight Deflectometer measurements. A choice of layered linear elastic analysis and Odemark-Boussinesq methods is included in the program to calculate pavement responses. In this report, the Odemark-Boussinesq method was used for all backcalculation. Parameter estimation was based on the minimization of the relative difference between the observed deflection and the calculated deflection. A Kalman filter was used in all calculations, and in some cases a genetic algorithm was used to search for the optimal values.

Pavement temperatures were calculated at one third depth of the asphalt concrete layer, using BELLS equation with the surface temperature and the average air temperature of the previous day as inputs. The surface temperature was measured by the FWD during the test, and the average air temperature was obtained from a nearby weather station.

Pavement layer thicknesses were measured using several methods, including the Dynamic Cone Penetrometer (DCP), coring, and trenching. The average of measurements from these methods was used in the backcalculation, as summarized in Table 3.1.

Table 3.1: Average Thickness of Pavement Layers Used in Backcalculation

Section	Overlay	Overlay (mm)	Underlying DGAC (mm)	Aggregate Base (mm)
586RF over 567RF	MB15-G	46	83	352
587RF over 568RF	RAC-G	48	82	349
588RF over 569RF	AR4000-D	95	88	337
589RF over 571RF	MB4-G (45 mm)	49	79	352
590RF over 572RF	MB4-G (45 mm)	86	83	349
591RF over 573RF	MAC15-G	46	77	337

3.2. Section Characterization

Each underlying section and corresponding overlay is discussed in Sections 3.2.1 through 3.2.6. Each data point discussed or illustrated is an average of the three FWD drops on each point. In all sections, it was noted that the asphalt concrete modulus was generally higher at both ends of the HVS test section. This was attributed to load reduction during the direction change of the test wheel carriage. Data from Stations 0 through 1 and Stations 14 through 16 were therefore excluded from the analysis.

On all sections excluding Section 591, the back-calculated moduli of the asphalt concrete and the aggregate base varied considerably along the section. To account for this variation in the analysis and to simplify reporting, the other five test sections were subdivided into two subsections as follows. Subdivision based purely on variation was not considered necessary.

- Subsection A: Stations 2 through 8
- Subsection B: Stations 8 through 14.

In this study the underlying layer and overlay were considered as a single layer in all analyses to account for the similarity in stiffnesses and to account for the depth of measurement of the FWD sensors in the backcalculation process.

3.2.1 Sections 567RF and 586RF: MB15-G

The backcalculated moduli for the three pavement layers on Sections 567RF and 586RF are presented in Figure 3.1 through Figure 3.9.

Asphalt Concrete

The asphalt concrete modulus of Section 586RF was generally higher than that of Section 567RF (Figure 3.1 and Figure 3.2). This was expected because the overlay modulus is a composite of the overlay and underlying DGAC layer, which was extensively cracked during Phase 1 HVS loading. Variation of the overlay modulus in Figure 3.1 and Figure 3.2 was attributed to temperature change, binder aging, and HVS loading. Temperature had a significant effect on the asphalt concrete modulus, which complicates the analysis of time and seasonal effects (Figure 3.3). Based on the data measured in the trafficked area after overlay construction (June 25, 2003) and before HVS testing on the section started (April 28, 2006) modulus increased from 2,282 MPa to 2,572 MPa on Subsection A, and from 2,516 MPa to 4,135 MPa on Subsection B, indicating an aging effect during the first 30 months after overlay construction. Modulus of the composite asphalt concrete layer in the trafficked area showed little difference from that in the untrafficked area before the HVS testing, but dropped significantly (approximately 50 percent) after HVS testing, illustrating the damage caused to the asphalt concrete layer by HVS loading.

Aggregate Base

The backcalculated modulus of the base changed between 1,000 and 4,000 MPa during the course of the study (Figure 3.4 through Figure 3.6). Much of the strength is attributed to recementation of the recycled concrete aggregate particles used in the base material (12). Temperature also affected the base modulus (Figure 3.6) but to a lesser extent compared to the asphalt concrete layers, with trends indicating that lower temperatures corresponded to higher base modulus. This could be due to the change of confinement

provided to the base by the asphalt concrete layer. A simple comparison of the aggregate base modulus before and after construction of the overlay illustrates the confinement effect. The base modulus after overlay construction (i.e., additional confinement) was generally higher than that before the overlay was placed. Apart from the temperature and overlay effects, the base modulus also tended to increase with time, particularly in the first two years after construction when recementation of the particles occurred. The base modulus in the trafficked area showed significant reduction (around 60 percent) after HVS loading, while the modulus in the untrafficked area showed little change.

Subgrade

The backcalculated modulus of the subgrade was relatively stable along the section (Figure 3.7 and Figure 3.8) and varied between 150 MPa and 350 MPa during the course of the study. Some temperature effects on the subgrade modulus were observed (Figure 3.9). Lower temperatures corresponded to higher subgrade modulus, which was attributed to the stiffening of the asphalt concrete and base layers at lower temperatures, which in turn reduced the level of stress on the subgrade (the modulus of cohesive subgrade typically increases with the reduction of stress level). The subgrade modulus increased with time in the first two years after construction and then stabilized, following a similar trend to the base modulus. Recementation of the base materials probably influenced the subgrade modulus in terms of increased confinement. The subgrade modulus in both the trafficked and untrafficked areas showed little change after HVS loading.

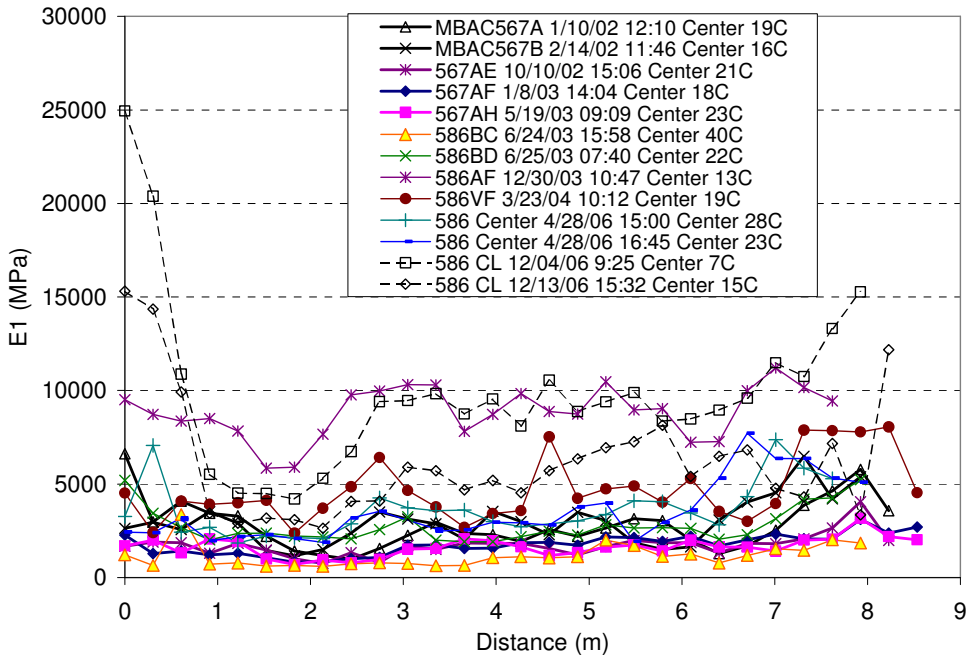

Figure 3.1: Modulus of asphalt concrete from FWD on Section 567RF/586RF (MB15-G)(center).

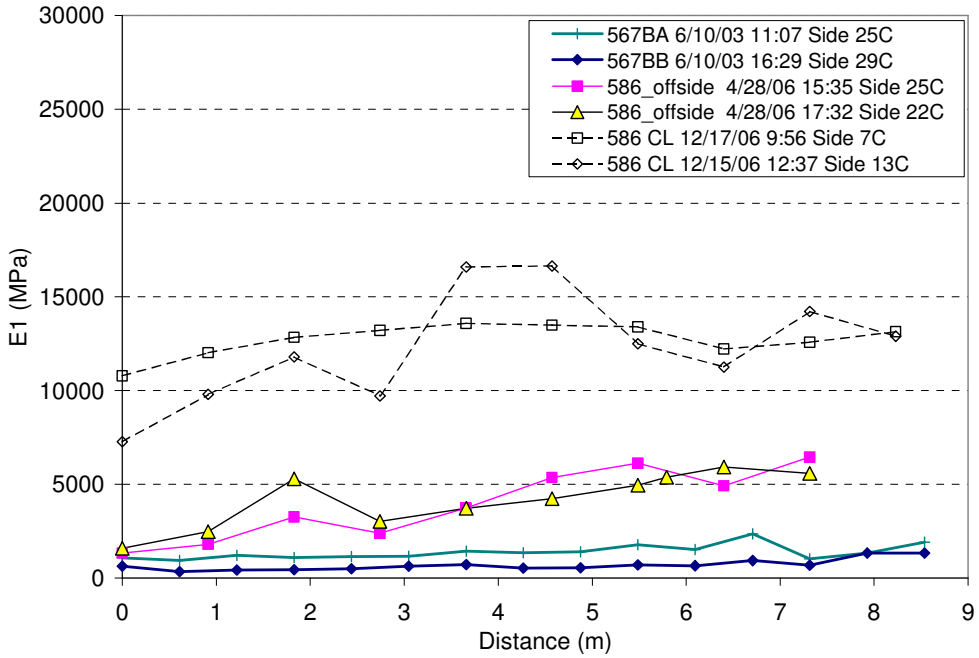

Figure 3.2: Modulus of asphalt concrete from FWD on Section 567RF/586RF (side).

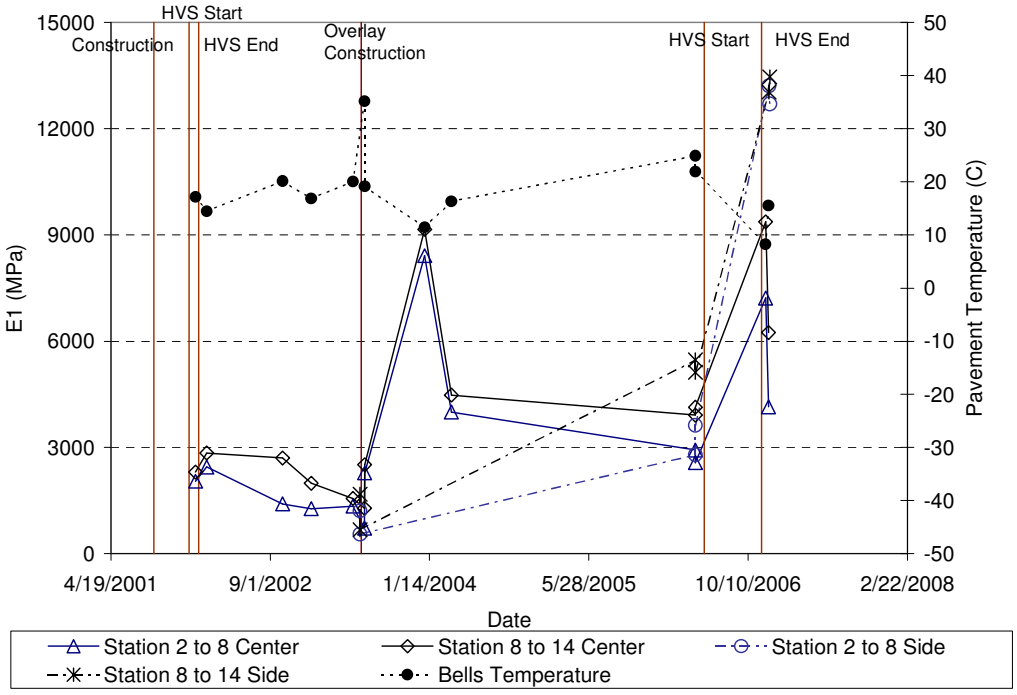

Figure 3.3: Modulus of asphalt concrete from FWD versus time on Section 567RF/586RF.

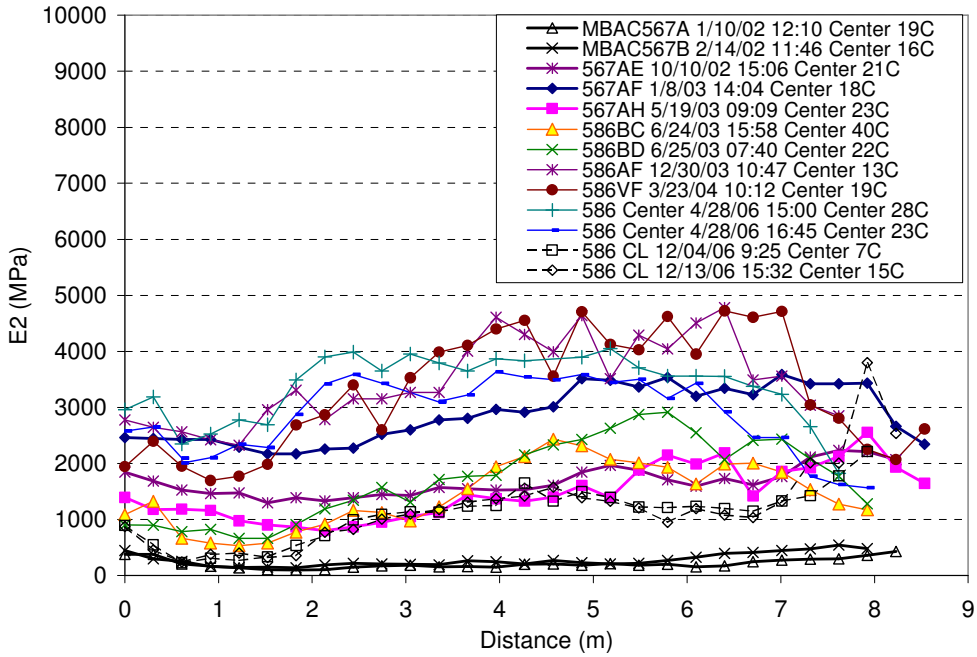

Figure 3.4: Modulus of aggregate base from FWD on Section 567RF/586RF (center).

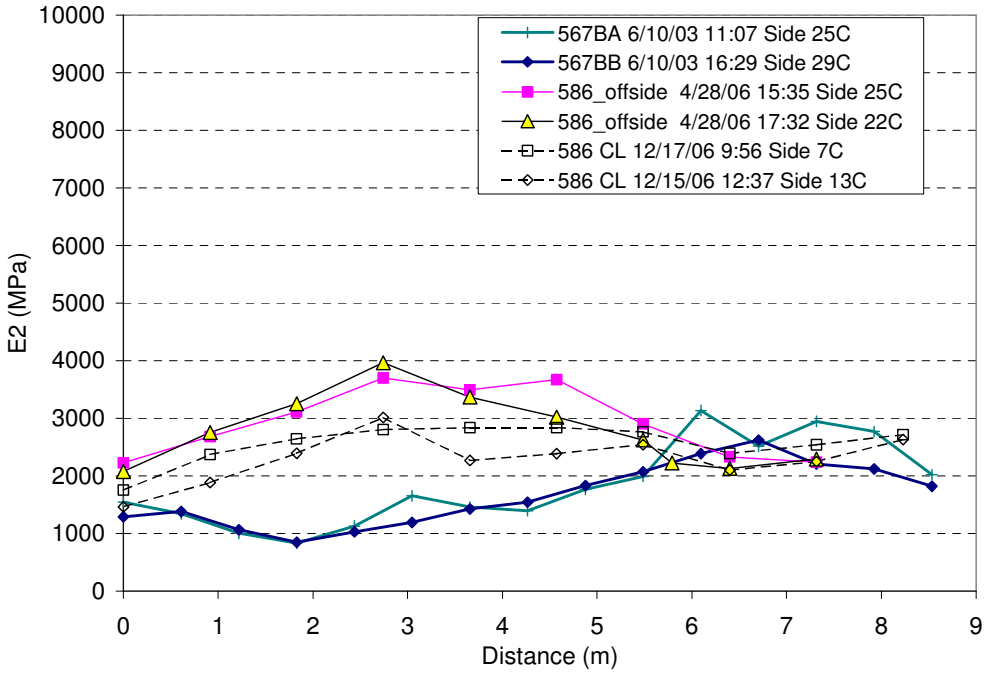

Figure 3.5: Modulus of aggregate base from FWD on Section 567RF/586RF (side).

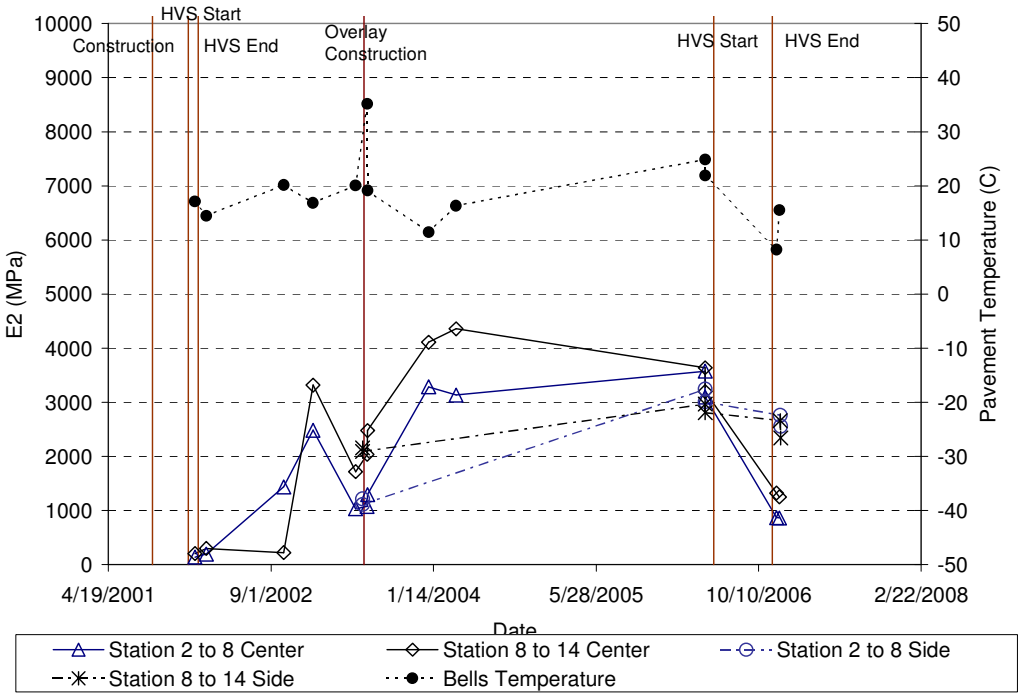

Figure 3.6: Modulus of aggregate base from FWD versus time on Section 567RF/586RF.

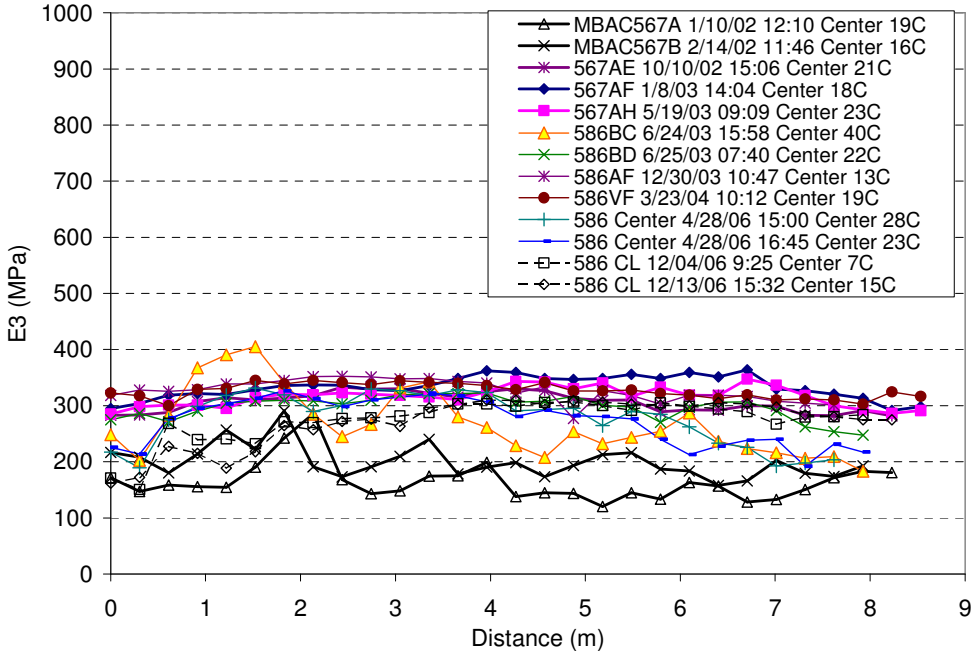

Figure 3.7: Modulus of subgrade from FWD on Section 567RF/586RF (center).

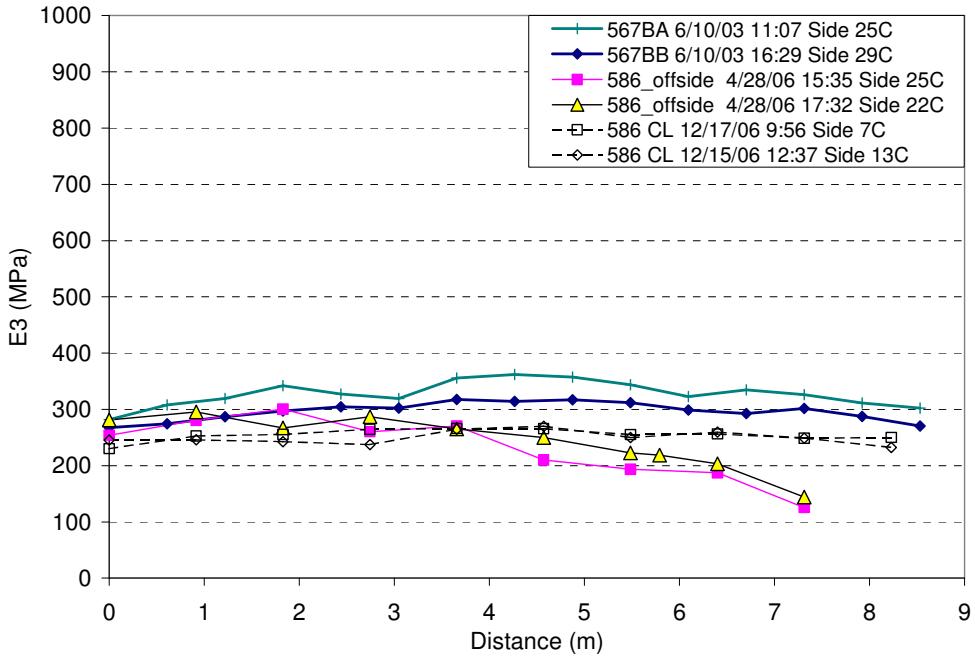

Figure 3.8: Modulus of subgrade from FWD on Section 567RF/586RF (side).

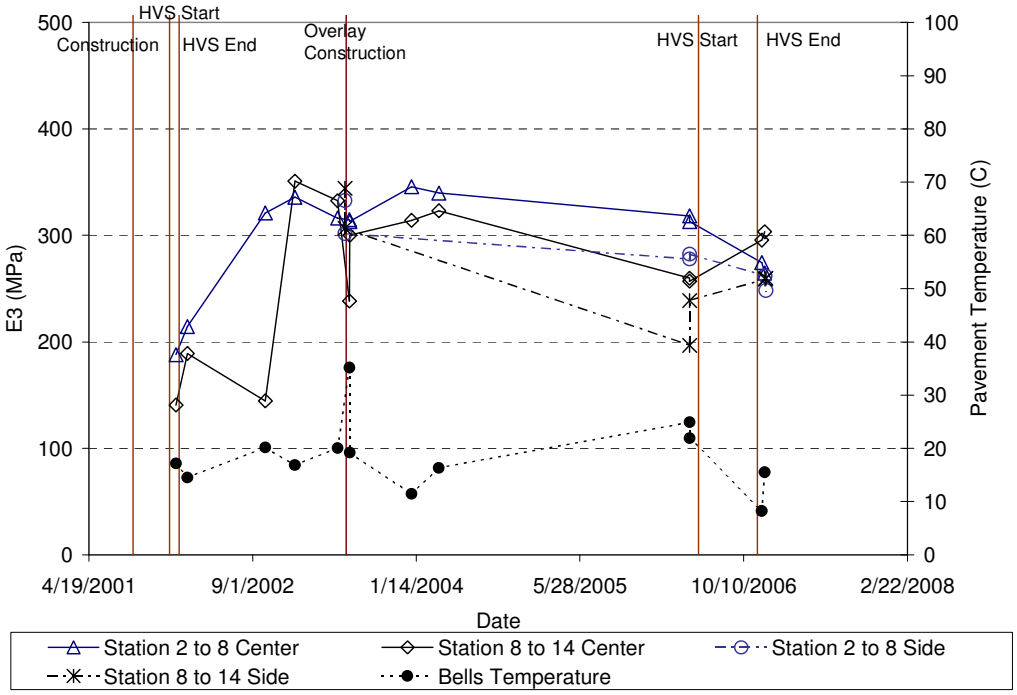

Figure 3.9: Modulus of subgrade from FWD versus time on Section 567RF/586RF.

3.2.2 Sections 568RF and 587RF: RAC-G

The backcalculated moduli for the three pavement layers on Sections 568RF and 587RF are presented in Figure 3.10 through Figure 3.18.

Asphalt Concrete

The asphalt concrete modulus varied significantly with time, generally in a range of 1,000 MPa to 10,000 MPa in the trafficked area and 1,000 MPa to 14,000 MPa in the untrafficked area (Figure 3.10 and Figure 3.11). Temperature had a significant effect on the asphalt concrete modulus (Figure 3.12). Based on the data measured in the trafficked area after overlay construction (June 25, 2003) and before HVS testing on the section started (February 18, 2005), modulus increased from 3,696 MPa to 7,310 MPa on Subsection A, and from 3,807 MPa to 8,171 MPa on Subsection B), indicating the effect of aging during the first 20 months after overlay construction. Modulus of the composite asphalt concrete layer in the trafficked area showed little difference from that in the untrafficked area before the HVS test, but dropped significantly (approximately 70 percent) after the HVS test.

Aggregate Base

The backcalculated modulus of the base changed significantly with time (Figure 3.13 and Figure 3.14) and was generally lower between Stations 2 and 8 than between Stations 8 and 14. In the untrafficked areas, the base on Sections 568RF/587RF (500 MPa to 2,000 MPa) was generally weaker than the base in the corresponding area on Sections 567RF/586RF (1,000 MPa to 4,000 MPa). The trend of variation with time of the base modulus (Figure 3.15) was similar to that observed on Sections 567RF/586RF. Modulus increases were again attributed to recementation of the base material. Modulus increased in the trafficked area from about 100 MPa after Phase 1 HVS testing to about 1,700 MPa before Phase 2 HVS testing, a period of about three years. At the end of Phase 2 HVS loading, the base modulus in the trafficked area had dropped to about 300 MPa. Reduced confinement from the damaged asphalt concrete layer and destruction of the cemented bonds between aggregate particles were identified as the probable causes of this modulus reduction. This observation was supported by little change in the base modulus in the untrafficked area. Temperature had a slight affect, with lower temperatures corresponding to higher modulus. This was consistent with the findings from Sections 567RF/586RF.

Subgrade

The backcalculated modulus of the subgrade under the trafficked test section varied in a similar pattern to that observed on the base (Figure 3.16 and Figure 3.17). Modulus ranged between 50 MPa and 330 MPa in the untrafficked area, which was generally lower than the subgrade modulus in the corresponding area on Sections 567RF/586RF (200 MPa to 350 MPa). Modulus appeared to be affected by HVS loading

(Figure 3.18), with modulus in the trafficked area of Subsection A dropping from 170 MPa to 140 MPa during Phase 1 HVS testing, then increasing to about 250 MPa between tests, before finally dropping to about 100 MPa after Phase 2 testing. The subgrade modulus of Subsection B followed a similar trend but with higher values. Changes were attributed to changes in the overlying base. The subgrade modulus in the untrafficked area was relatively stable over time, with generally lower values than the modulus in the trafficked area.

3.2.3 Sections 569RF and 588RF: AR4000-D

The backcalculated moduli for the three pavement layers on Sections 569RF and 588RF are presented in Figure 3.19 through Figure 3.27.

Asphalt Concrete

The asphalt concrete modulus varied significantly with time, generally in a range of 700 MPa to 13,000 MPa in the trafficked area and 500 MPa to 15,000 MPa in the untrafficked area. As with the other sections, temperature had a significant effect on the asphalt concrete modulus (Figure 3.21). Based on the data measured in the trafficked area after overlay construction (June 25, 2003) and before HVS testing on the section started (October 19, 2005), modulus increased from 5,000 MPa to 8,400 MPa on Subsection A, and from 4,000 MPa to 6,900 MPa on Subsection B. Modulus of the composite asphalt concrete layer in the trafficked area showed little difference from that in the untrafficked area before the HVS test, but showed a significant reduction (approximately 80 percent) after the HVS test.

Aggregate Base

A clear trend in the backcalculated base modulus was observed along the section with higher values between Stations 2 and 8 than between Stations 8 and 14 (Figure 3.22 and Figure 3.23). This is consistent with the measurements after construction (3). The untrafficked base was generally weaker (100 to 1,400 MPa) compared to that on Sections 567RF/586RF (1,000 to 4,000 MPa). Trends in the base modulus over time (Figure 3.24) were similar to those observed on Sections 567RF/ 586RF and Sections 568RF/ 587RF. After Phase 1 HVS testing, the base modulus increased significantly over time to about 1,200 MPa, but had dropped to 200 MPa after Phase 2 testing. Modulus showed little change in the untrafficked area. Temperature had minimal affect on the base modulus.

Subgrade

The backcalculated modulus of the subgrade also varied along the section in a similar pattern to the base (Figure 3.25 and Figure 3.26). Moduli in the untrafficked area ranged between 50 MPa and 180 MPa, which was generally lower than that recorded on Sections 567RF/586RF (200 MPa to 350 MPa). The

modulus mirrored trends in the base (Figure 3.27) but with smaller variation (100 MPa and 200 MPa at 20°C). Temperature and HVS loading had a minor effect on the subgrade modulus.

3.2.4 Sections 571RF and 589RF: 45 mm MB4-G

The backcalculated moduli for the three pavement layers on Sections 571RF and 589RF are presented in Figure 3.28 through Figure 3.36.

Asphalt Concrete

The asphalt concrete modulus varied significantly with time, generally in a range of 800 MPa to 9,000 MPa in the trafficked area and 1,000 MPa to 12,000 MPa in the untrafficked area. Variance of the backcalculated asphalt concrete modulus before overlay construction (Section 571RF) was significantly larger than that after overlay construction (Section 589RF), probably due the thickness of the underlying DGAC layer (about 80 mm) being close to the recommended minimum value for appropriate backcalculation of 75 mm (half the radius of the FWD loading plate). Phase 1 HVS testing did not appear to have a significant affect on the underlying DGAC modulus (Figure 3.30), but reduced the moduli of the aggregate base and the subgrade (Figure 3.33 and Figure 3.36). Phase 2 HVS testing started approximately one year after overlay construction, and FWD testing did not indicate any significant aging effect on the asphalt concrete modulus during this period. Measurements at similar temperatures after Phase 2 testing, however, showed an increase in composite asphalt concrete modulus. Modulus in the trafficked area showed small differences from that in the untrafficked area before the HVS test, but showed a significant reduction (around 70 percent) after the HVS test.

Aggregate Base

The aggregate base modulus was relatively uniform along the section (Figure 3.31 and Figure 3.32) and varied between 100 MPa and 800 MPa in the trafficked area, and between 300 MPa and 800 MPa in the untrafficked area over the course of the study. There are two outliers in Figure 3.31, which were backcalculated from FWD tests performed in December 2003. The test data was considered suspect and was excluded from any further analyses. The modulus in the untrafficked area was generally weaker than that in the corresponding area on Sections 567RF/586RF, Sections 568RF/587RF, and Sections 569RF/588RF. The trend of variation with time of the base modulus (Figure 3.33) was similar to that on other sections, dropping from 600 MPa to 300 MPa during Phase 1 testing, then increased continuously over a period of 20 months to about 700 MPa. This value was less than that on Sections 586RF, 587RF, and 588RF. During Phase 2 loading, the aggregate base modulus in the trafficked area dropped back to about 250 MPa, but showed little change in the untrafficked area. After Phase 2

testing, the base modulus increased by about 150 MPa over a two-year period. Some temperature affect was noted, with lower temperatures corresponding to higher modulus.

Subgrade

The backcalculated modulus of the subgrade was lower in Subsection A compared to Subsection B (Figure 3.34 and Figure 3.35). It ranged between and 80 MPa and 260 MPa in the untrafficked area and was generally lower than that on Sections 567RF/586RF, Sections 568RF/587RF, but higher than that on Sections 569RF/588RF. The subgrade modulus followed similar trends to that of the base modulus (Figure 3.36), but with smaller variation (200 MPa and 300 MPa at 20°C). Phase 2 HVS loading appeared to have an effect on the modulus, which was reduced from 220 MPa to 130 MPa during the test.

3.2.5 Sections 572RF and 590RF: 90 mm MB4-G

The backcalculated moduli for the three pavement layers on Sections 572RF and 590RF are presented in Figure 3.37 through Figure 3.45.

Asphalt Concrete

Modulus varied in a range of 500 MPa to 13,000 MPa in the trafficked area and 1,000 MPa to 13,000 MPa in the untrafficked area. Variance of the backcalculated modulus of the underlying DGAC was significantly larger than that after overlay construction, which was again related to the relationship between layer thickness and FWD configuration. Based on the FWD data measured at a pavement temperature of about 18°C, the modulus dropped from about 4,000 MPa to about 3,000 MPa during Phase 1 testing (Figure 3.39), and from about 4,000 MPa to about 2,200 MPa during Phase 2 testing. An aging effect was apparent after Phase 2 testing.

Aggregate Base

Base modulus was consistent along the section (Figure 3.40 and Figure 3.41), but varied from 50 MPa to 1,000 MPa in the trafficked area, and from 80 MPa to 800 MPa in the untrafficked area over the duration of the study. Base modulus in the untrafficked area was comparable to that on Sections 571RF/589RF, and generally weaker than that on Sections 567RF/586RF, Sections 568RF/587RF, and Sections 569RF/588RF. The trend of variation with time of the base modulus (Figure 3.42) was similar to that of the asphalt concrete modulus, increasing from about 600 MPa to 1,100 MPa (measured at 18°C pavement temperature) in the eight months before Phase 1 testing. It dropped to about 100 MPa (measured at 26°C pavement temperature) after Phase 1 testing, increased to about 770 MPa (measured at 5°C pavement temperature) in the nine months between HVS testing, and then dropped again to 270 MPa (measured at 19°C pavement temperature) after Phase 2 testing. The effects of recementation on the

backcalculated modulus were not as apparent as that in Sections 567/586RF, 568/587RF, 569/588RF, and 572/589RF.

Subgrade

The backcalculated modulus of the subgrade was generally lower in Subsection A compared to that in Subsection B (Figure 3.43 and Figure 3.44), ranging between 50 MPa and 140 MPa in the untrafficked area. Results were comparable to those on Sections 569RF/588RF, and generally lower than those on Sections 567RF/586RF, Sections 568RF/587RF, and Sections 571RF/589RF. The subgrade modulus followed a similar trend to that of the base modulus (Figure 3.45), ranging between 180 MPa and 300 MPa before HVS testing, and between 50 MPa and 200 MPa after the testing.

3.2.6 Sections 573RF and 591RF: MAC15-G

The backcalculated moduli for the three pavement layers on Sections 573RF and 591RF are presented in Figure 3.46 through Figure 3.54. This section was analyzed as a single entity and was not subdivided.

Asphalt Concrete

The asphalt concrete modulus varied in the ranges 1,000 MPa to 12,000 MPa in the trafficked area and 1,000 MPa to 15,000 MPa in the untrafficked area. Temperature affected the modulus (Figure 3.48) as expected, but Phase 1 testing did not have a significant influence.

Aggregate Base

The base modulus generally varied from 150 MPa to 2,000 MPa in the trafficked area, and from 500 MPa to 1,500 MPa in the untrafficked area (Figure 3.49 and Figure 3.50), similar to that on Section 569RF/588RF, weaker than that on Sections 567RF/586RF and 568RF/587RF, and stiffer than that on Sections 571RF/589RF and 572RF/590RF. The trend of variation with time of the base modulus (Figure 3.51) was similar to that of the subgrade (Figure 3.54). Recementation effects were not obvious from the backcalculated aggregate base data, although the forensic investigation indicated that relatively strong cementation had occurred (12).

Subgrade

The subgrade modulus was generally uniform along the section (Figure 3.52 and Figure 3.53), ranging between 100 MPa and 150 MPa in the untrafficked area over the duration of the study, comparable to that on Sections 569RF/588RF, 571RF/589RF, and 572RF/590RF, but lower than the subgrade modulus on Sections 567RF/586RF and 568RF/587RF. Modulus ranged between 110 MPa and 280 MPa before Phase 2 testing, and between 50 MPa and 150 MPa after testing.

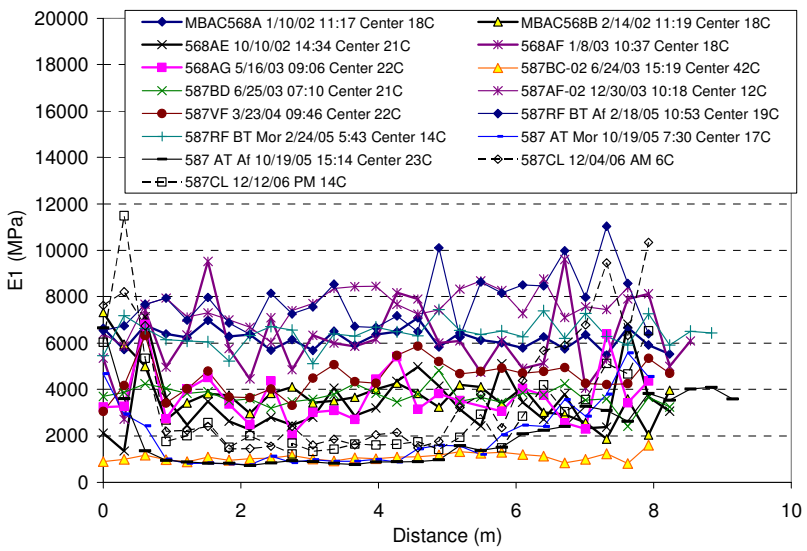

Figure 3.10: Modulus of asphalt concrete from FWD on Section 568RF/587RF (RAC-G)(center).

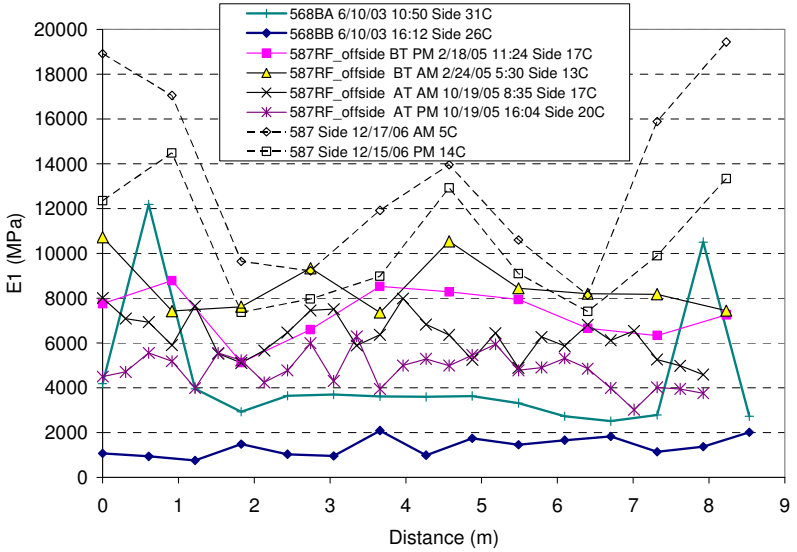

Figure 3.11: Modulus of asphalt concrete from FWD on Section 568RF/587RF (side).

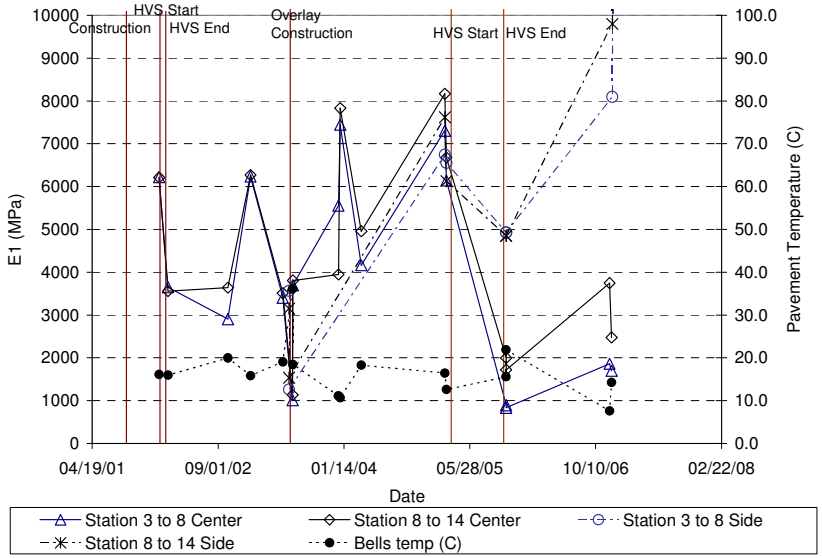

Figure 3.12: Modulus of asphalt concrete from FWD versus time on Section 568RF/587RF.

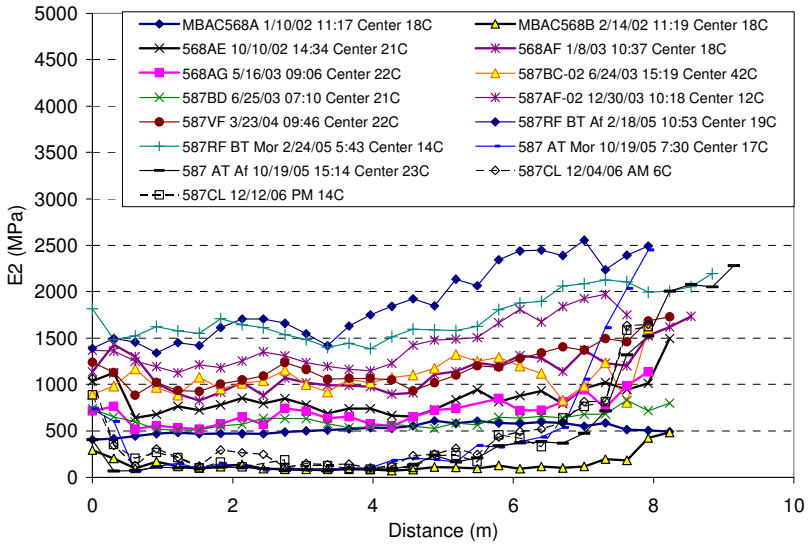

Figure 3.13: Modulus of aggregate base from FWD on Section 568RF/587RF (center).

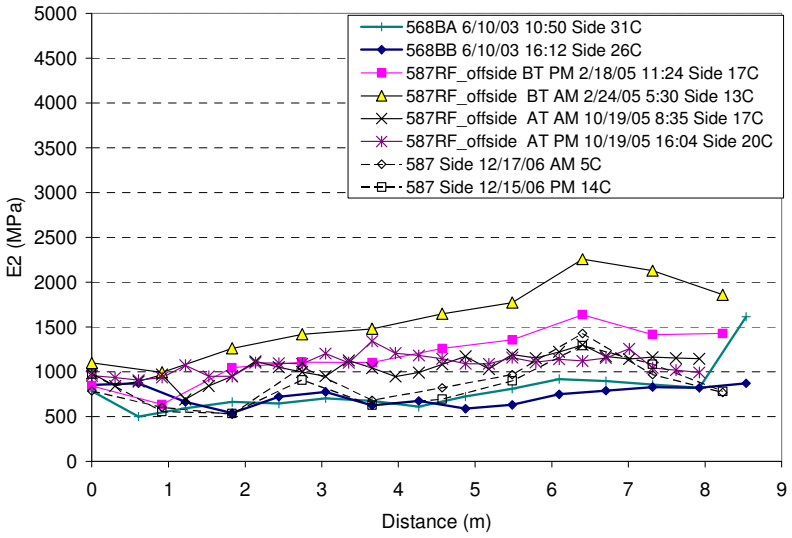

Figure 3.14: Modulus of aggregate base from FWD on Section 568RF/587RF (side).

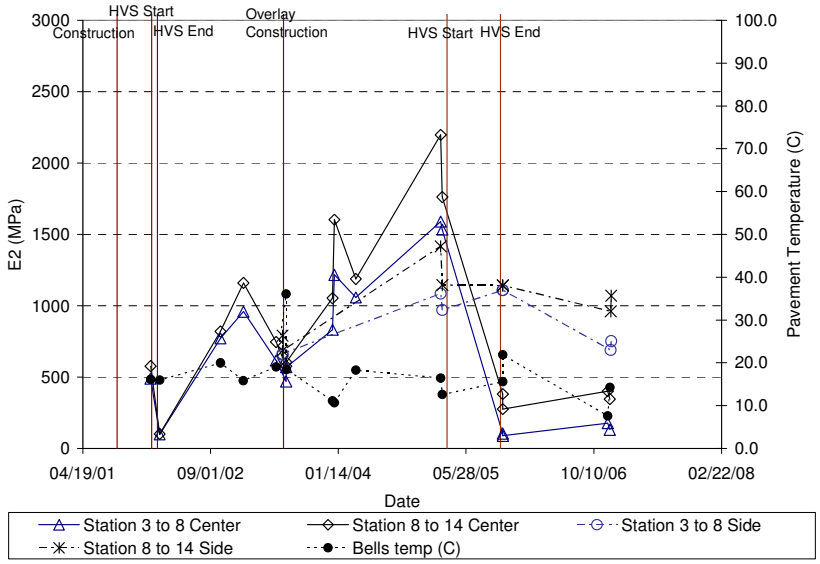

Figure 3.15: Modulus of aggregate base from FWD versus time on Section 568RF/587RF.

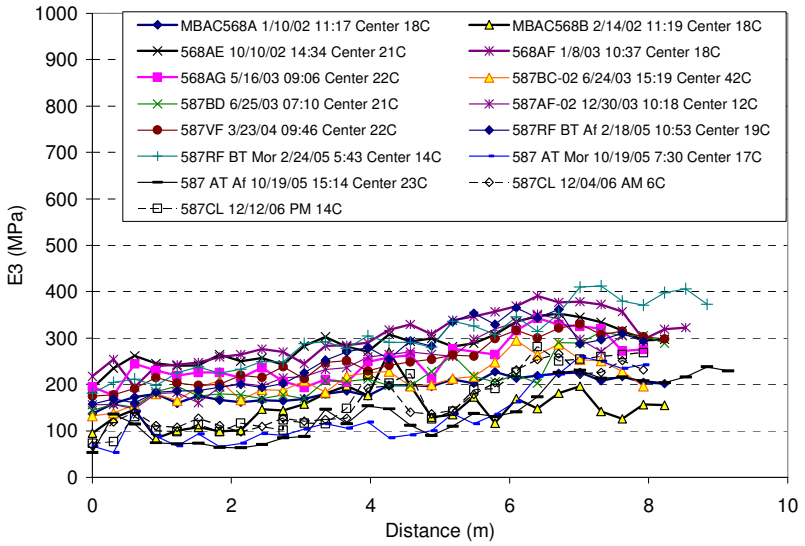

Figure 3.16: Modulus of subgrade from FWD on Section 568RF/587RF (center).

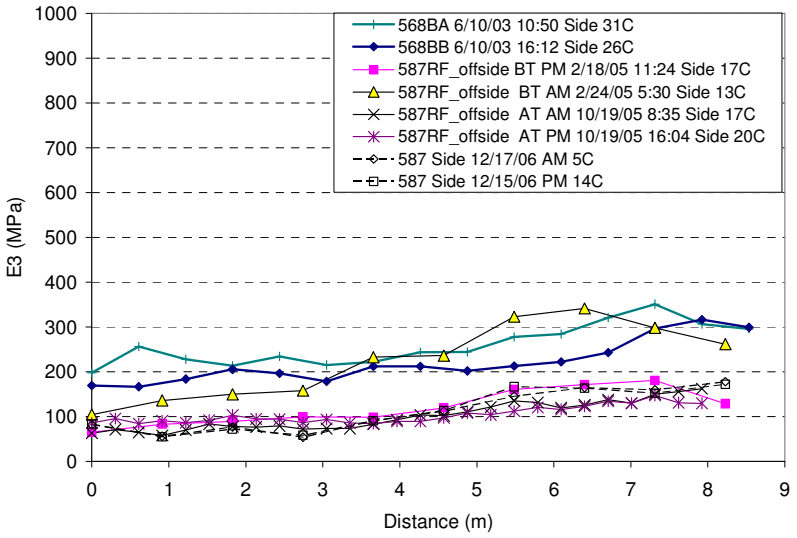

Figure 3.17: Modulus of subgrade from FWD on Section 568RF/587RF (side).

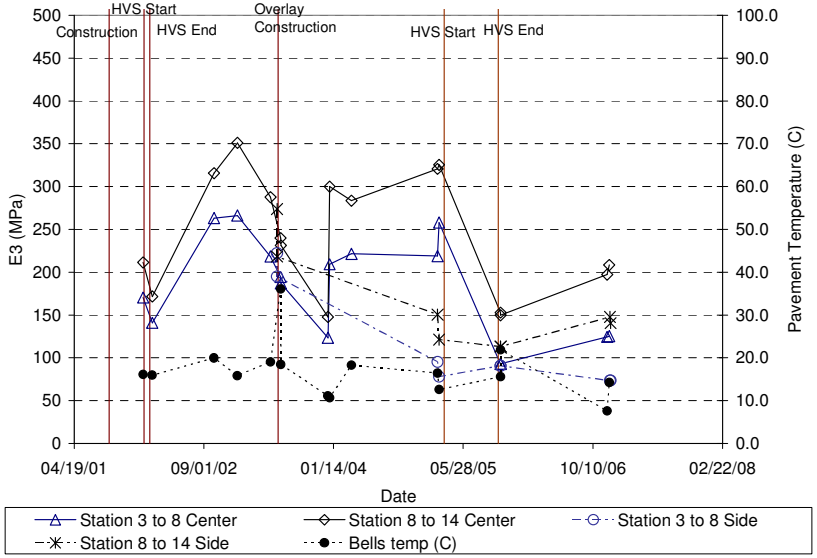

Figure 3.18: Modulus of subgrade from FWD versus time on Section 568RF/587RF.

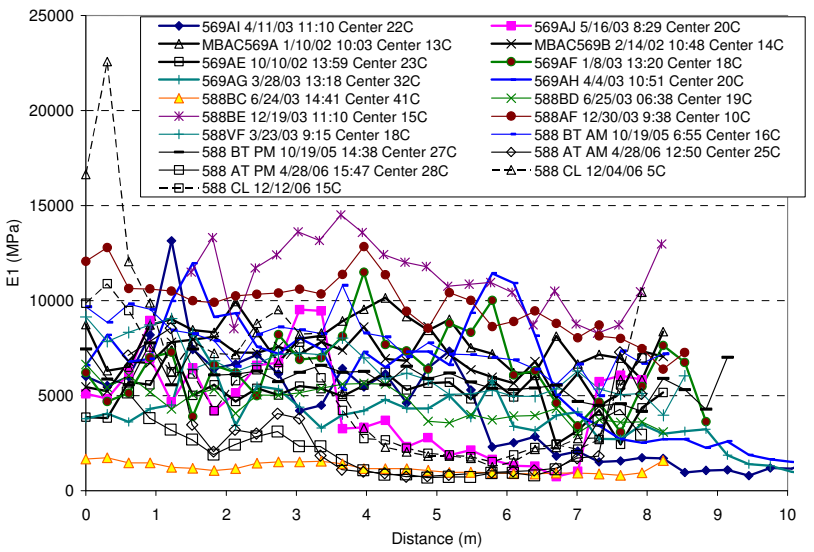

Figure 3.19: Modulus of asphalt concrete from FWD on Section 569RF/588RF (AR4000-D)(center).

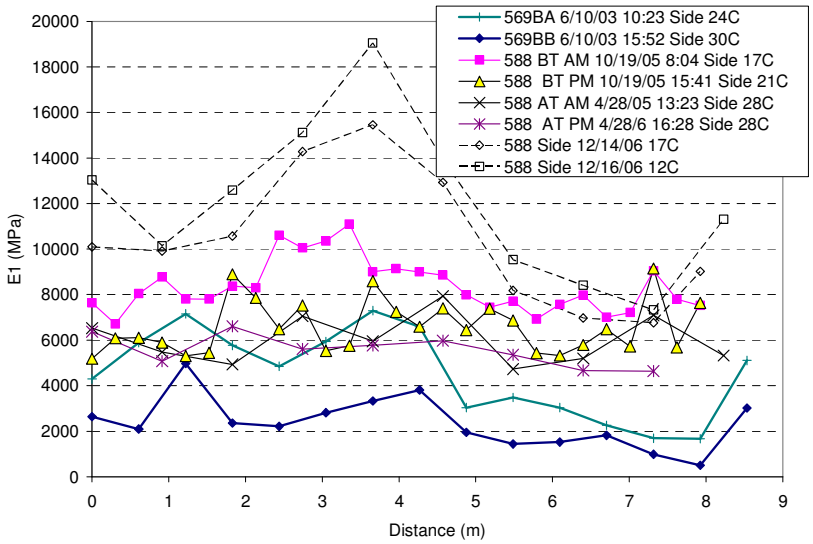

Figure 3.20: Modulus of asphalt concrete from FWD on Section 569RF/588RF (side).

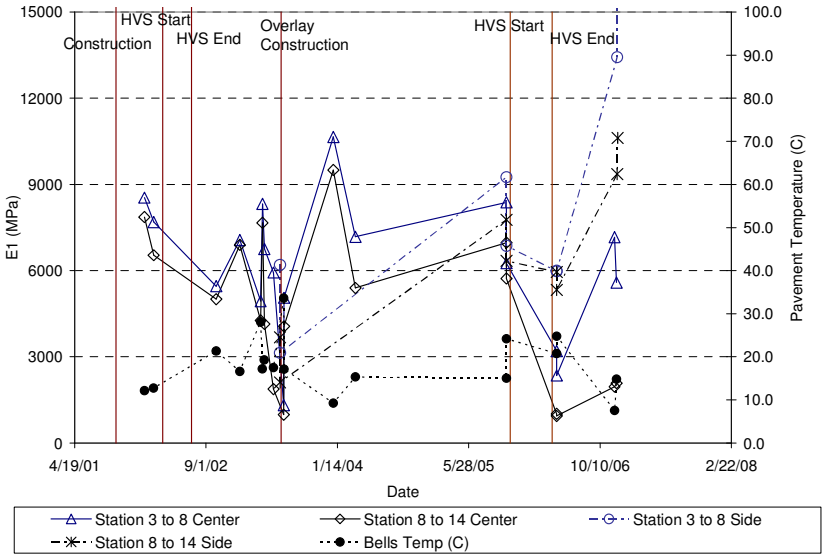

Figure 3.21: Modulus of asphalt concrete from FWD versus time on Section 569RF/588RF.

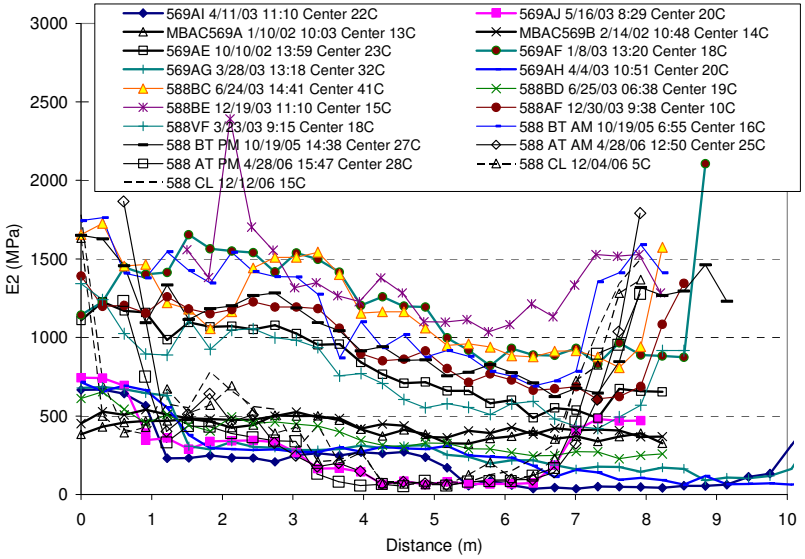

Figure 3.22: Modulus of aggregate base from FWD on Section 569RF/588RF (center).

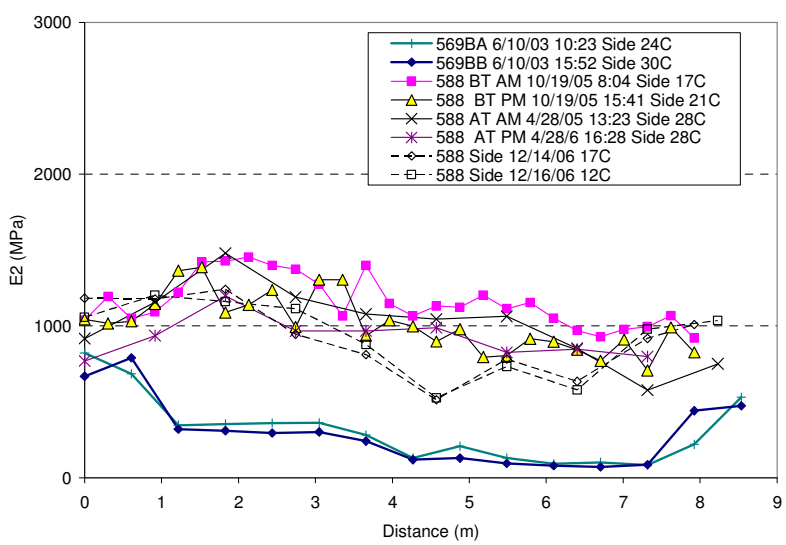

Figure 3.23: Modulus of aggregate base from FWD on Section 569RF/588RF (side).

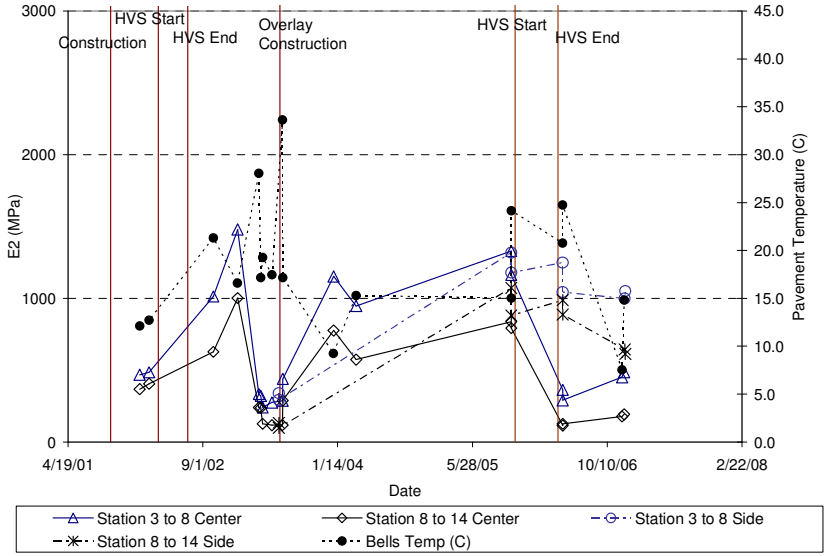

Figure 3.24: Modulus of aggregate base from FWD versus time on Section 569RF/588RF.

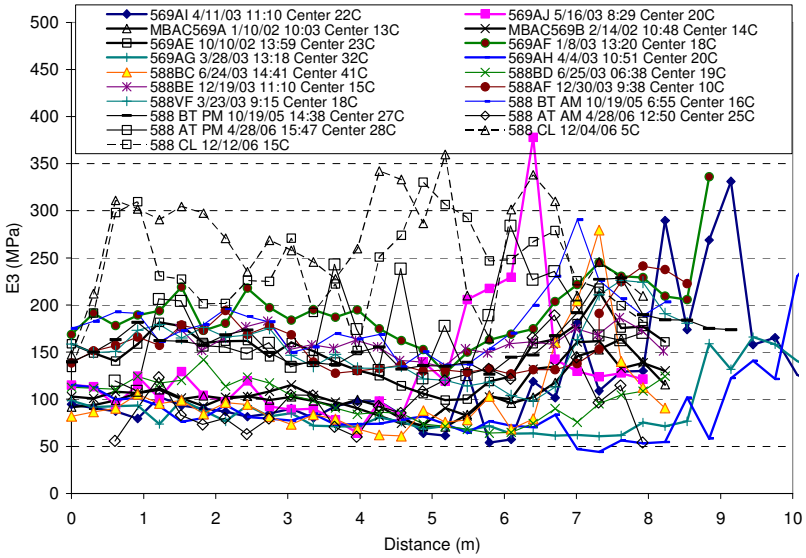

Figure 3.25: Modulus of subgrade from FWD on Section 569RF/588RF (center).

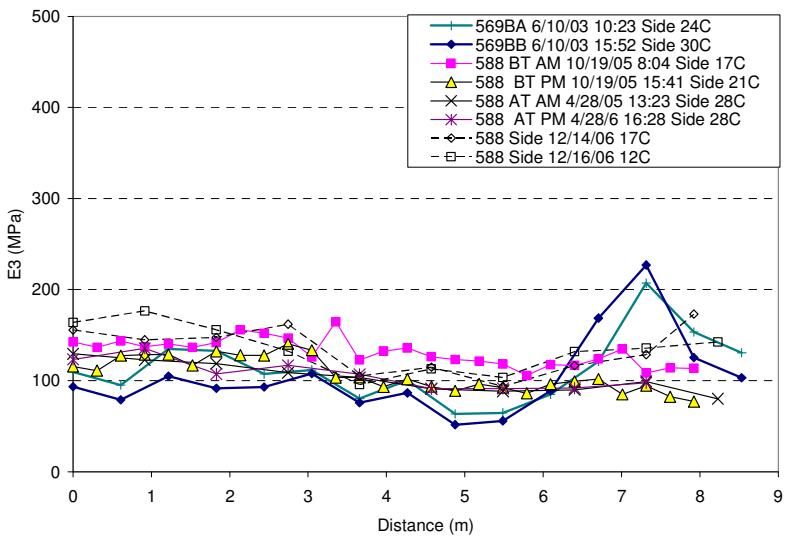

Figure 3.26: Modulus of subgrade from FWD on Section 569RF/588RF (side).

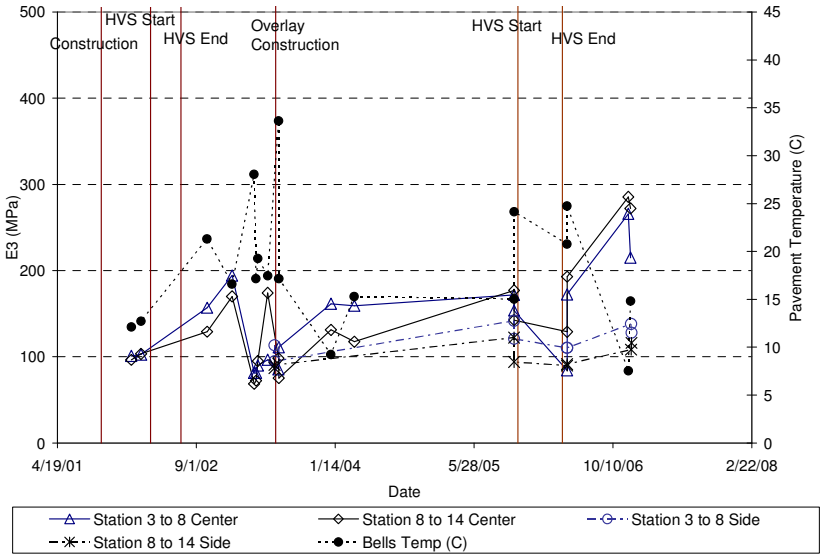

Figure 3.27: Modulus of subgrade from FWD versus time on Section 569RF/588RF.

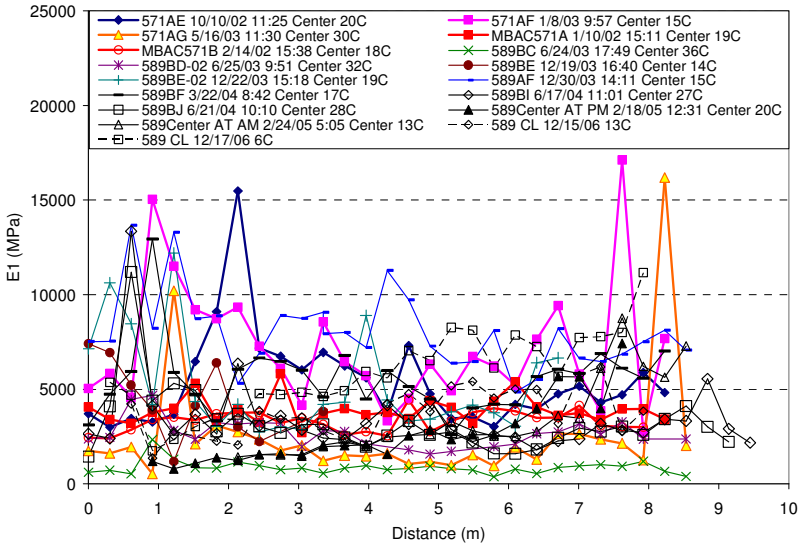

Figure 3.28: Modulus of asphalt concrete from FWD on Section 571RF/589RF (MB4-G-45)(center).

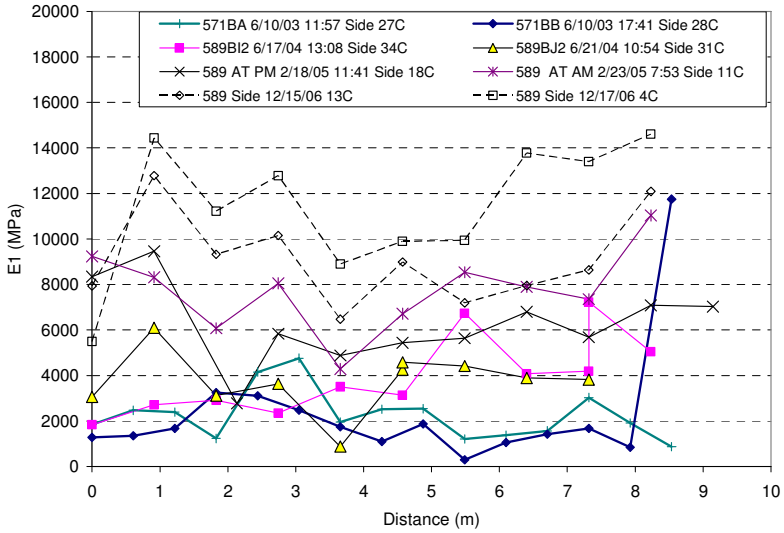

Figure 3.29: Modulus of asphalt concrete from FWD on Section 571RF/589RF (side).

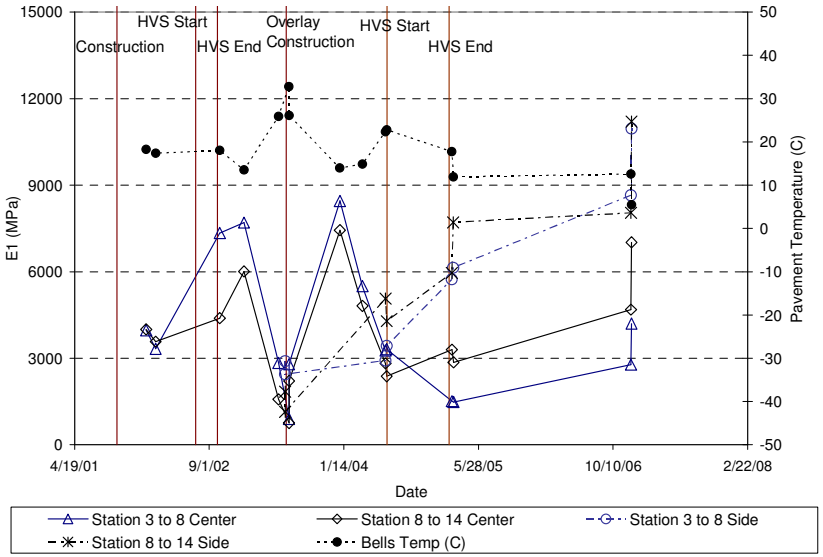

Figure 3.30: Modulus of asphalt concrete from FWD versus time on Section 571RF/589RF.

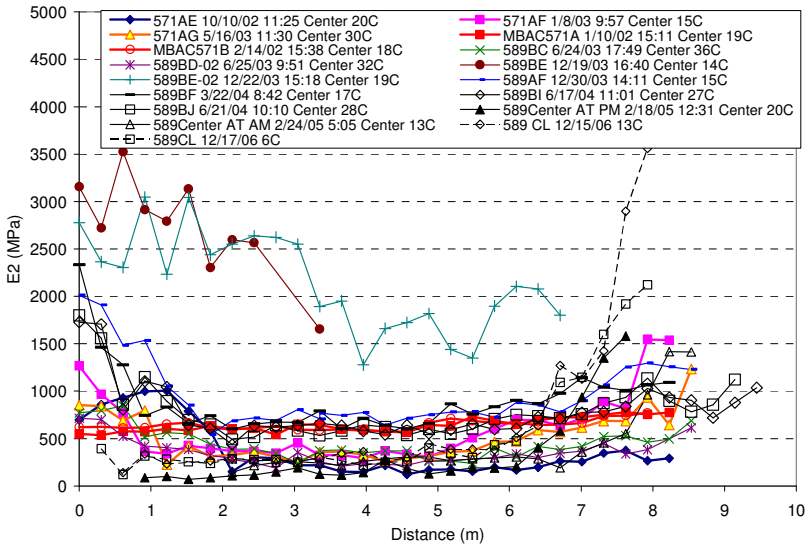

Figure 3.31: Modulus of aggregate base from FWD on Section 571RF589RF (center).

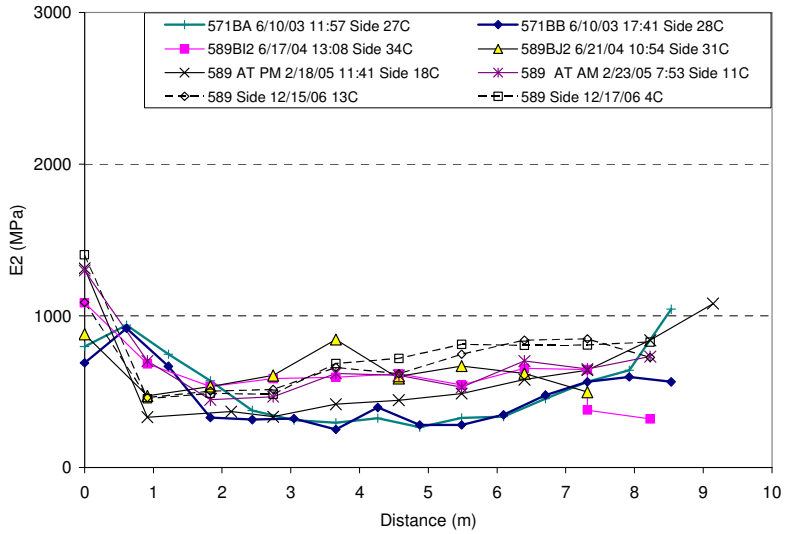

Figure 3.32: Modulus of aggregate base from FWD on Section 571RF/589RF (side).

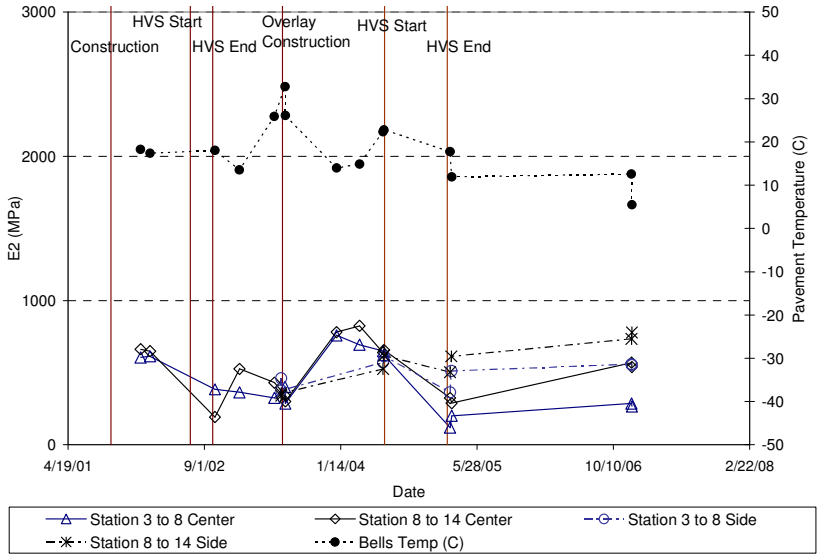

Figure 3.33: Modulus of aggregate base from FWD versus time on Section 571RF/589RF.

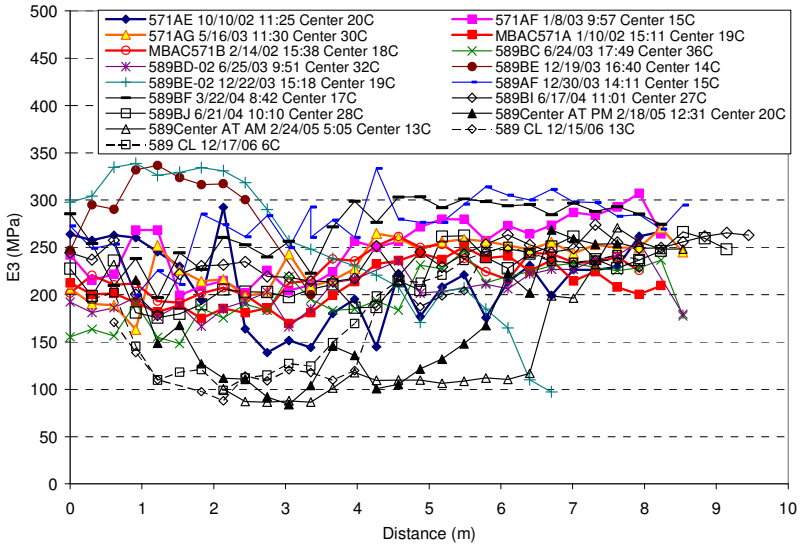

Figure 3.34: Modulus of subgrade from FWD on Section 571RF/589RF (center).

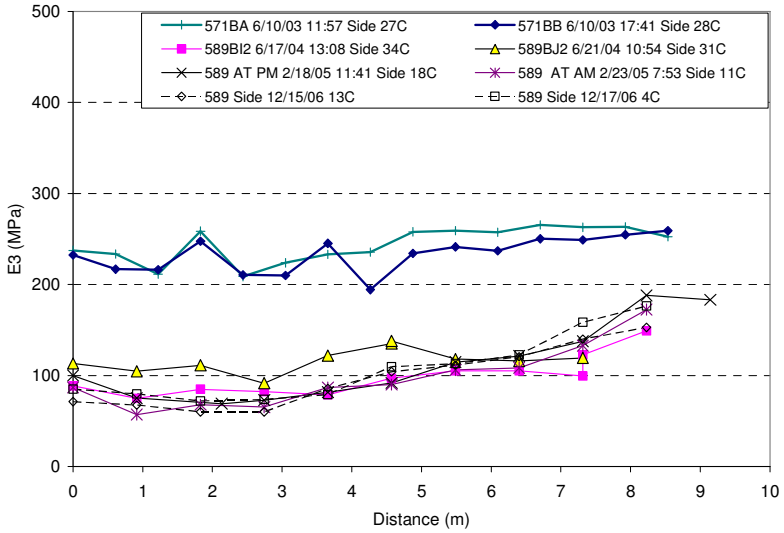

Figure 3.35: Modulus of subgrade from FWD on Section 571RF/and 589RF (side).

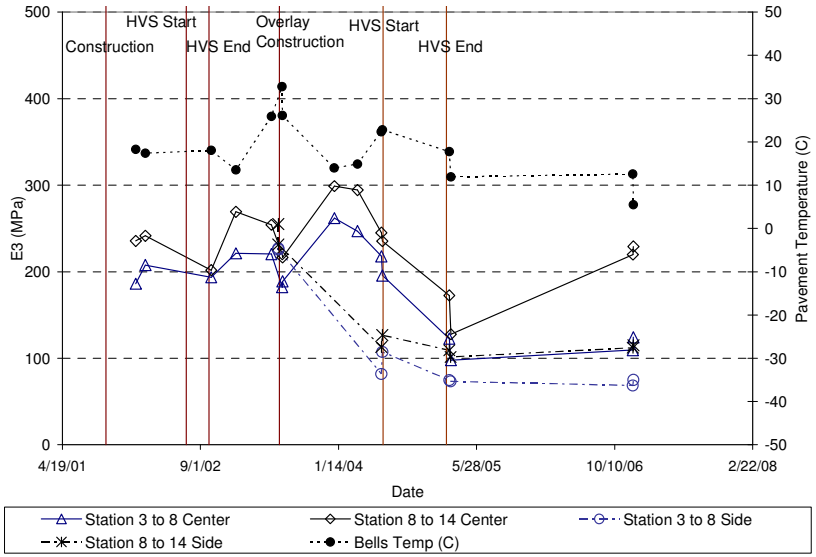

Figure 3.36: Modulus of subgrade from FWD versus time on Section 571RF/589RF.

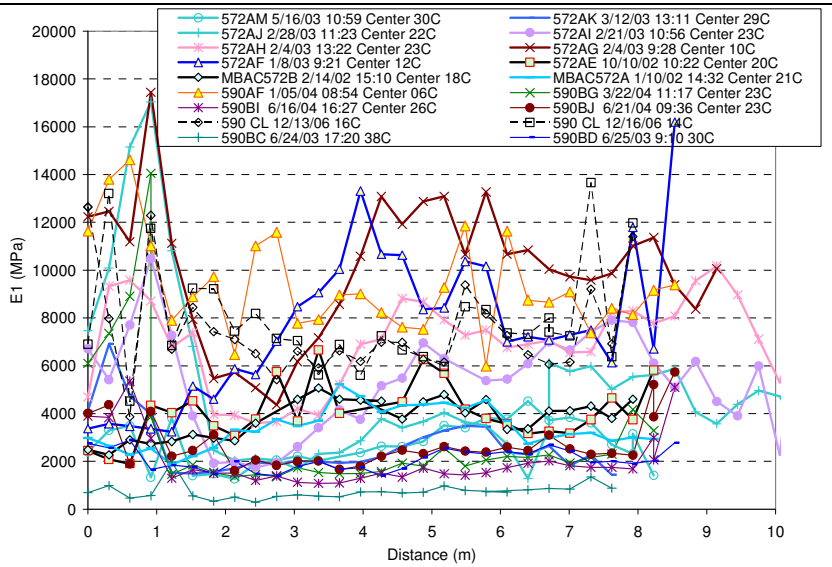

Figure 3.37: Modulus of asphalt concrete from FWD on Section 572RF/590RF (MB4-G-90)(center).

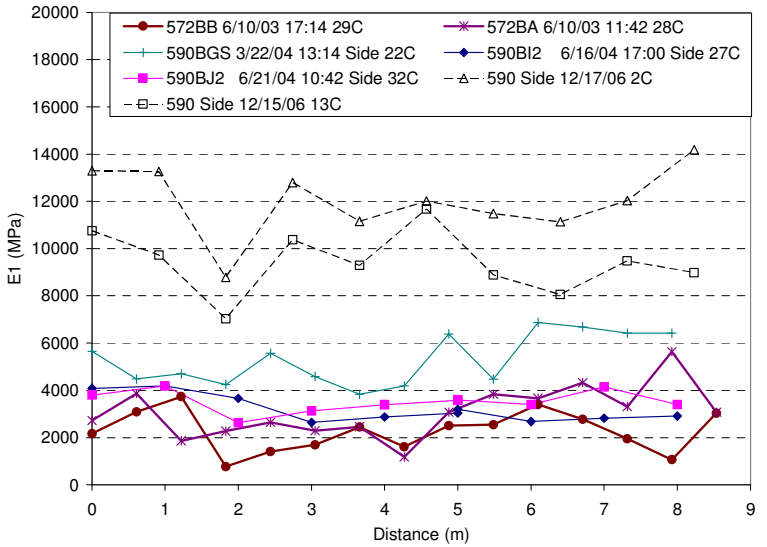

Figure 3.38: Modulus of asphalt concrete from FWD on Section 572RF590RF (side).

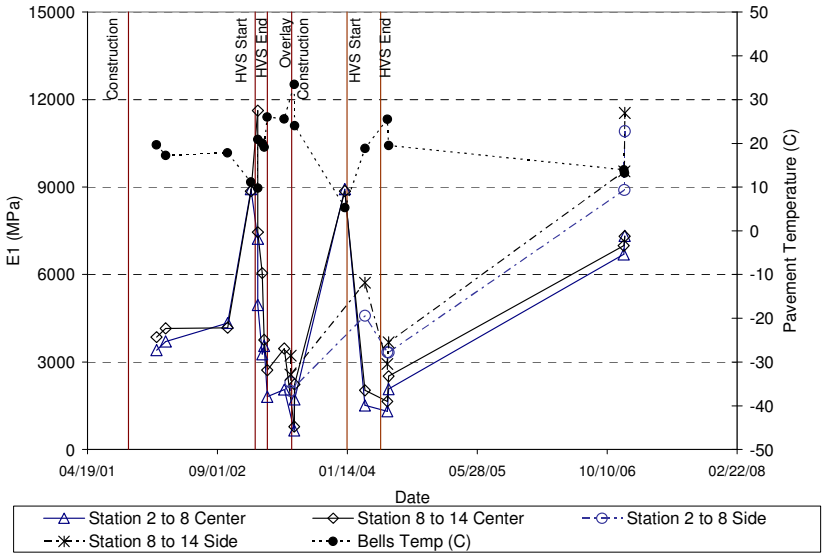

Figure 3.39: Modulus of asphalt concrete from FWD versus time on Section 572RF/590RF.

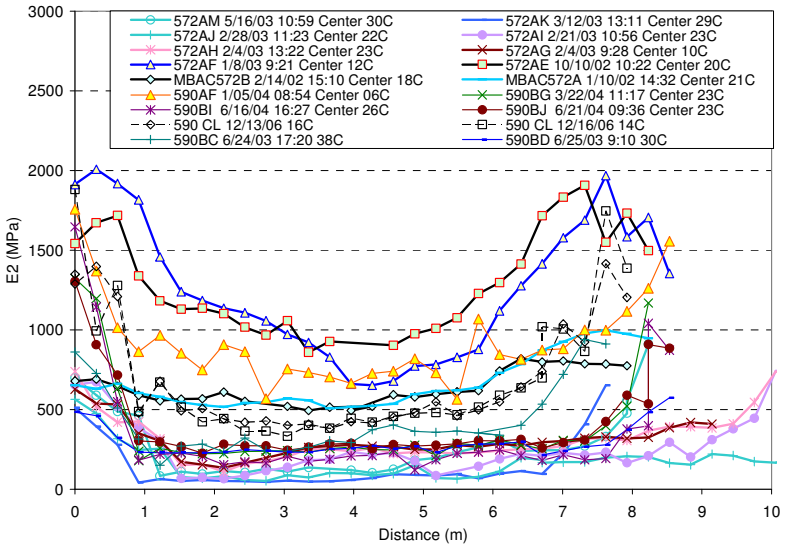

Figure 3.40: Modulus of aggregate base from FWD on Sections 572RF/590RF (center).

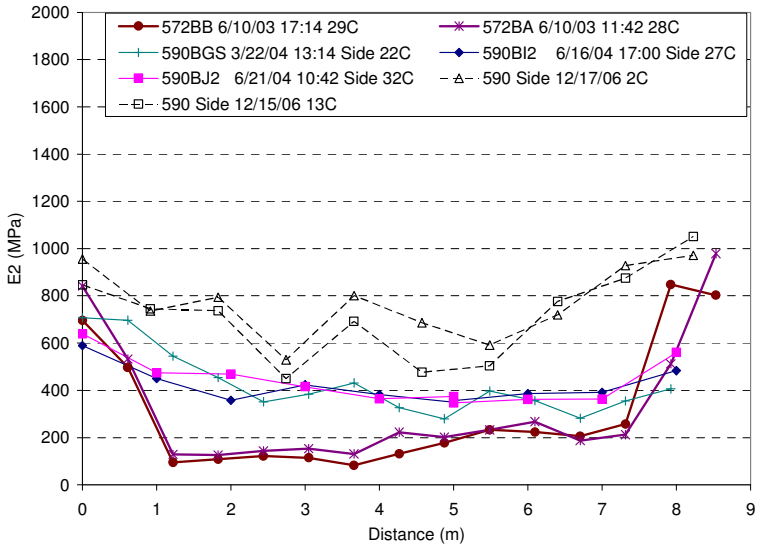

Figure 3.41: Modulus of aggregate base from FWD on Section 572RF/590RF (side).

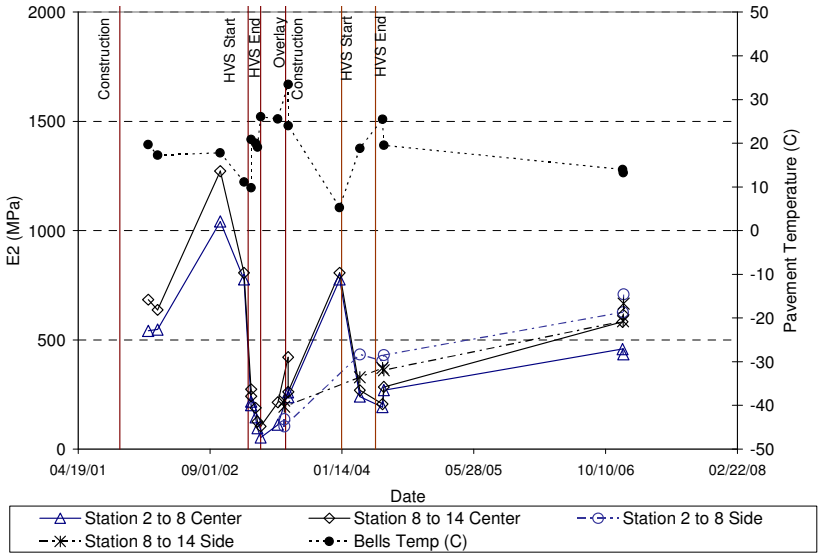

Figure 3.42: Modulus of aggregate base from FWD versus time on Section 572RF/590RF.

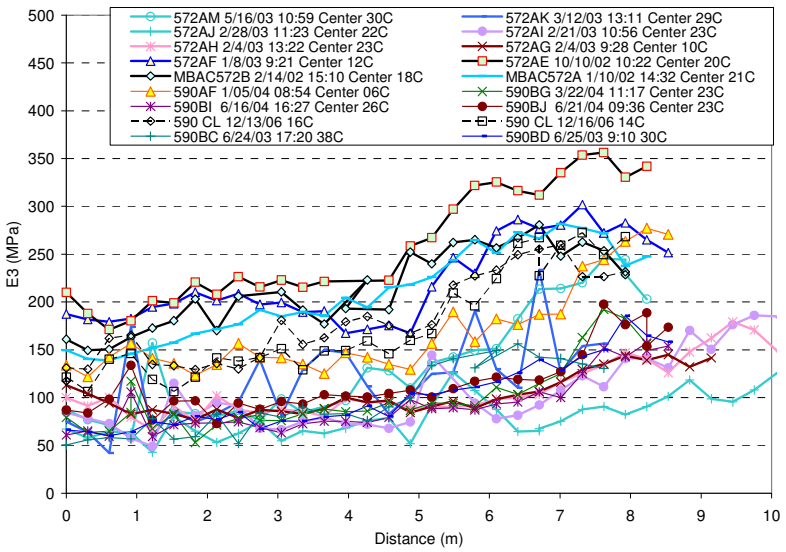

Figure 3.43: Modulus of subgrade from FWD on Section 572RF/590RF (center).

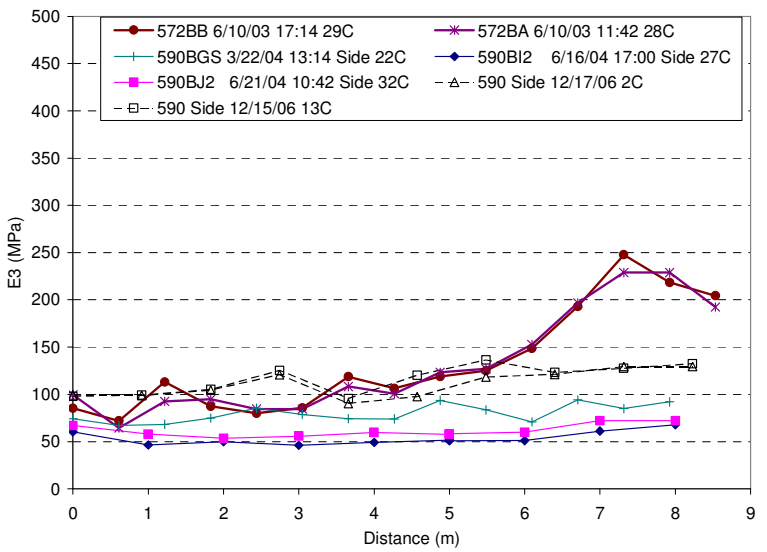

Figure 3.44: Modulus of subgrade from FWD on Section 572RF/590RF (side).

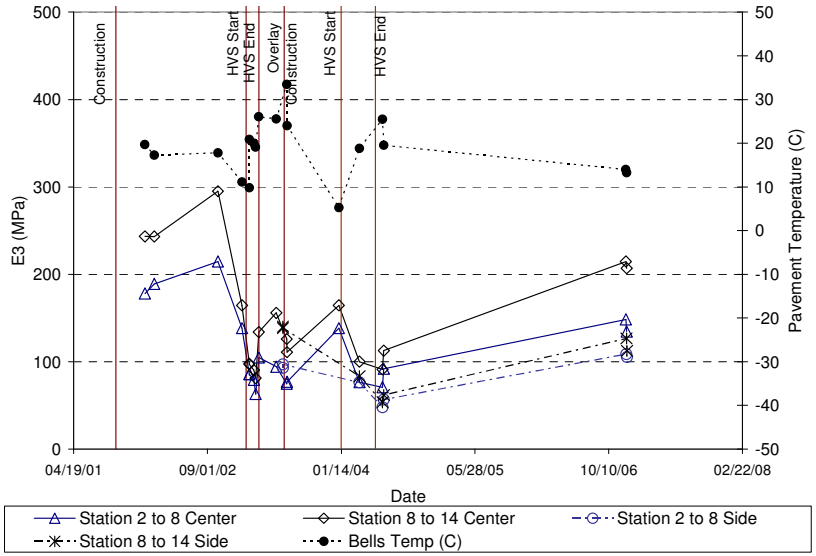

Figure 3.45: Modulus of subgrade from FWD versus time on Section 572RF/590RF.

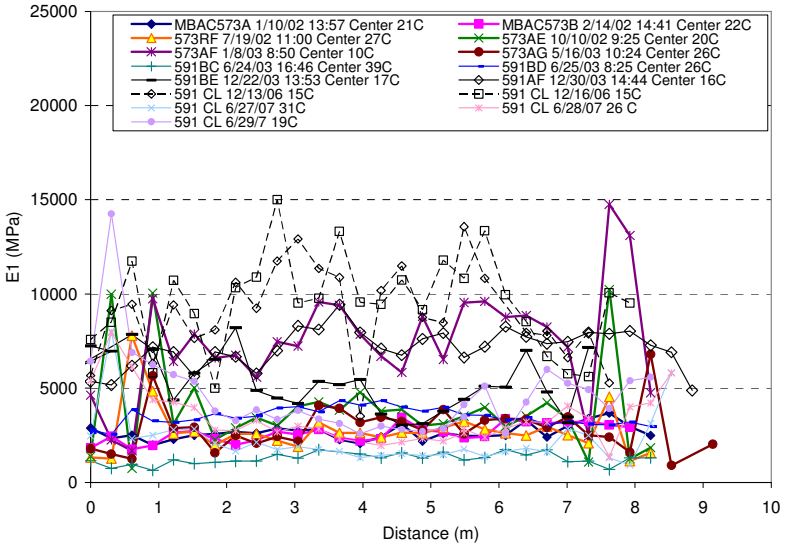

Figure 3.46: Modulus of asphalt concrete from FWD on Section 573RF/591RF (MAC15-G)(center).

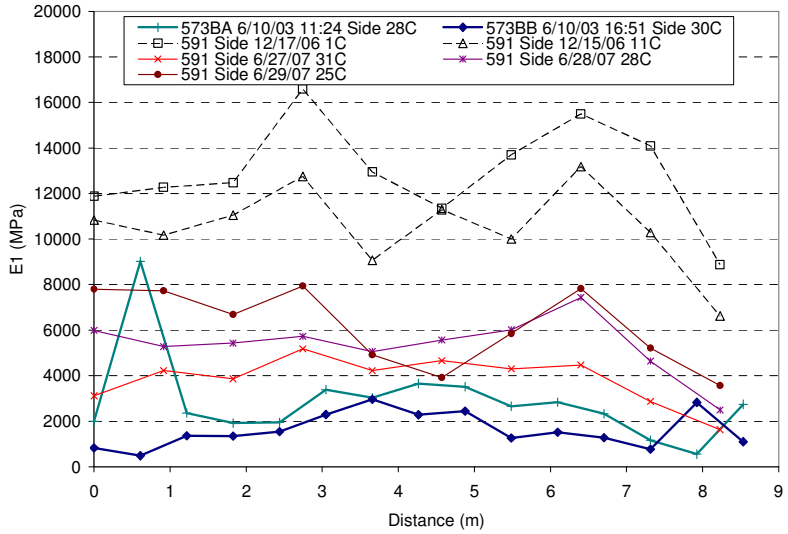

Figure 3.47: Modulus of asphalt concrete from FWD on Section 573RF/591RF (side).

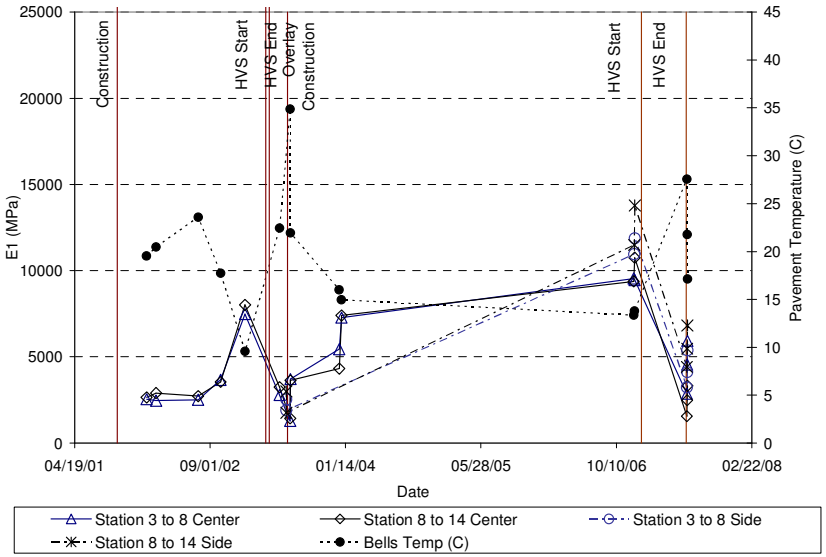

Figure 3.48 Modulus of asphalt concrete from FWD versus time on Section 573RF/591RF.

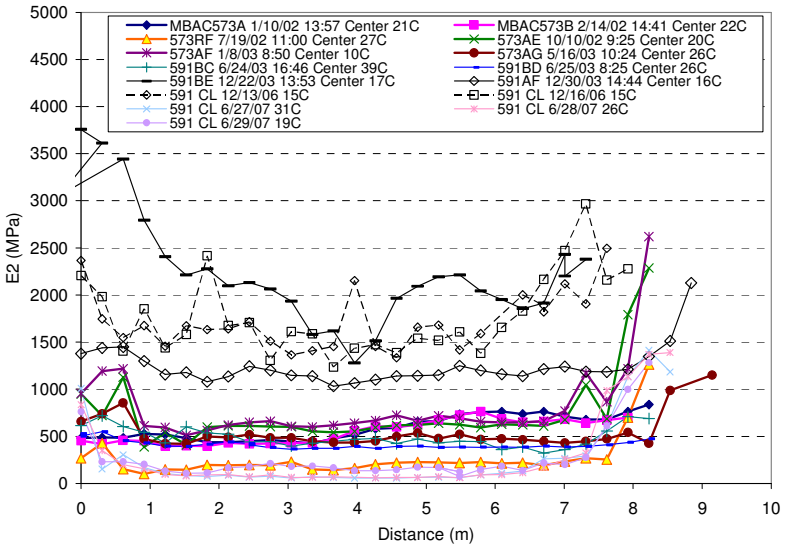

Figure 3.49: Modulus of aggregate base from FWD on Section 573RF/591RF (center).

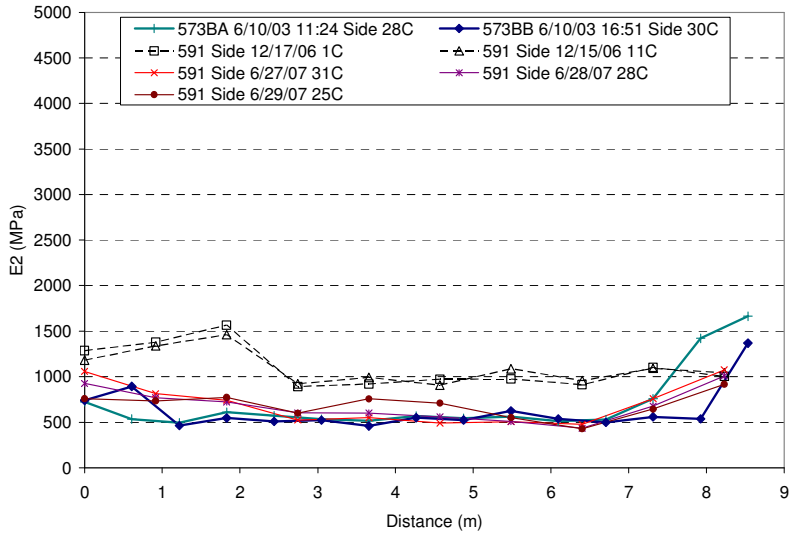

Figure 3.50: Modulus of aggregate base from FWD on Section 573RF/591RF (side).

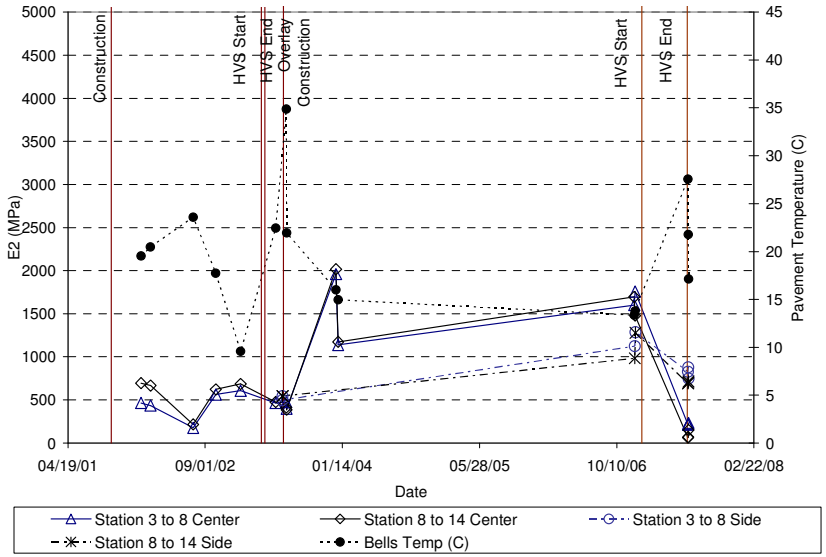

Figure 3.51: Modulus of aggregate base from FWD versus time on Section 573RF/591RF.

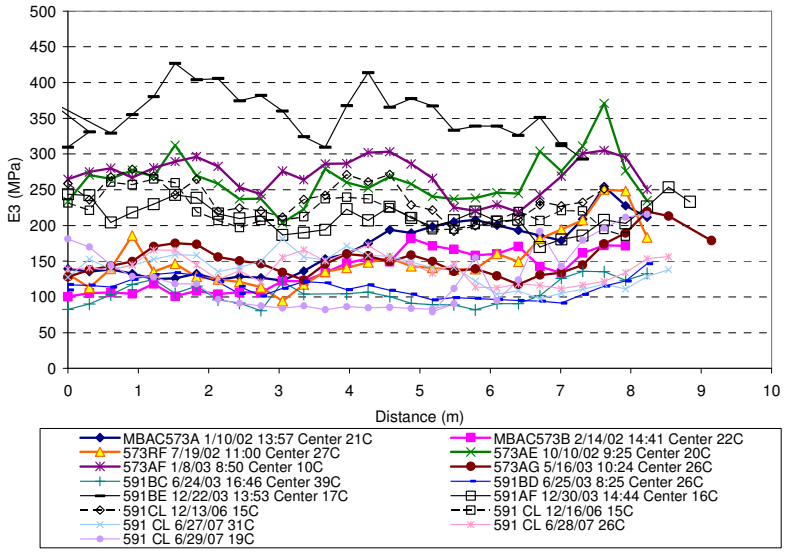

Figure 3.52: Modulus of subgrade from FWD on Section 573RF/591RF (center).

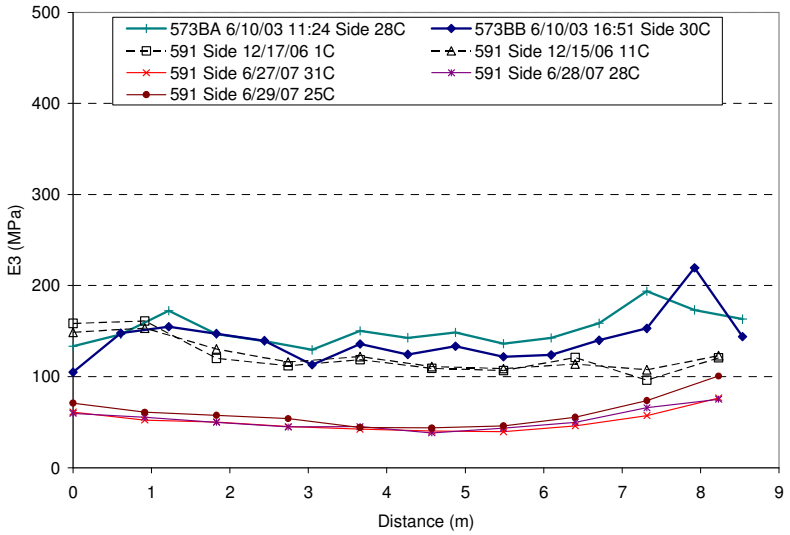

Figure 3.53: Modulus of subgrade from FWD on Section 573RF/591RF (side).

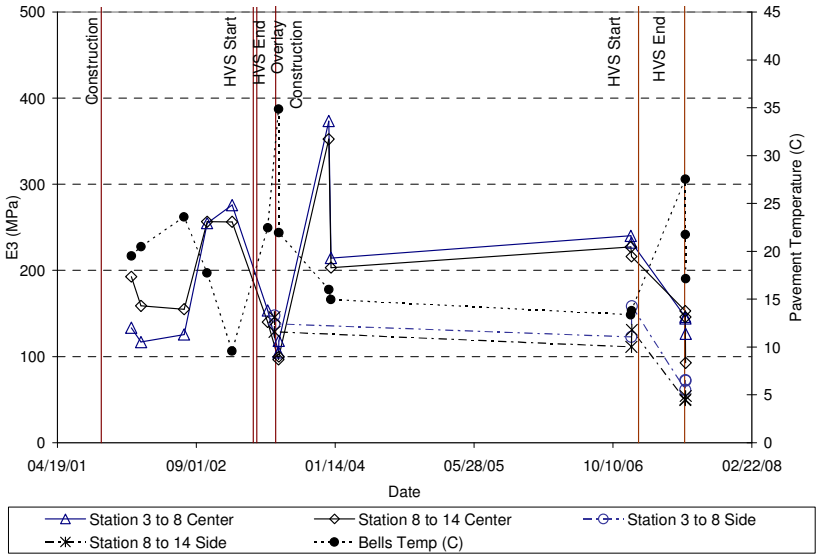

Figure 3.54: Modulus of subgrade from FWD versus time on Section 573RF/591RF.

3.3. Comparison between HVS Sections

Comparison of the pavement structure after Phase 1 HVS testing was discussed in the Phase 1 report (3) and is not discussed further.

The moduli of the three pavement layers before and after Phase 2 HVS testing are summarized in Table 3.2, and plotted in Figure 3.55 through Figure 3.57. For simplicity, subsectioning was omitted in this discussion.

Asphalt Concrete

When considering the temperature effect before Phase 2 HVS testing, Figure 3.55 shows that the composite asphalt concrete layers on the sections overlaid with RAC-G, AR4000-D, and MAC15-G had comparable moduli. The modulus of Section 586RF (MB15-G) was similar to that of Sections 589RF (45 mm MB4-G) and 590RF (90 mm MB4-G), but was lower than the moduli of other sections. After Phase 2 HVS testing, the moduli of the RAC-G, AR4000-D, both MB4-G, and the MAC15-G overlays had all dropped, with the reduction of the RAC-G most significant. The modulus of the MB15-G overlay was not affected by HVS loading.

Aggregate Base

The base in the vicinity of the section overlaid with the MB15-G mix was very stiff (3,500 MPa) before Phase 2 testing (Figure 3.56), attributed to recementation of the particles. At comparable temperatures, the base in the vicinity of the sections overlaid with RAC-G, AR4000-D, or MAC15-G mixes was also relatively stiff, also attributed to recementation, with an average modulus of more than 1,000 MPa before the Phase 2 HVS test. The base in the vicinity of the two sections overlaid with the MB4-G mix had the lowest measured aggregate base modulus. HVS loading resulted in damage to the base under all the sections. The modulus of the base under the sections overlaid with RAC-G, AR4000-D, MB4-G (45 mm), MB4-G (90 mm), and MAC15-G dropped to similar levels (about 250 MPa) after Phase 2 testing, while the MB15-G section retained the highest aggregate base modulus (around 1,000 MPa).

Subgrade

Subgrade modulus was highest (about 340 MPa) in the vicinity of Section 586RF before Phase 2 testing (Figure 3.57) and was similar (about 270 MPa) under the sections overlaid with RAC-G and MB4-G (45 mm). Slightly lower moduli were recorded on the remainder of the sections. This is consistent with the analysis after Phase 1 testing (3), which attributed weaker sections of the subgrade to significantly higher moisture contents in some areas during compaction. After HVS testing the subgrade modulus was

approximately 50 percent lower on the sections overlaid with RAC-G, MB4-G (45 mm), and MAC15-G, and relatively unchanged on the remainder of the sections. It is not clear whether this was attributed to loading or to the effects of moisture.

Table 3.2: Summary of Moduli Before and After Phase 2 HVS Test

Layer	Section	Before HVS Test				After HVS Test			
		Mean (MPa)	Standard Deviation (MPa)	BELLS Temp. (°C)	RSD* Peak (µmm)	Mean (MPa)	Standard Deviation (MPa)	BELLS Temp. (°C)	RSD* Peak (µmm)
AC	586RF	4,239	1,211	16.3	174	5,193	1,162	15.5	279
	587RF	7,740	1,004	16.5	368	1,445	469	15.6	1,718
	588RF	5,991	463	24.1	257	1,747	1,069	24.7	2,099
	589RF	5,157	1,131	14.9	562	2,406	902	17.7	1,375
	590RF	1,977	302	24.0	493	1,483	210	25.5	1,228
	591RF	9,460	2,391	13.4	280	4,621	1,979	17.1	1,058
AB	586RF	3,746	654	16.3		1,057	294	15.5	
	587RF	1,894	197	16.5		243	147	15.6	
	588RF	977	109	24.1	Not	263	255	24.7	Not
	589RF	760	121	14.9	measured	222	145	17.7	measured
	590RF	250	18	24.0		199	31	25.5	
	591RF	1,649	244	13.4		193	111	17.1	
SG	586RF	332	7	16.3		284	21	15.5	
	587RF	270	37	16.5		123	40	15.6	
	588RF	148	13	24.1	Not	179	45	24.7	Not
	589RF	271	18	14.9	measured	148	44	17.7	measured
	590RF	94	11	24.0		81	8	25.5	
	591RF	234	23	13.4		110	26	17.1	

* Road Surface Deflectometer - average of RSD deflection measurements on AC only at 5 stations

586RF - MB15-G 587RF - RAC-G 588RF - AR4000-D
589RF - MB4-G (45mm) 590RF - MB4-G (90mm) 591RF - MAC15-G

The above discussion indicates considerable variation in the modulus measured over the length of the test road. The calculated moduli also do not relate to the average of the peak deflections measured on each section with the RSD. The subgrade, base and asphalt layers were each constructed in a single day. Although there was some variation in the aggregate used in the base (recycled portland cement concrete) and some variation in the thickness of the base and asphalt layers, aggregate compaction, asphalt paving, and asphalt compaction were all carried out as a continuous process. Therefore, there should not have been a significant variation in the modulus of the subgrade, base and underlying DGAC along the length of the section. Anomalies and discrepancies in the measurements are instead attributed to:

- Limitations of FWD measurements on cracked surfaces (587RF and 588RF) and on uneven surfaces (589RF)
- Limitations of the backcalculation procedure in terms of layer differentiation, temperature correction, and seed and baseline value inputs
- Variation in the degree of recementation of the recycled aggregate particles and subgrade moisture content along the length of the section

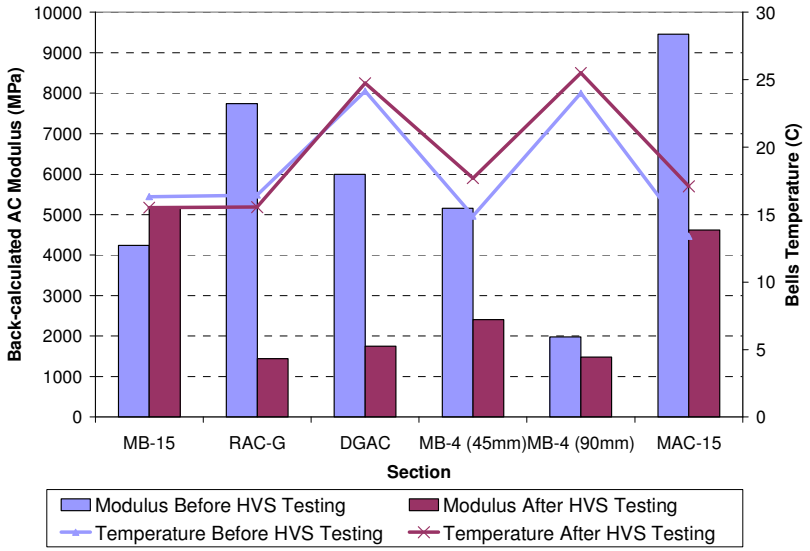

Figure 3.55: Modulus of asphalt concrete before and after Phase 2 HVS testing.

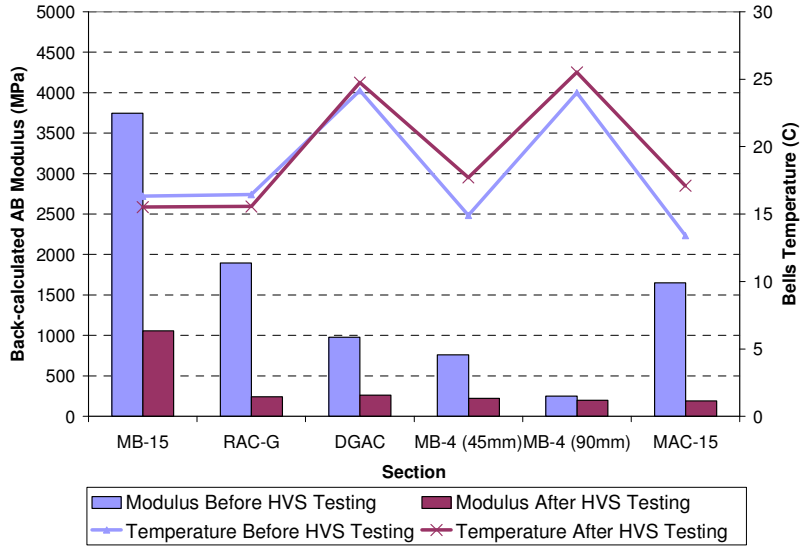

Figure 3.56: Modulus of aggregate base before and after Phase 2 HVS testing.

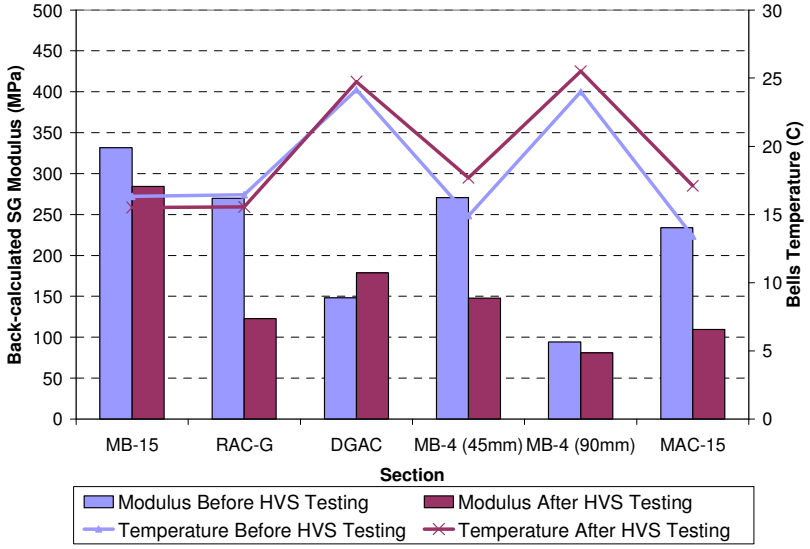

Figure 3.57: Modulus of subgrade before and after Phase 2 HVS testing.

3.4. Correlation of Moduli of Different Layers

The modulus of the aggregate base was generally positively correlated with the moduli of the asphalt concrete and the subgrade. Figure 3.58 through Figure 3.64 show the relationship between the asphalt concrete, base and subgrade moduli in the trafficked area before and after HVS testing, and in the untrafficked area. Observations from the figures show that:

- The correlation between the asphalt concrete layers and the base in the trafficked area after Phase 1 (Figure 3.58) was poor. This was attributed to the very cracked nature of the asphalt concrete which impacts on the accuracy of FWD testing, variability in cracking between the sections, and possibly also to partial destruction of cemented bonds between the aggregate particles (formed by recementation of the recycled concrete particles) during HVS trafficking.
- The correlation improved in the period between tests and after the construction of the overlay. This is attributed to the rest period from HVS loading, and to the confinement provided by the overlays. Recementation of the aggregate particles probably also continued.
- The correlation between the asphalt concrete and base in the trafficked area was relatively good after HVS testing. This was attributed to there being no cracking on four of the six sections, and a systematic breakdown of the cemented bonds under trafficking on all the sections (Figure 3.59).
- The correlation in the untrafficked area was poor, particularly for those sections with a high modulus aggregate base (Figure 3.60). This is probably due to variance in the degree of recementation of the material, and consequent differences in confining pressure.
- The effect of the subgrade on the behavior of the base follows similar trends to that of the asphalt concrete. The weaker subgrade areas provided less confining pressure to the base, resulting in lower base moduli.
- No significant correlation was found between the asphalt concrete modulus and the subgrade modulus.

3.5. Load Effect on Backcalculated Stiffness

Each FWD test consisted of three drops at each test spot beginning with the lightest load. The relationship between the load level and the backcalculated pavement stiffnesses is shown in Figure 3.65 through Figure 3.70 for each HVS section. The drop load level had little effect on the backcalculated pavement stiffnesses.

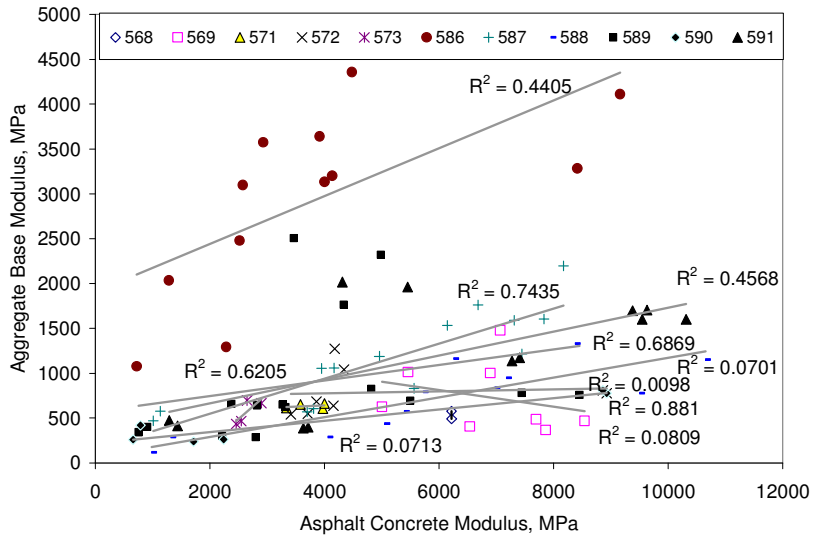

Figure 3.58: Variation of AC and base and modulus in the trafficked area before HVS testing.

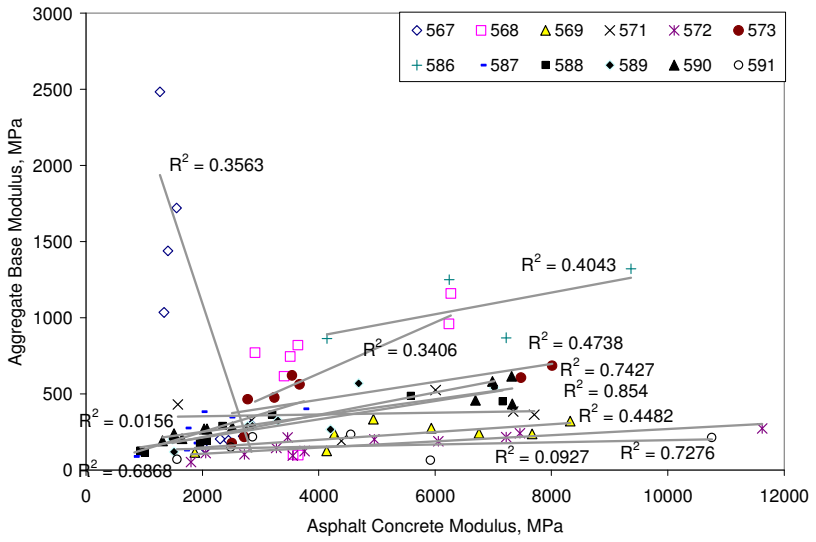

Figure 3.59: Variation of AC and base modulus in the trafficked area after HVS testing.

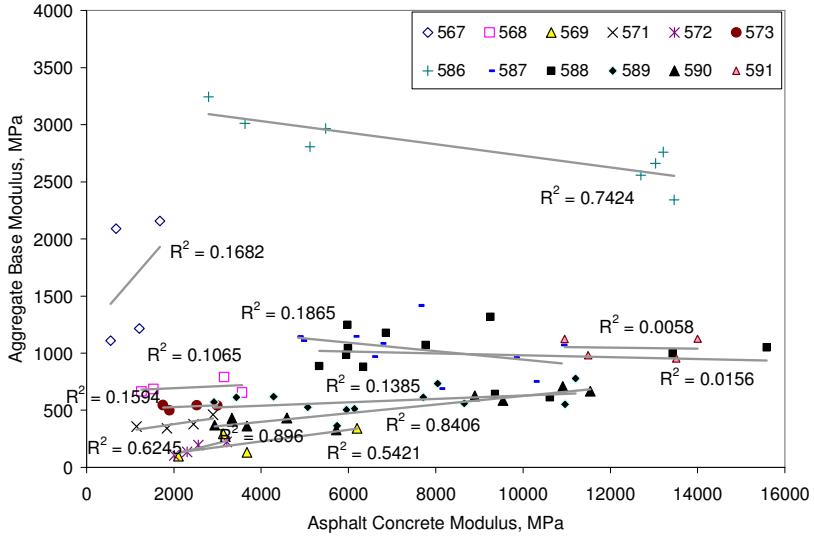

Figure 3.60: Variation of AC and base modulus in the untrafficked area.

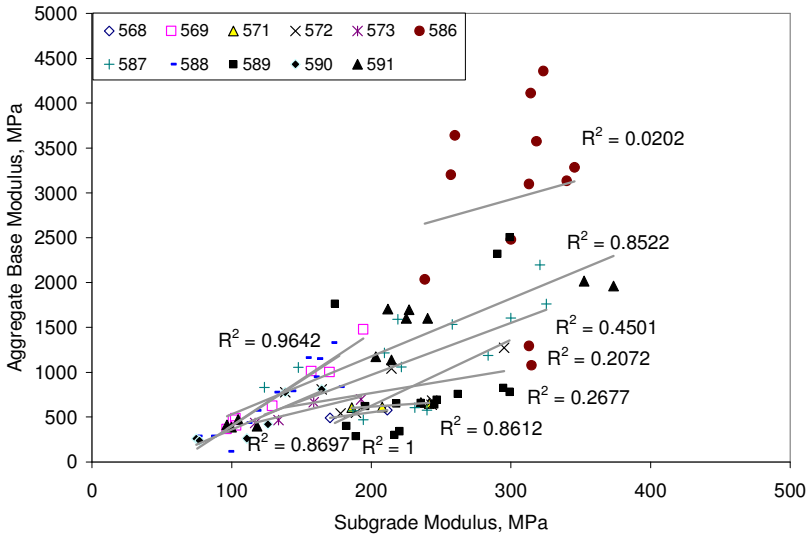

Figure 3.61: Variation of base and subgrade modulus in the trafficked area before HVS test.

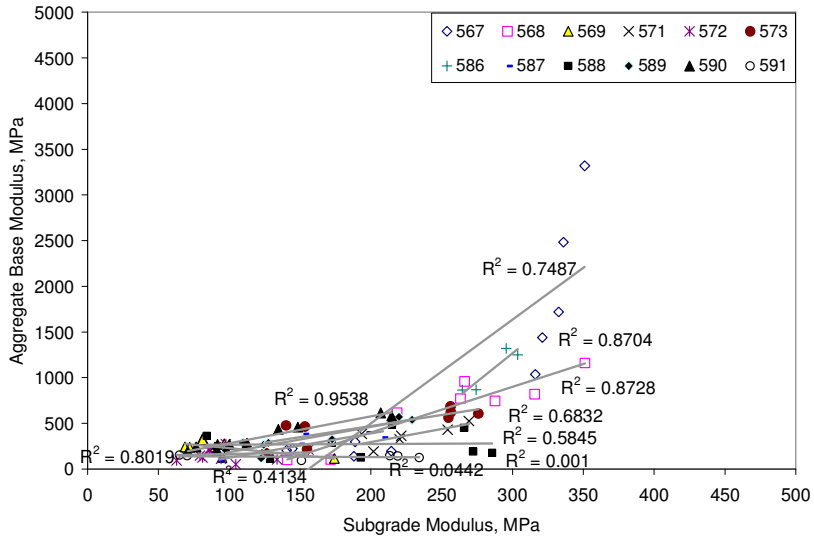

Figure 3.62: Variation of base and subgrade modulus in the trafficked area after HVS test.

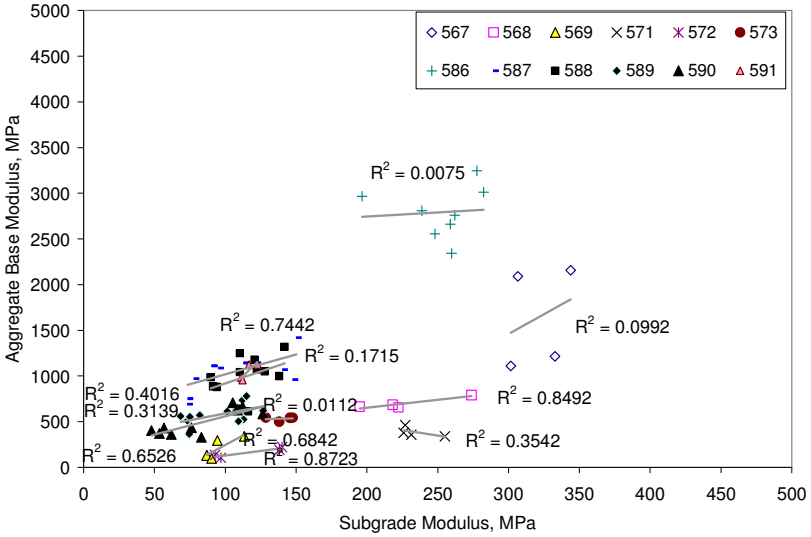

Figure 3.63: Variation of base and subgrade modulus in the untrafficked area.

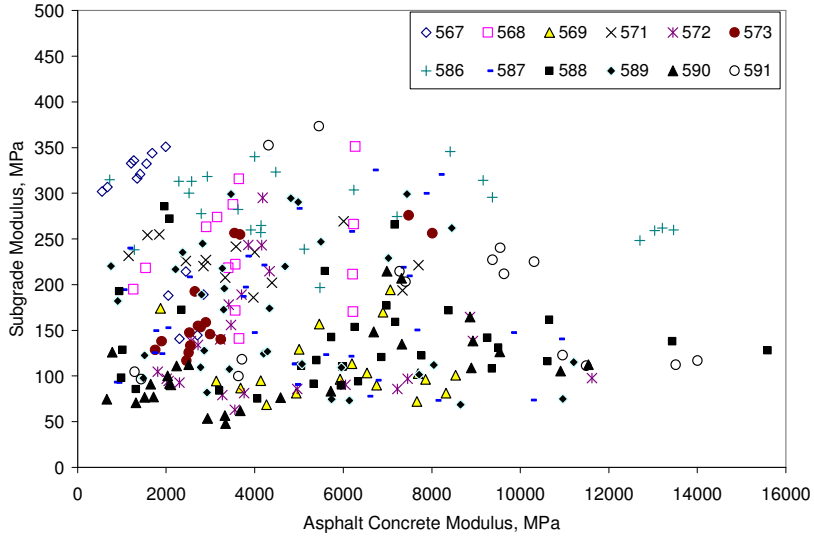

Figure 3.64: Variation of AC modulus with subgrade modulus.

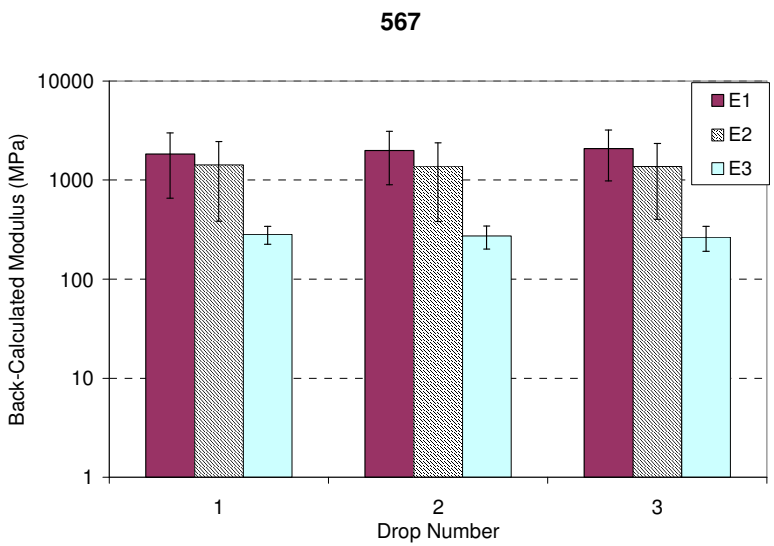

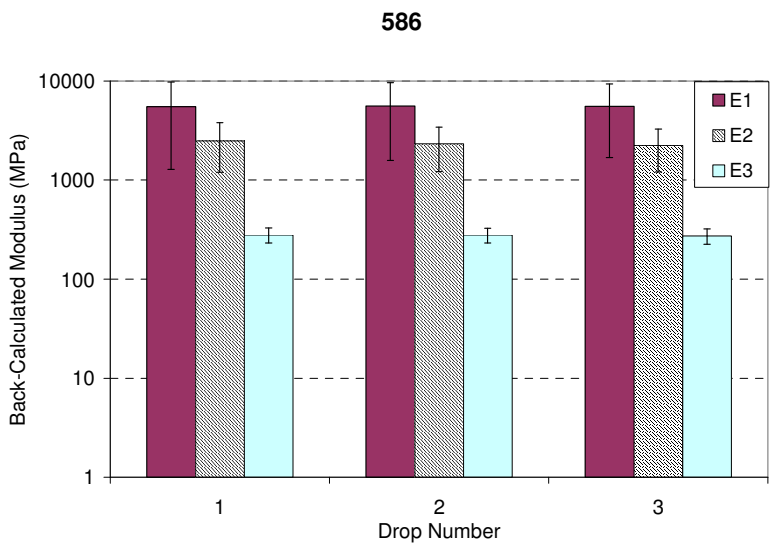

Figure 3.65: Average backcalculated modulus vs drop number on Section 567RF/586RF (MB15-G).

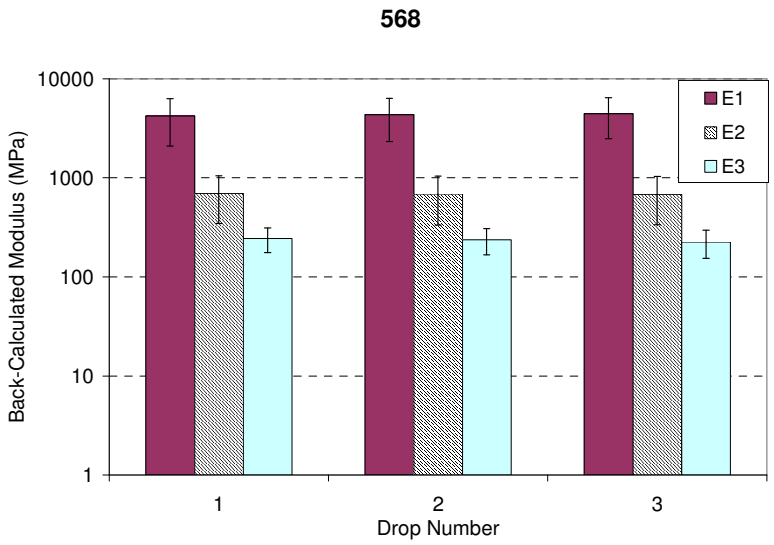

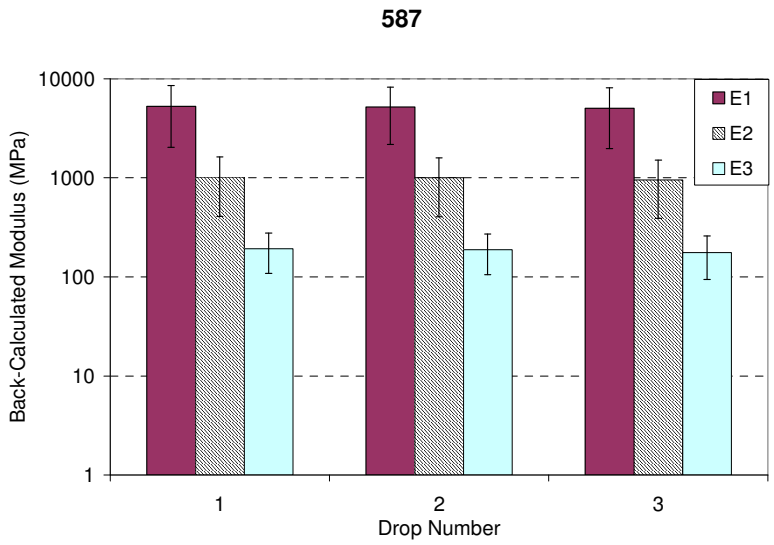

Figure 3.66: Average backcalculated modulus vs drop number on Section 568RF/587RF (RAC-G).

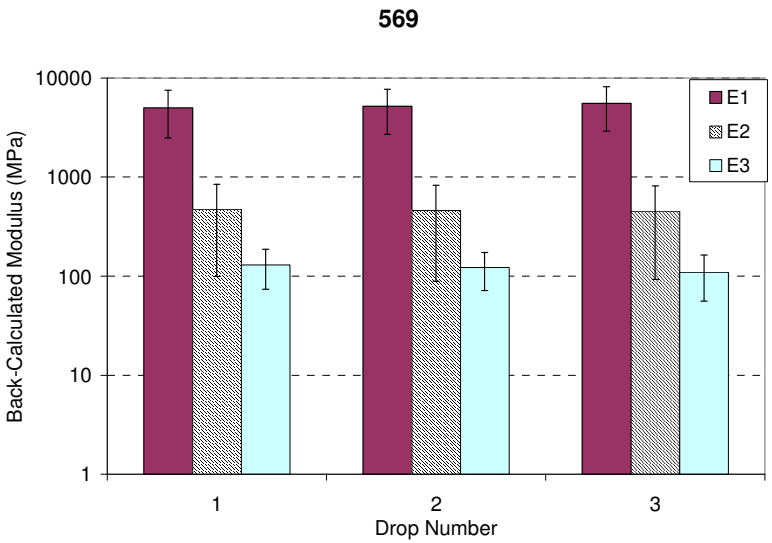

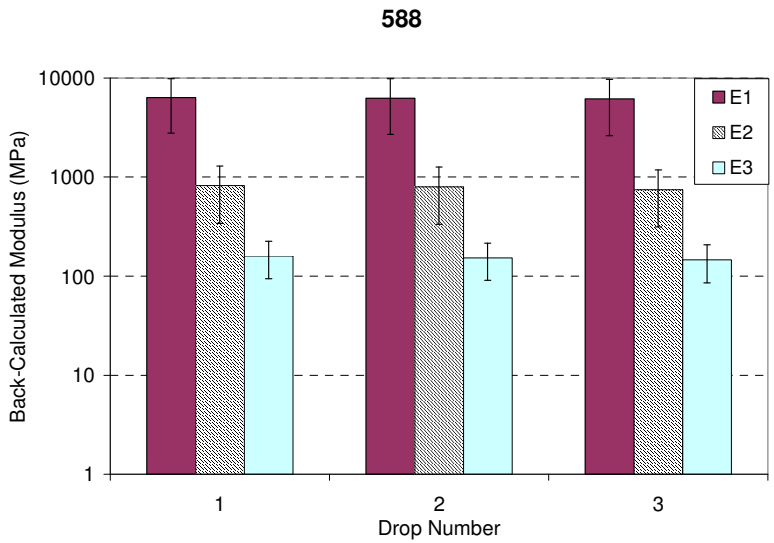

Figure 3.67: Average backcalculated modulus vs drop number on Section 569RF/588RF (AR4000-D).

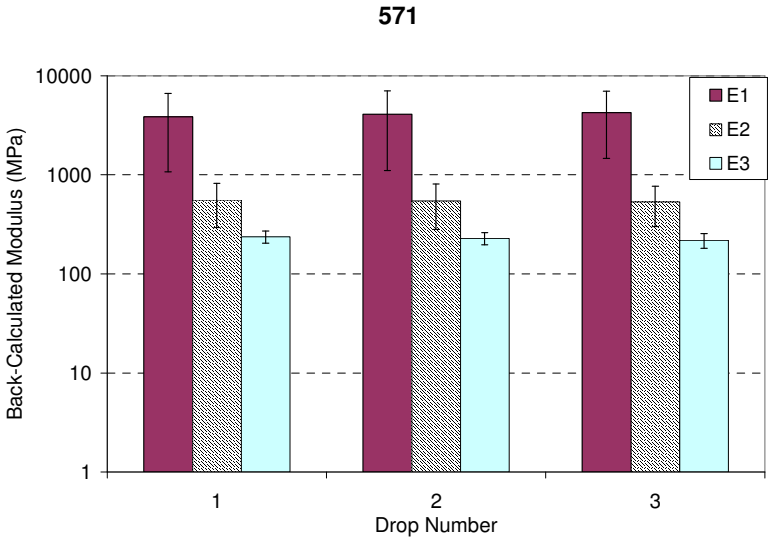

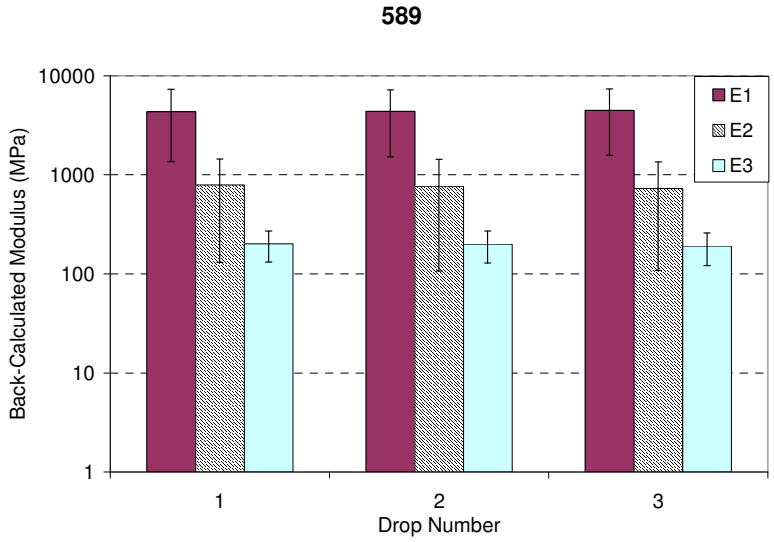

Figure 3.68: Average backcalculated modulus vs drop number on Section 571RF/589RF (MB4-G-45).

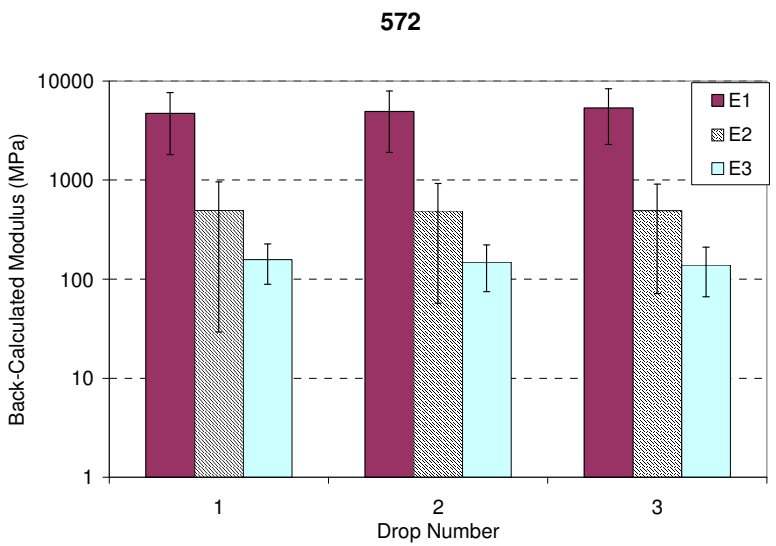

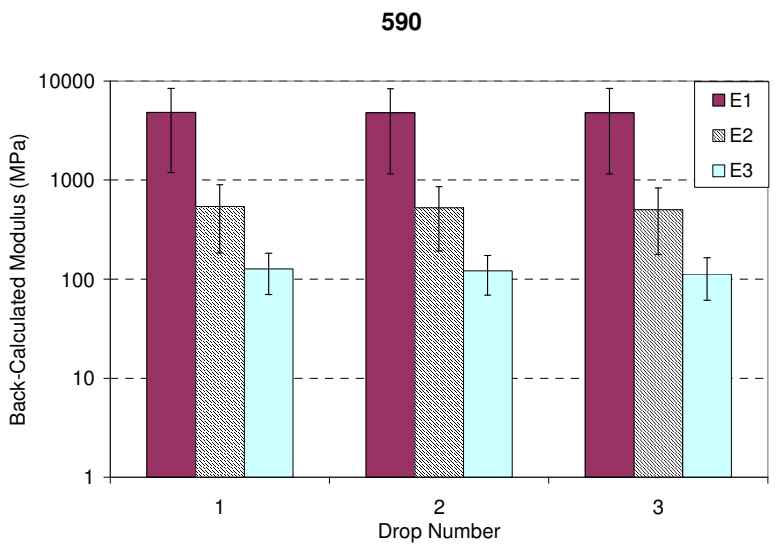

Figure 3.69: Average backcalculated modulus vs drop number on Section 572RF/590RF (MB4-G-90).

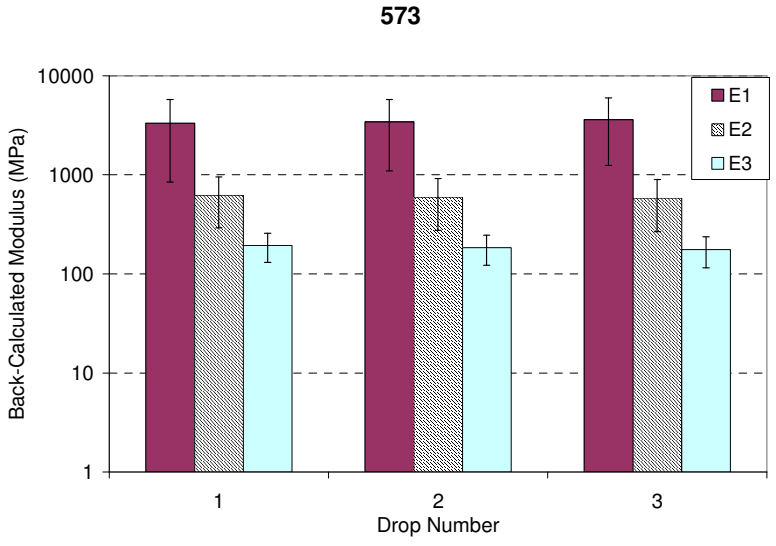

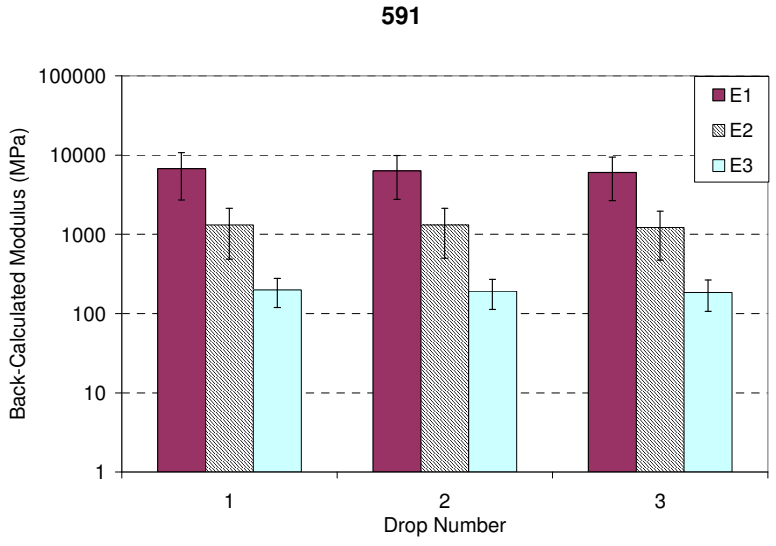

Figure 3.70: Average backcalculated modulus vs drop number on Section 573RF/591RF (MAC15-G).

4. AGING, SEASONAL EFFECTS, AND STIFFNESS RECOVERY

4.1. Temperature Adjustment

Temperature had a significant effect on the backcalculated modulus of the asphalt concrete, which in turn affected the aggregate base modulus. In order to analyze the aging and seasonal effects on material moduli, the temperature effect has to be removed.

The M-E PDG master curve formula (Equation 4.1) was used to develop the modulus master curve for each asphalt mix:

$$\log(E) = \log(E_{\min}) + \frac{\log\left(E_{\max}/E_{\min}\right)}{1+\exp(\beta+\gamma\times\log(t_r))},$$

$$t_r = lt\times\left(\frac{v_{ref}}{v}\right)^{aT},$$

$$\log(\log(v\ cPoise)) = A + VTS\times\log(T°K) \qquad \textbf{(4.1)}$$

Where: E is the modulus at a specific loading time t_r and temperature T

E_{min} is the minimum modulus

E_{max} is the maximum modulus

t_r is reduced time

lt is loading time (for creep test loading)

v is viscosity of the binder at the actual temperature

v_{ref} is viscosity of the binder at the reference temperature

T is the temperature in degrees Kelvin

β, γ, aT, A and VTS are constants, and log is to base 10.

The binder parameters A and VTS do not significantly affect the fitted curve. Good fit-to-measured moduli can be obtained with parameters from a number of different binders. Values of A = 9.6307 and VTS = -3.5047.

Other curve parameters were determined by minimizing the Root Mean Square (RMS) difference between the measured values and the values calculated using Solver in Excel.

4.1.1 Original (Underlying) Sections

The backcalcuated moduli of the underlying DGAC layer (all locations) were used to develop the master curve of the intact DGAC layer. Only the FWD data measured in the first 12 months after original construction were used in order to minimize the effect of aging.

The estimated master curve is shown in Figure 4.1. The following parameters were used:

E_{min} = 100 MPa,

E_{max} = 17909 MPa,

β = 0.136, γ = 0.439, and aT = 1.9406.

The master curve developed from laboratory flexural beam frequency sweep testing is also shown in the figure for comparison. The laboratory determined modulus was generally higher (7,300 MPa at 20 C) than the modulus backcalculated from the test road (3,077 MPa at 20 C). The difference was attributed to uncertainties associated with backcalculating the modulus of thin layers as well as differences in other factors such as test configuration, air-void content, and strain level. This is discussed in more detail in Section 4.1.2.

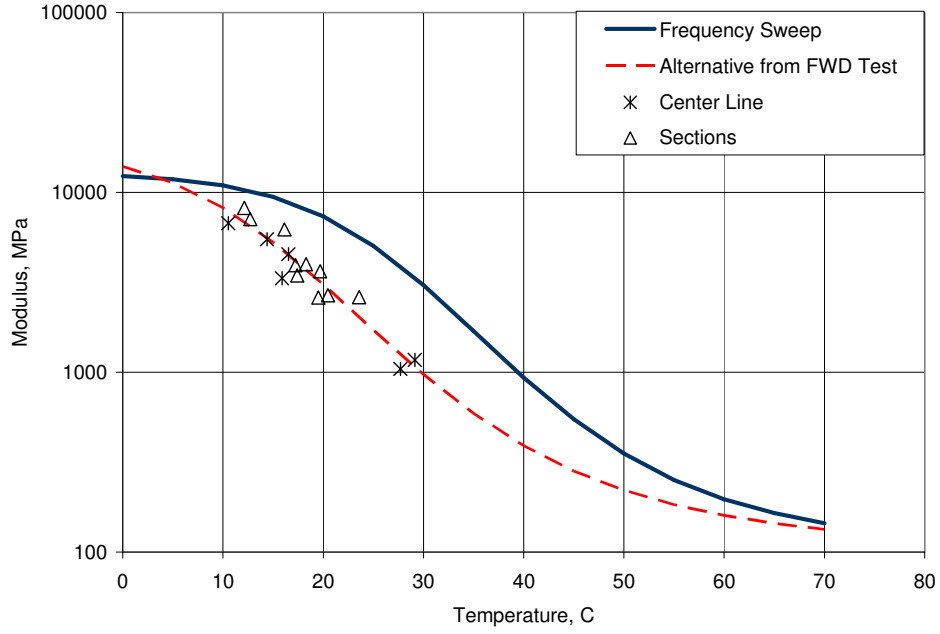

Figure 4.1: Master curves of DGAC estimated from laboratory and FWD data.

4.1.2 Overlay Sections

For analysis purposes, the underlying DGAC and the overlay were considered as one composite layer, since the individual layers were too thin to model separately. A master curve was developed for each intact composite asphalt concrete layer from FWD data. Since the dataset from the untrafficked areas of

each test section was limited, the FWD data measured in the trafficked areas of the test sections before Phase 2 testing were also used to develop the master curves. Although the underlying DGAC in the trafficked areas was damaged during Phase 1 testing, the modulus of the composite asphalt concrete layer did not appear to be significantly affected, as discussed in Chapter 3, and the data was therefore considered appropriate for master curve development.

Master curves were estimated by minimizing the root mean square (RMS) of the differences between observed and predicted values. Both absolute and relative differences were considered for the analysis. Use of the absolute difference applies less weight to the moduli measured at high temperatures. The estimated master curves for all test sections are shown in Figure 4.2 and Figure 4.3 for the two types of differences, respectively, with the corresponding parameters listed in Tables 4.1 and 4.2. The minimum modulus for all materials was fixed at 100 MPa during estimation.

The figures show that:

- The master curves, based on absolute difference, of Sections 586RF (MB15-G+DGAC) and 591RF (MAC15-G+DGAC) were similar (Figure 4.2).
- The composite asphalt concrete layers on Sections 586RF, 587RF, 590RF, and 591RF were more temperature sensitive than those on Sections 588RF and 589RF.
- The master curves, based on relative difference, of Sections 586RF (MB15-G+DGAC), 587RF (RAC-G+DGAC), and 591RF (MAC15-G+DGAC) were similar to each other (Figure 4.3).

The two asphalt concrete layers on Section 588RF consisted of similar AR4000-D mixes. A comparison of the master curve developed from the composite layer with those developed from the original layer and the laboratory test reveals that the former is similar to that developed from the laboratory frequency sweep test data (Figure 4.4). The significantly lower modulus master curve from the original layer illustrates the uncertainty associated with backcalculation of thin layers.

Table 4.1: Parameters of Master Curves of Intact Composite AC Layers:Absolute Difference

Section	Overlay	β	γ	aT	A	VTS	E_{min} (MPa)	E_{max} (MPa)
Underlying	-	0.1317	0.4375	1.9498	9.6307	-3.5047	100	17,887
586RF/567RF	MB15-G	0.3236	0.7560	1.7491	9.6307	-3.5047	100	15,000
587RF/568RF	RAC-G	-0.1370	0.8633	3.2237	9.6307	-3.5047	100	7,744
588RF/569RF	AR4000-D	-0.7635	0.5971	1.5310	9.6307	-3.5047	100	13,275
589RF/571RF	45 mm MB4-G	-0.3311	0.3814	1.7319	9.6307	-3.5047	100	15,000
590RF/572RF	90 mm MB4-G	-0.7619	0.4866	2.7905	9.6307	-3.5047	100	10,846
591RF/573RF	MAC15-G	-0.1620	0.4725	3.0239	9.6307	-3.5047	100	15,061

Table 4.2: Parameters of Master Curves of Intact Composite AC Layers: Relative Difference

Mix	Overlay	β	γ	aT	A	VTS	E_{min} (MPa)	E_{max} (MPa)
Underlying	-	0.1004	0.4380	1.9368	9.6307	-3.5047	100	17,887
586RF/567RF	MB15-G	-0.0577	0.6726	1.4136	9.6307	-3.5047	100	15,000
587RF/568RF	RAC-G	-0.2855	0.4928	1.5887	9.6307	-3.5047	100	14,958
588RF/569RF	AR4000-D	-0.7762	1.0440	1.7205	9.6307	-3.5047	100	10,599
589RF/571RF	45 mm MB4-G	-0.5467	0.3547	1.6354	9.6307	-3.5047	100	15,000
590RF/572RF	90 mm MB4-G	-0.8439	0.5318	2.7688	9.6307	-3.5047	100	10,556
591RF/573RF	MAC15-G	-0.7740	0.2933	2.8968	9.6307	-3.5047	100	16,000

4.2. Aging Analysis of Untrafficked Areas

The developed master curves were used to adjust the backcalculated asphalt concrete moduli to values at a reference temperature of 20°C. Moduli of the underlying aggregate base and subgrade were also adjusted correspondingly because change in asphalt concrete modulus changes the confinement pressure to the underlying layer. The modulus adjustment was completed in *CalBack*.

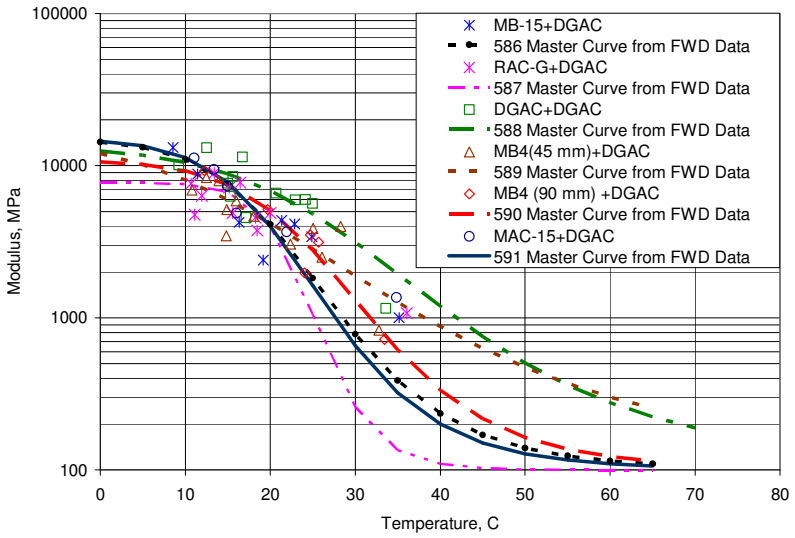

Figure 4.2: Master curves of AC layers estimated from FWD data based on absolute difference.

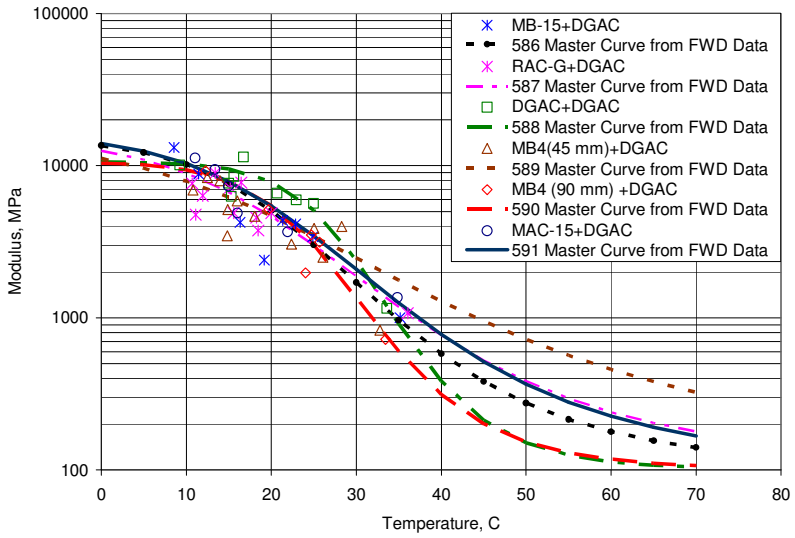

Figure 4.3: Master curves of AC layers estimated from FWD data based on relative difference.

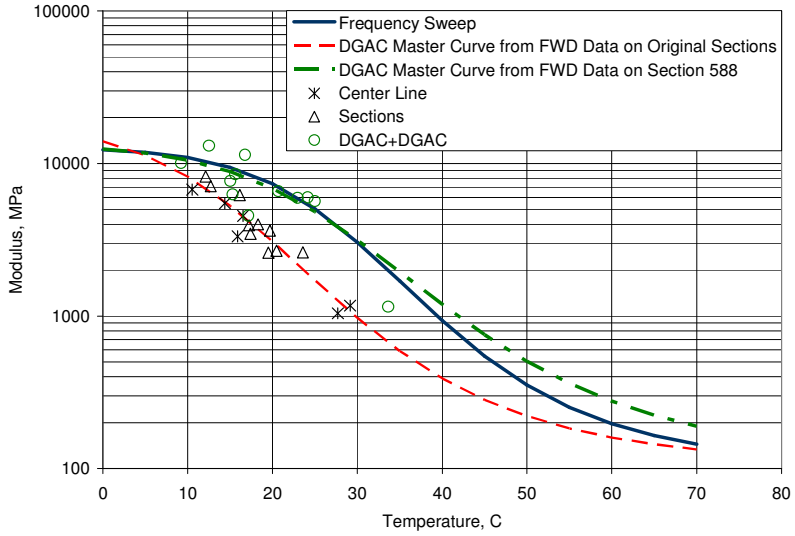

Figure 4.4: Master curves of DGAC estimated from laboratory and different FWD data.

4.2.1 Original (Underlying) Sections

The adjusted moduli of the intact original section layers are presented in Figure 4.5. A logarithm function was used to fit the time series data. The estimated parameters shown in the figure indicate that an aging effect was evident. The moduli of the asphalt concrete, aggregate base, and subgrade generally increased with time. The low R-square values, however, indicate that age alone cannot sufficiently describe the variation in observed data. Changes in material properties thus also need to be considered, specifically those in the aggregate base. Figure 3.56 shows non-uniformity in this layer. To minimize this variation, the age effect on the base was analyzed for each section (Figure 4.6). Age effect on the base modulus was most significant on Section 567RF, followed by Section 568RF. The goodness-of-fit (R-square) of the corresponding logarithm functions was considered acceptable.

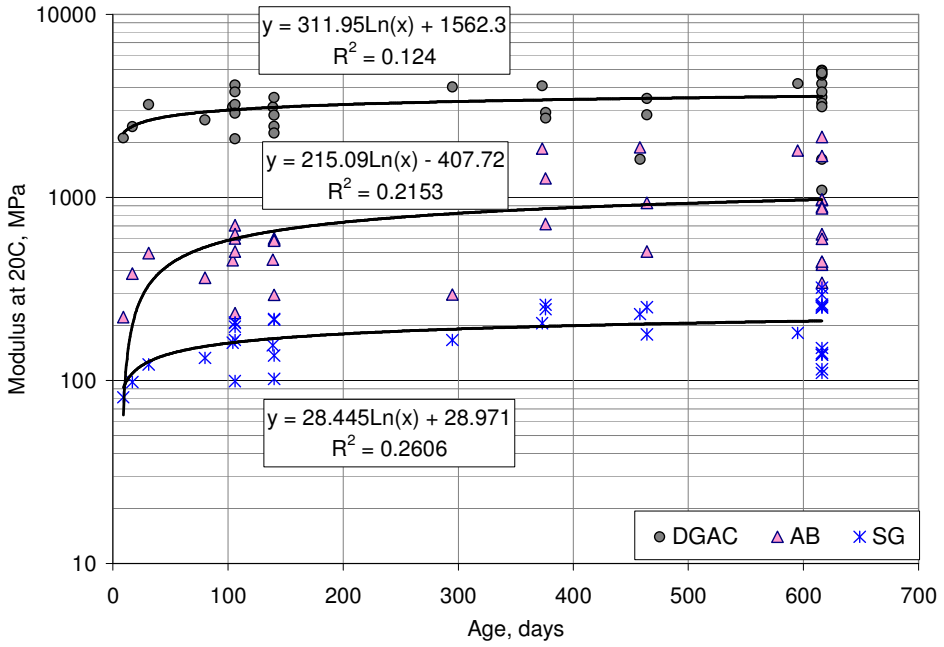

Figure 4.5: Temperature adjusted moduli of original sections versus age.

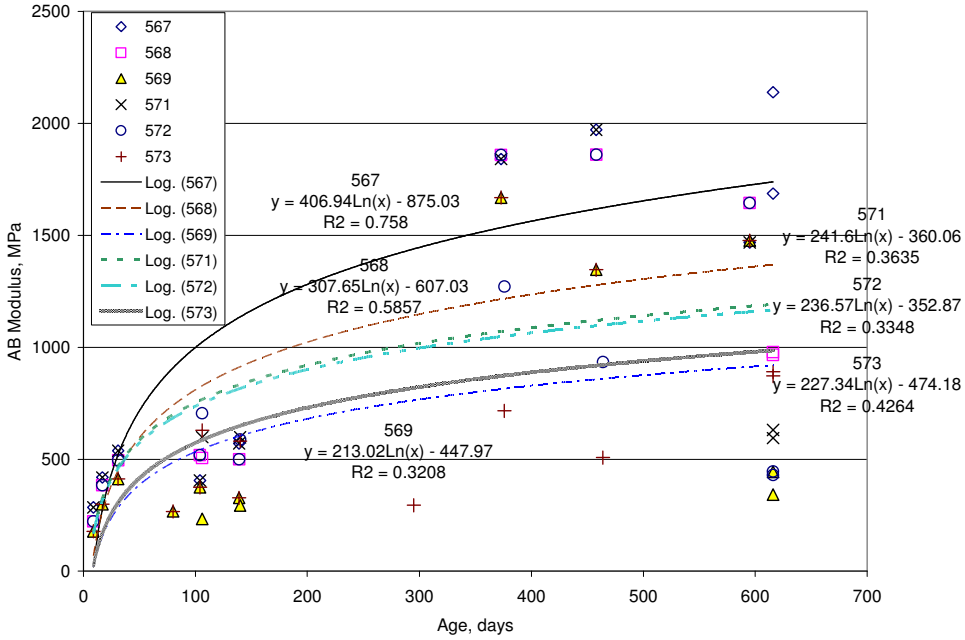

Figure 4.6: Temperature adjusted modulus of aggregate base for each section.

Changes in the subgrade modulus over time were mostly attributed to changes in confinement from the base (and asphalt concrete) layers and the seasonal moisture content variation. Although the material was consistent, some non-linearity may have also existed. The effects of this were treated as a function of the load level in the simulations with *CalME*, in order to separate them from the confinement effects.

The modulus of the subgrade was calculated from:

$$E = A + B \times S$$

$$S = \left(\sum_{i=1}^{n-1} h_i \times \sqrt[3]{E_i} \right)^3 \qquad \textbf{(4.2)}$$

Where: A and B are parameters

E_i and h_i are the modulus and thickness of layer i above subgrade.

Figure 4.7 presents the estimated function for each section.

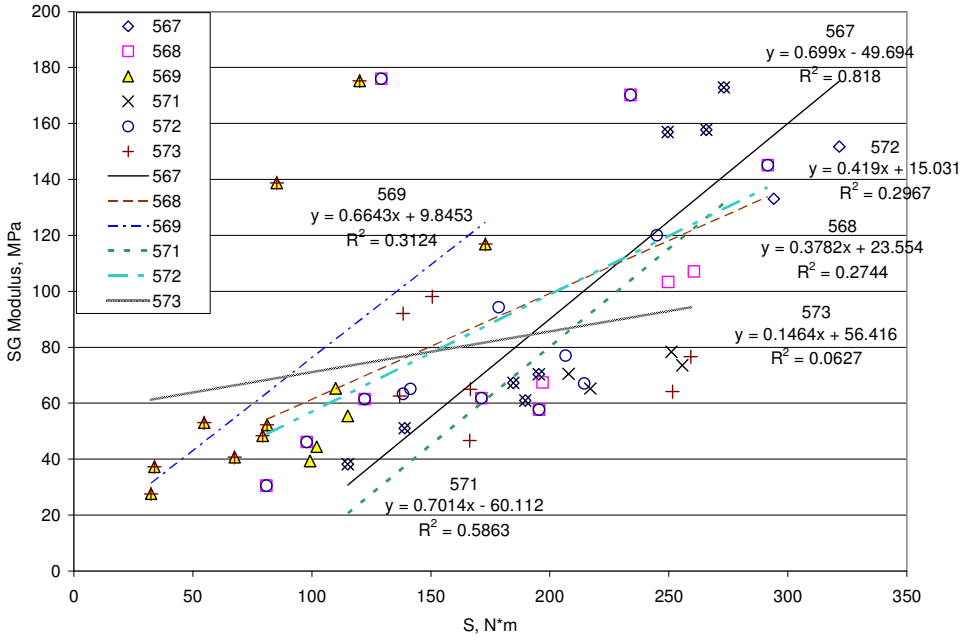

Figure 4.7: Modulus of the subgrade as a function of the stiffness of the pavement layers.

4.2.2 Overlay Sections

The adjusted moduli of the three layers in the overlay sections are presented in Figure 4.8 through Figure 4.13. The age was determined from the time of overlay construction (June 14, 2003). A logarithm function was used to fit the time series data. Aging of the asphalt concrete was apparent in all sections except Section 591RF (MAC15-G), and the logarithm function appears to fit the data well. Base modulus increased with time on Sections 586RF and 588RF, but did not change significantly on the other sections. This is attributed to differences in the degree of recementation and seasonal changes in moisture content. The correlation between subgrade modulus and age was considered poor.

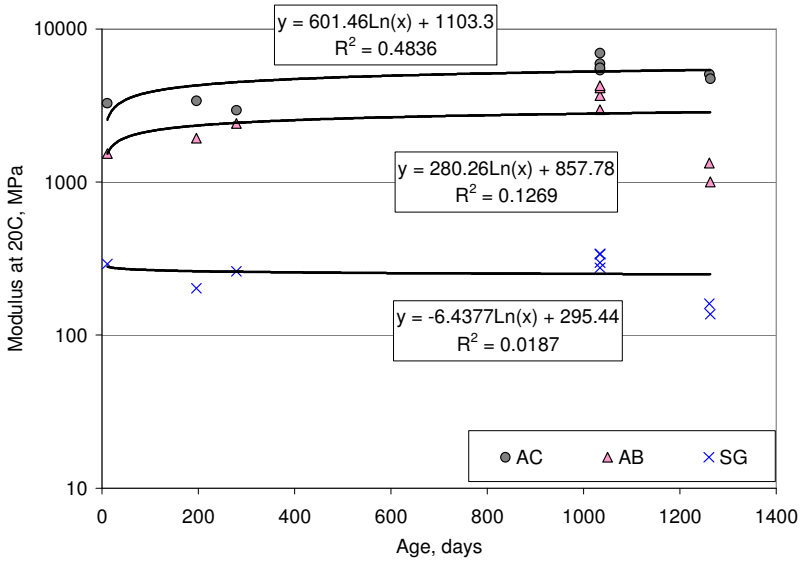

Figure 4.8: Temperature adjusted moduli of Section 586RF (MB15-G) versus age.

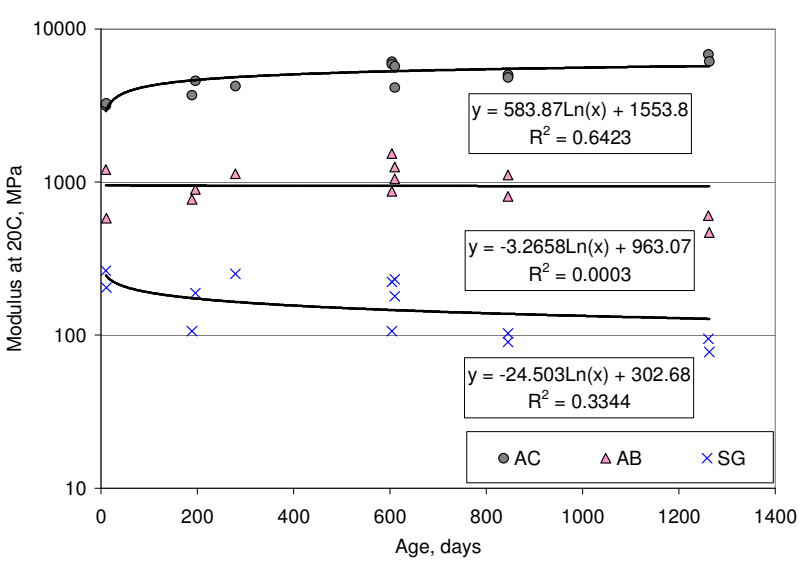

Figure 4.9: Temperature adjusted moduli of Section 587RF (RAC-G) versus age.

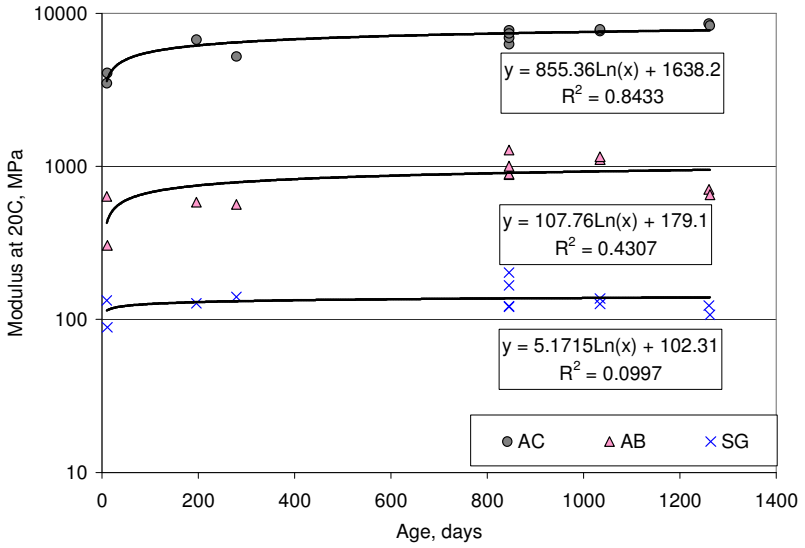

Figure 4.10: Temperature adjusted moduli of Section 588RF (AR4000-D) versus age.

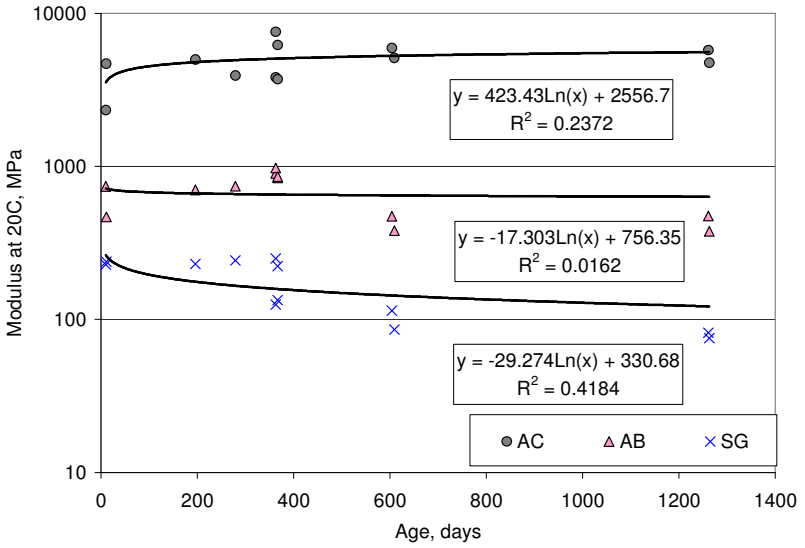

Figure 4.11: Temperature adjusted moduli of Section 589RF (MB4-G-45) versus age.

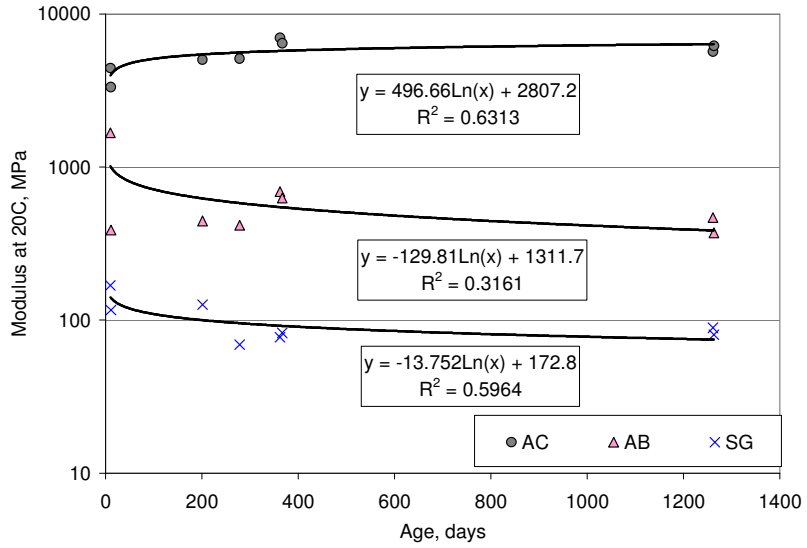

Figure 4.12: Temperature adjusted moduli of Section 590RF (MB4-G-90) versus age.

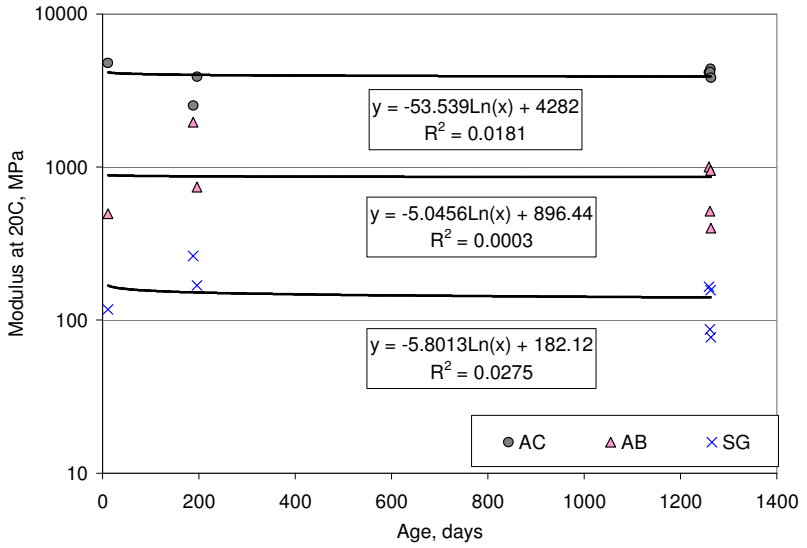

Figure 4.13: Temperature adjusted moduli of Section 591RF (MAC15-G) versus age.

4.3. Seasonal Effects on Untrafficked Areas

In-service pavements are affected by seasonal variations of several important factors, including traffic volume and load, temperature, precipitation, freeze-thaw cycles, and other potential environmental variables. In this experiment, traffic load was controlled and was not considered in the analysis of seasonal effects. Temperature effect was adjusted from the master curves, and there were no freeze-thaw cycles. The potential seasonal effects, therefore, were mainly attributed to changes in moisture content in the pavement layers resulting from precipitation and underground water table.

The water table fluctuates between 3.0 and 5.0 m below the surface of the pavement (3). Figure 4.14 and Figure 4.15 show the monthly precipitation and moisture content in the aggregate base and subgrade for the duration of the study. Water content is shown as a relative number. After June 2003 the base moisture content was not measured. The peak monthly precipitation occurred in December through February, with little rain between May and September. Moisture content in the base fluctuated with precipitation, but with rates of moisture content decrease lower than rates of moisture content increase. The subgrade moisture content was lower in July through October (dry season), and remained relatively constant during other months. Moisture content increases in the subgrade closely followed increases in monthly precipitation, but the decrease of moisture content in the subgrade was significantly slower than the corresponding decrease in monthly precipitation. This reflects the slow drainage rate of the subgrade.

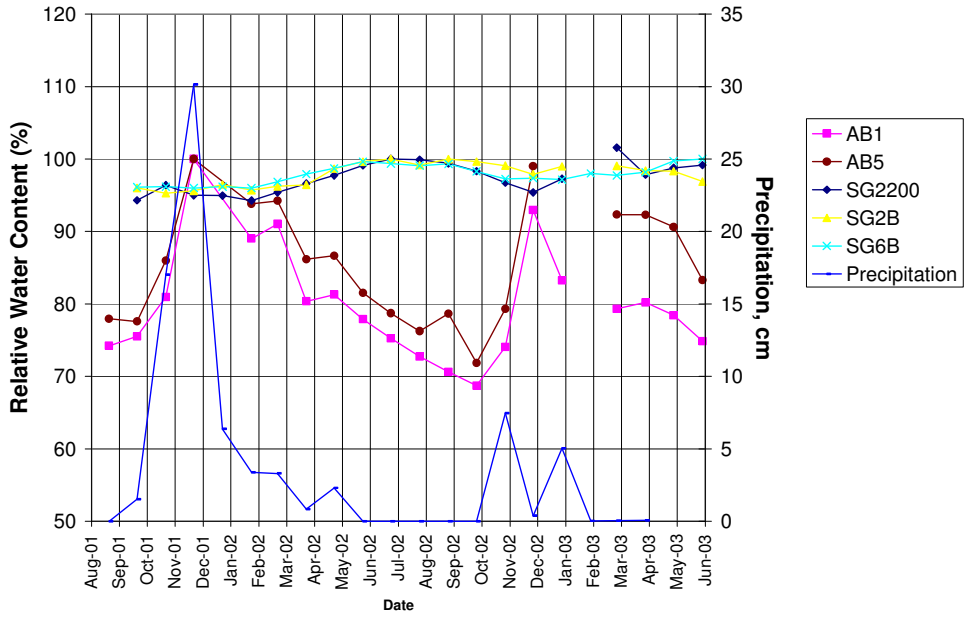

Figure 4.14: Time variation of moisture content with precipitation before June 2003.

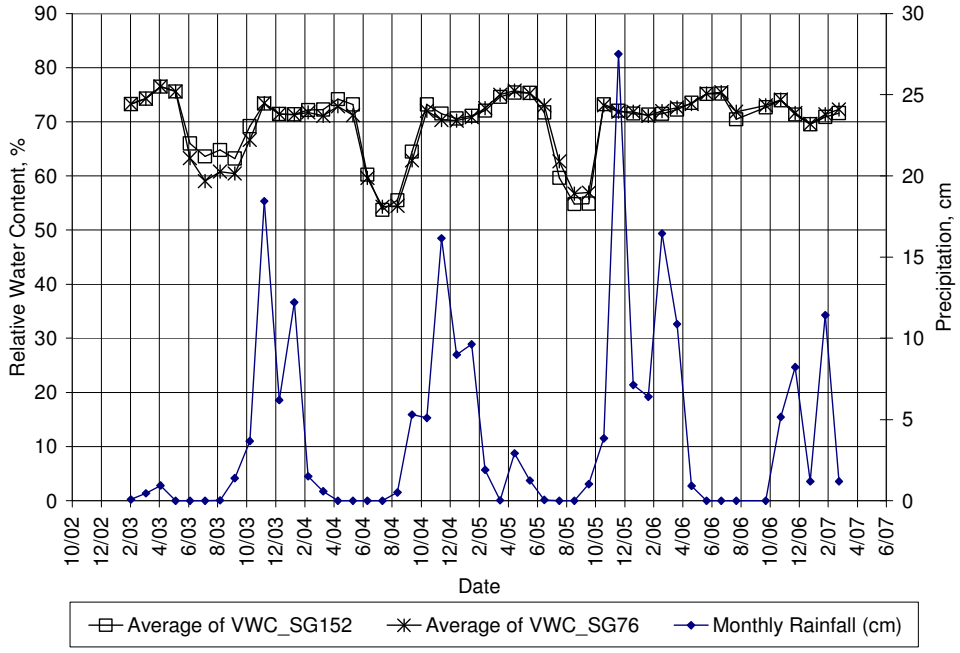

Figure 4.15: Time variation of moisture content with precipitation after June 2003.

4.3.1 Original (Underlying) Sections

The residual data after subtracting the aging functions fitted in Section 4.2 from the temperature adjusted moduli were used to study seasonal effects. The residual moduli of the three layers in the original sections are presented in Figure 4.16. The residual asphalt concrete modulus generally appeared higher in July through September (dry season), and lower in October through January (wet season), however, no significant seasonal patterns in the residual moduli of the three pavement layers were observed.

4.3.2 Overlay Sections

The residual moduli of the three layers in the overlay sections, after subtracting the aging functions from corresponding temperature adjusted moduli are shown in Figure 4.17 through Figure 4.22. The detection of any seasonal effects is difficult due to the scatter and limited amount of data points in each plot.

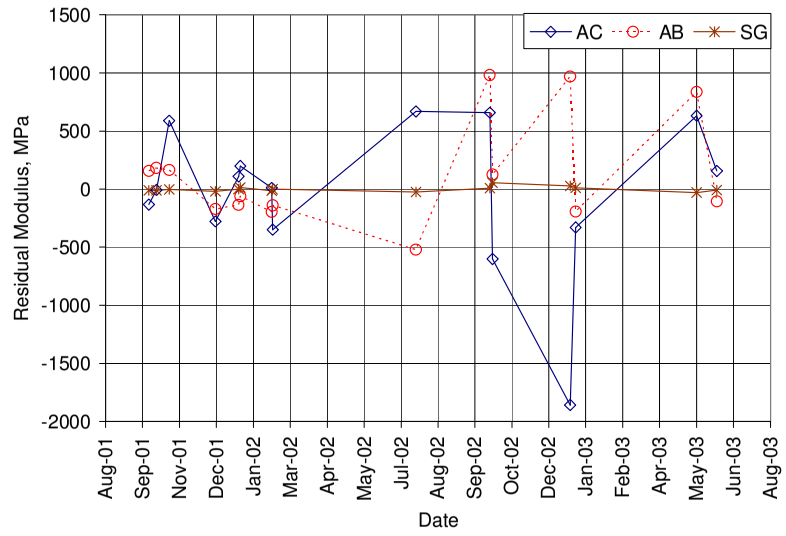

Figure 4.16: Time variation of residual moduli of original sections.

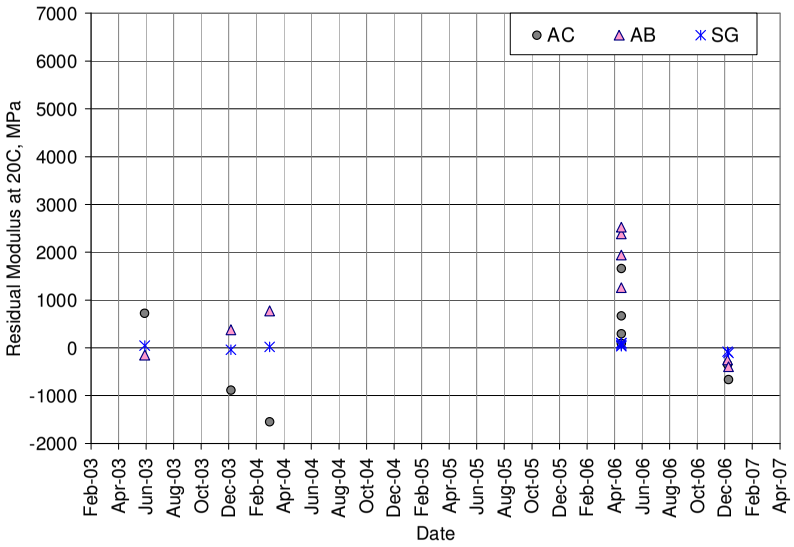

Figure 4.17: Time variation of residual moduli of Section 586RF (MB15-G).

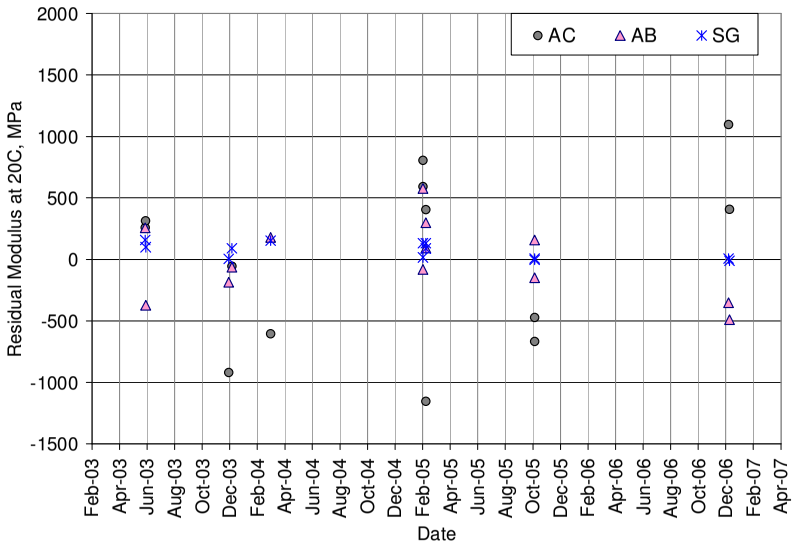

Figure 4.18: Time variation of residual moduli of Section 587RF (RAC-G).

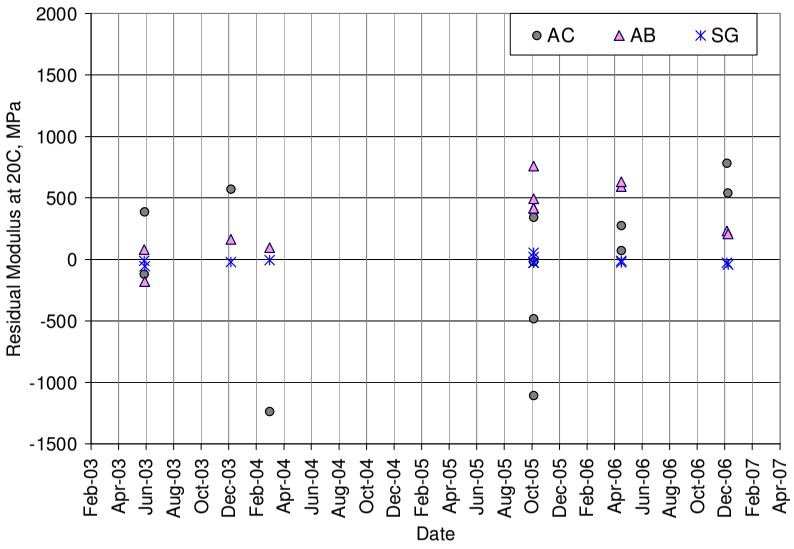

Figure 4.19: Time variation of residual moduli of Section 588RF (AR4000-D).

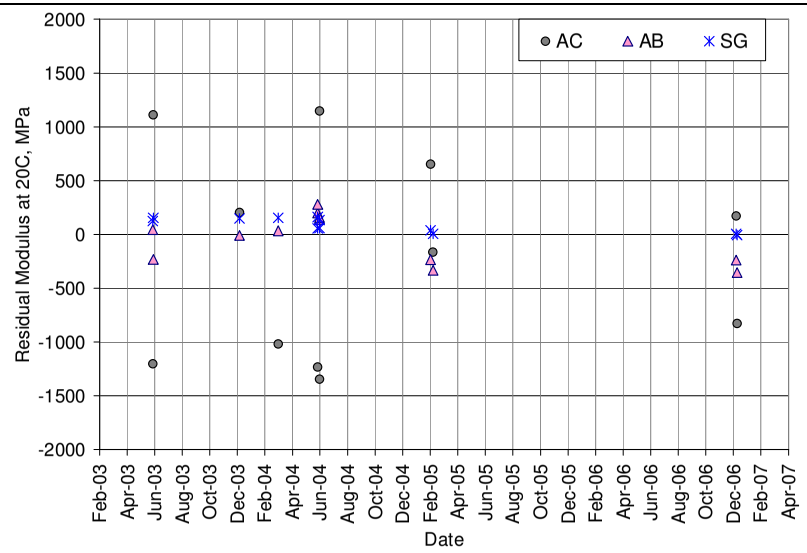

Figure 4.20: Time variation of residual moduli of Section 589RF (MB4-G-45).

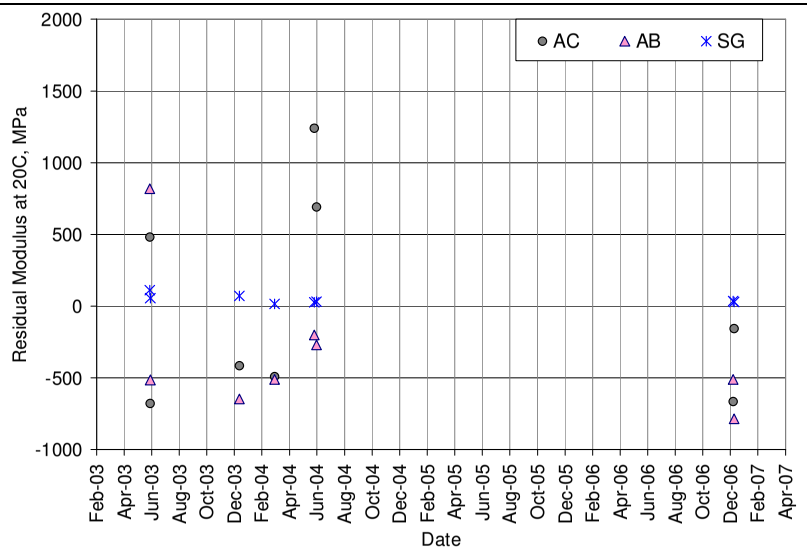

Figure 4.21: Time variation of residual moduli of Section 590RF (MB4-G-90).

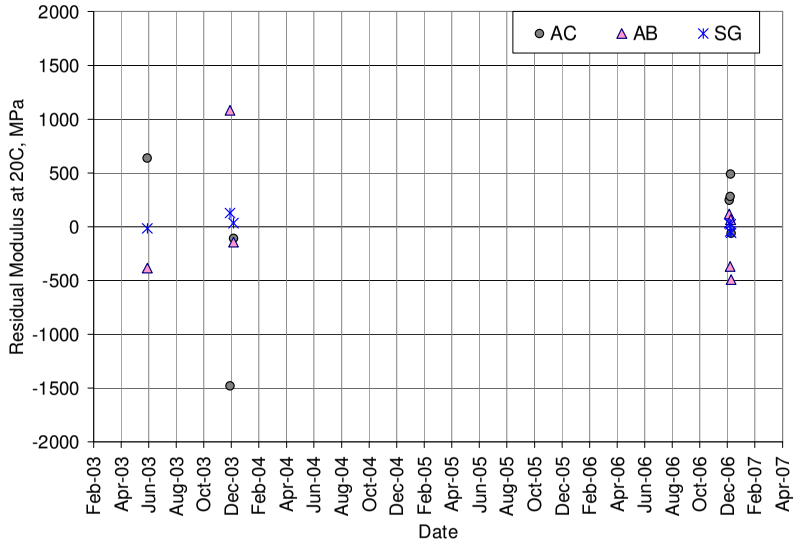

Figure 4.22: Time variation of residual moduli of Section 591RF (MAC15-G).

4.4. Stiffness Recovery after HVS testing

The modulus plots in Section 3.2 show that the modulus of the asphalt concrete tended to recover with time after HVS testing. These moduli can be adjusted to values at a reference temperature to better detect this trend using the master curves developed in Section 4.1. However, these curves are only applicable for undamaged mixes and a different master curve, modeled by the following equation (Equation 4.3), was used for fatigue-damaged asphalt mixes.

$$\log(E) = \log(E_{\min}) + \frac{\log\left(E_{\max} / E_{\min}\right) \times (1-\omega)}{1+\exp(\beta+\gamma\times\log(t_r))} \quad \textbf{(4.3)}$$

Where: ω is a damage parameter and the remaining parameters are the same as those defined in Equation 4.1.

Shortly after each HVS test, FWD measurements were taken at two different temperatures on the same day on each section. These data were used to develop the master curves of damaged mixes. Table 4.3 presents the estimated damage parameter (ω) for each composite mix. Higher values of ω represent more fatigue damage. The section overlaid with the MB15-G mix had minimal fatigue damage in the asphalt concrete mix, while the section overlaid with the RAC-G mix had the most fatigue damage.

Table 4.3: Summary of Parameters of Master Curves of Damaged Composite AC Layers

Section	Mix	ω	E_{max} (MPa)
586RF	MB15-G + DGAC	0.006	14,664
587RF	RAC-G +DGAC	0.337	2,762
588RF	AR4000-D + DGAC	0.275	3,469
589RF	MB4-G (45 mm) + DGAC	0.246	4,368
590RF	MB4-G (90 mm) + DGAC	0.205	4,159
591RF	MAC15-G + DGAC	NA	NA

Calback was re-run with the inputs of the damaged master curves, to adjust the backcalculated modui to the reference temperature (20°C). The results are presented in Figure 4.23 through Figure 4.26. The results are grouped into subsections to account for the within-section variation.

The modulus of the fatigue-damaged asphalt concrete generally recovered to some extent after between one and three years, depending on the section. There was little change in the moduli of the base and subgrade. Section 588RF (AR4000-D overlay) showed distinctly different modulus recovery for the two subsections. A lower modulus was measured immediately after the HVS test on Subsection A compared to Subsection B, and it recovered very little modulus over time. The first-level analysis report for this section (9) revealed that this subsection had severe interconnected cracking after both Phase 1 and Phase 2 HVS tests, while Subsection B had very few cracks. The other overlay sections had predominantly

transverse cracks that were far less interconnected after Phase 2 testing. Modulus recovery therefore appeared to only occur in asphalt concrete with few interconnected cracks.

The moduli of the asphalt concrete were normalized for each section by the corresponding values right after HVS testing to compare the recovery rate of the different mixes (Figure 4.27). The recovery rates of the sections overlaid with RAC-G and MB4-G (45 mm) were similar, while that of the MB4-G (90 mm) overlay section was slightly higher. If the severely cracked subsection is excluded, the AR4000-D overlay section had the highest recovery rate.

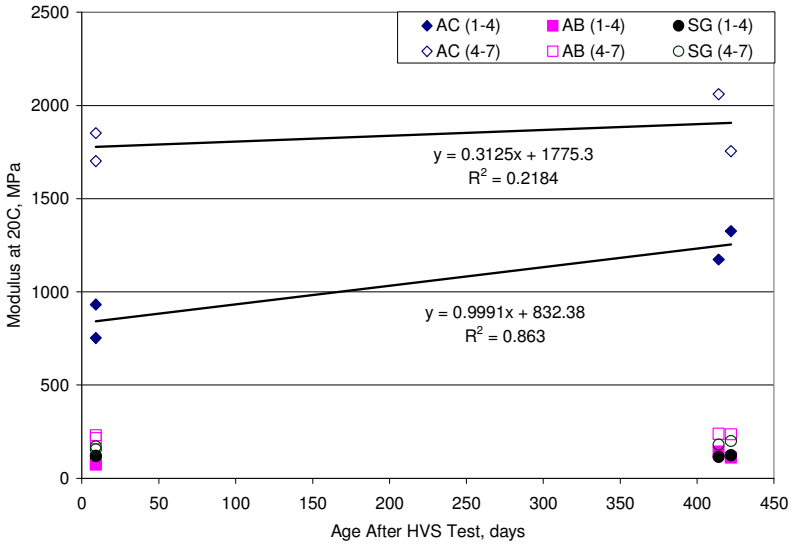

Figure 4.23: Moduli versus age after HVS testing for Section 587RF (RAG-G).

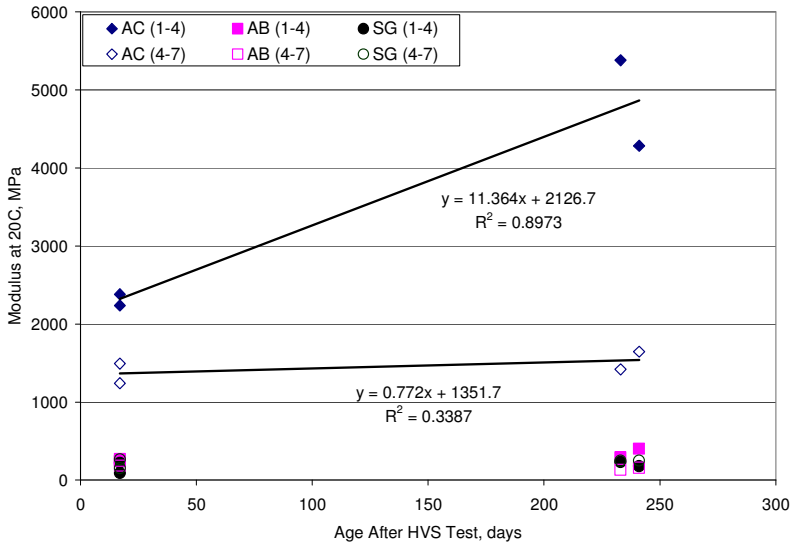

Figure 4.24: Moduli versus age after HVS testing for Section 588RF (AR4000-D).

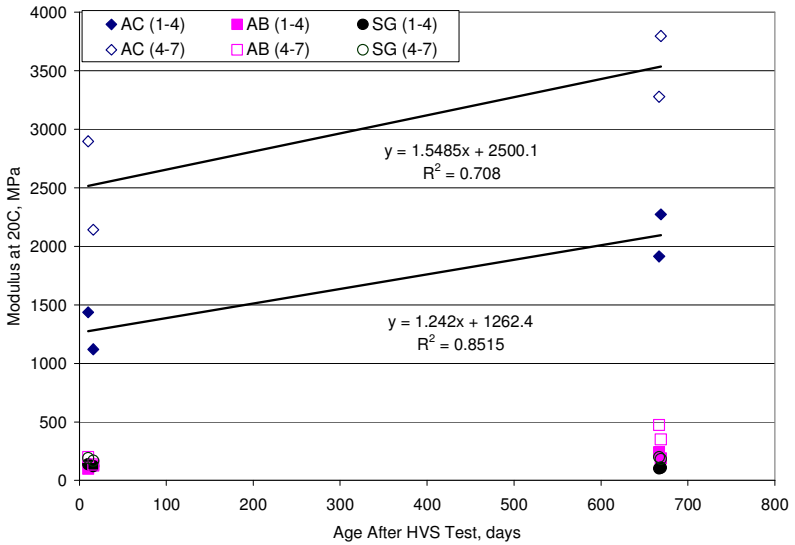

Figure 4.25: Moduli versus age after HVS testing for Section 589RF (MB4-G-45).

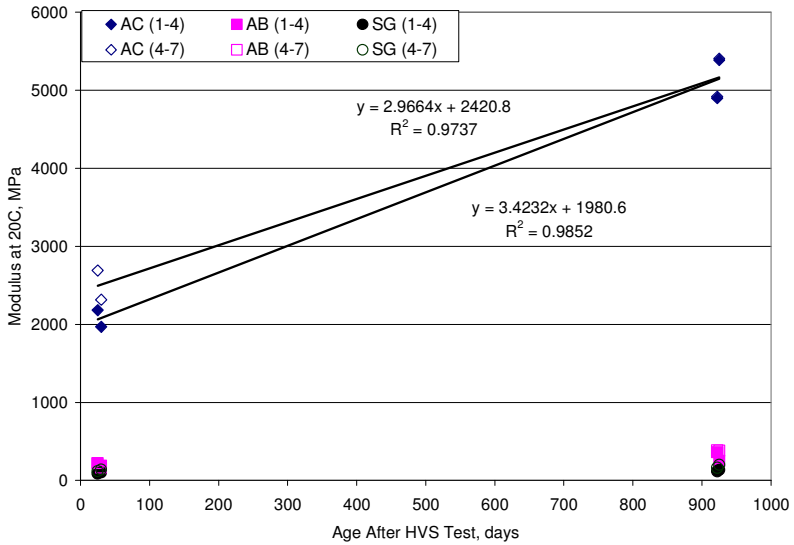

Figure 4.26: Moduli versus age after HVS testing for Section 590RF (MB4-G-90).

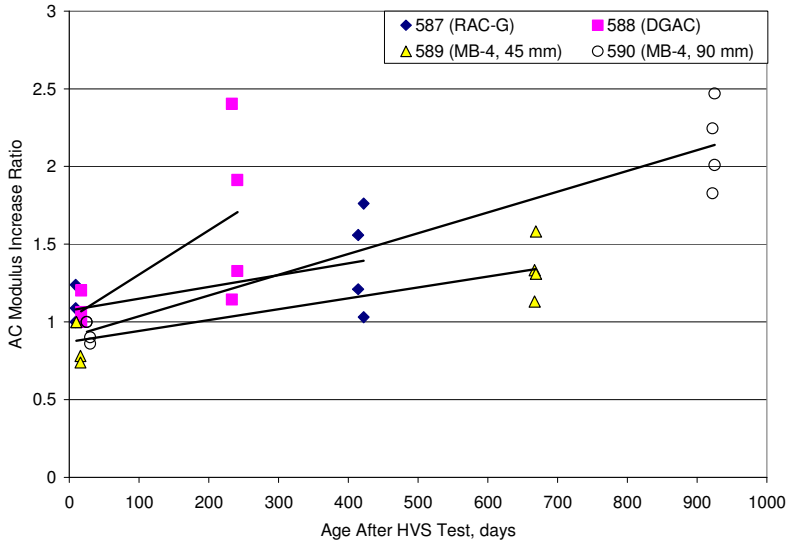

Figure 4.27: Normalized moduli versus age after HVS test.

5. COMPARISON OF BACKCALUCLATED AND LABORATORY RESULTS

This chapter compares the moduli backcalculated from FWD data to those measured in the laboratory, and to those backcalculated from Road Surface Deflectometer (RSD) data.

5.1. Comparison of Predicted and Measured Composite Asphalt Layer Stiffness

In backcalculation, it is generally not recommended to backcalculate the modulus of an asphalt layer if the thickness is less than half the radius of the loading plate (75 mm in this study). Because the thicknesses of the overlays were generally less than the minimum allowable thickness for reliable backcalculation, both the overlay and the underlying DGAC layer were treated as one composite layer in all FWD deflection analyses. However, in the laboratory the modulus of each mix was measured separately from flexural beam specimens. To compare the moduli backcalculated from field data to those measured in the laboratory, the moduli of individual mixes need to be converted into composite moduli. The Odemark's method was used for this conversion (Equation 5.1). The overlay was first converted into an equivalent layer with a different thickness (h_e) and the same modulus as the underlying layer. This equivalent layer, along with the underlying layer, was then converted into a composite layer with the thickness equal to the sum of the overlay thickness (h_1) and the existing layer thickness (h_2).

$$h_e = f_1 h_1 \sqrt[3]{E_1 / E_2} + h_2$$
$$E_c = f_2 \frac{h_e^3}{(h_1 + h_2)^3} E_2 \qquad \textbf{(5.1)}$$

Where: E_c is the calculated composite modulus

E_1 is the overlay modulus obtained from a frequency sweep test

E_2 is the modulus of existing layer obtained from the frequency sweep test

f_1 and f_2 are correction factors (f_1=0.9, f_2=1.0).

The backcalculated composite moduli of each test section are shown in Figure 4.2.

Figure 5.1 through Figure 5.6 show the master curves, estimated from laboratory and FWD tests, of the composite asphalt concrete layer for each test section. The data points (composite asphalt concrete moduli backcalculated from FWD measurements) used to fit the master curve from the FWD test are also shown. The following was observed:

- The data points generally fall around the master curve obtained from the laboratory frequency sweep test.
- The data from Section 587RF (RAC-G) fall slightly below the laboratory master curve at 10°C to 20°C, while the data from Section 590RF (90 mm MB4-G) are slightly above. The master curves estimated from these FWD data points are generally in good agreement with the corresponding laboratory master curves.
- The FWD master curves based on relative difference for Sections 586RF (MB15-G), 587RF (RAC-G), and 591RF (MAC15-G) fit the laboratory master curves better than the FWD master curves based on the absolute difference. For Section 588RF (AR4000-D), the opposite is apparent, while there is no significant difference for Sections 589RF (45 mm MB4-G) and 590RF (90 mm MB4-G).
- If the number of data points for minimization is large enough, the difference between master curves based on the absolute difference and relative difference should be small.

5.2. Comparison of Backcalculated and Laboratory Stiffness of the Base Layer

Samples of the base were taken during construction of the test road and tested in the laboratory for resilient modulus (M_r), following the LTPP P46 Test Protocol ("Resilient Modulus of Unbound Granular Base/Subbase Materials and Subgrade Soils"). In this test, a repeated axial cyclic stress is applied to a cylindrical test specimen, 152 mm in diameter and 300 mm high. The specimen is also subjected to a static confining stress provided by a triaxial pressure chamber.

The tests were conducted with different combinations of confining pressure, axial pressure, and water content. The results are presented in Figure 5.7, and the parameters estimated for the generalized model of aggregate base used in the M-E PDG design procedure (Equation 5.1) are shown in Table 5.1.

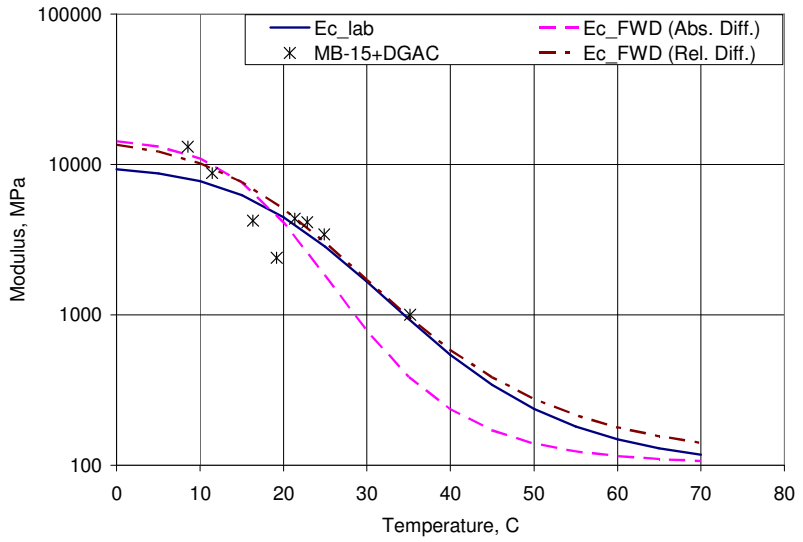

Figure 5.1: Composite AC moduli from laboratory and FWD tests for Section 586RF (MB15-G).

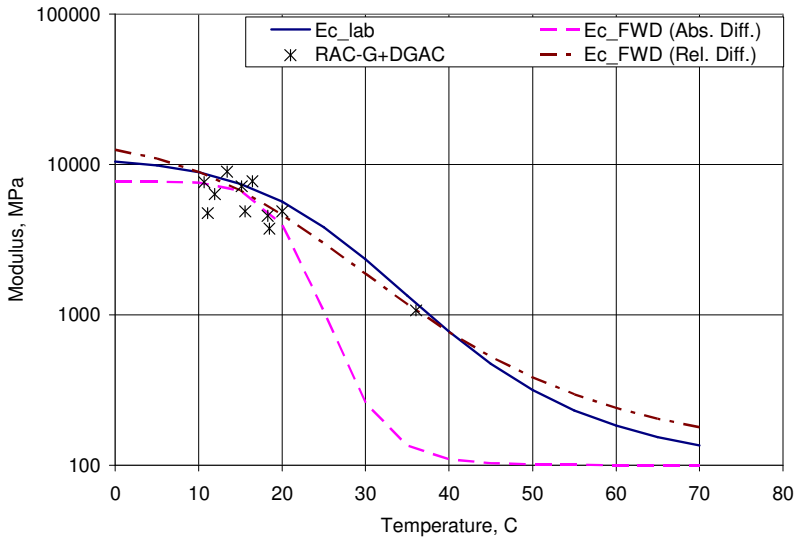

Figure 5.2: Composite AC moduli from laboratory and FWD tests for Section 587RF (RAC-G).

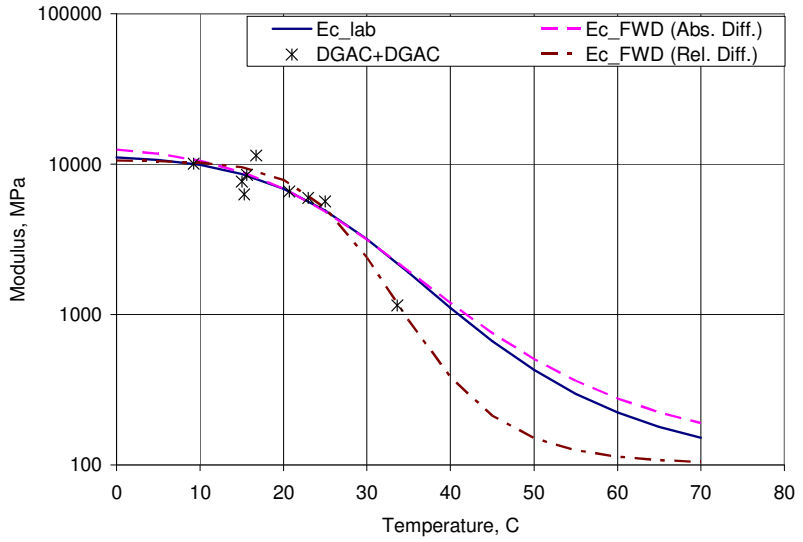

Figure 5.3: Composite AC moduli from laboratory and FWD tests for Section 588RF (AR4000-D).

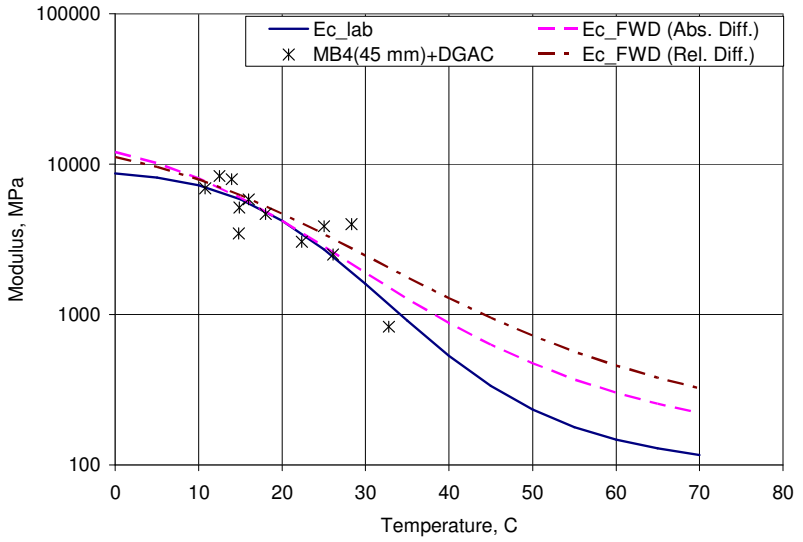

Figure 5.4: Composite AC moduli from laboratory and FWD tests for Section 589RF (MB4-G-45).

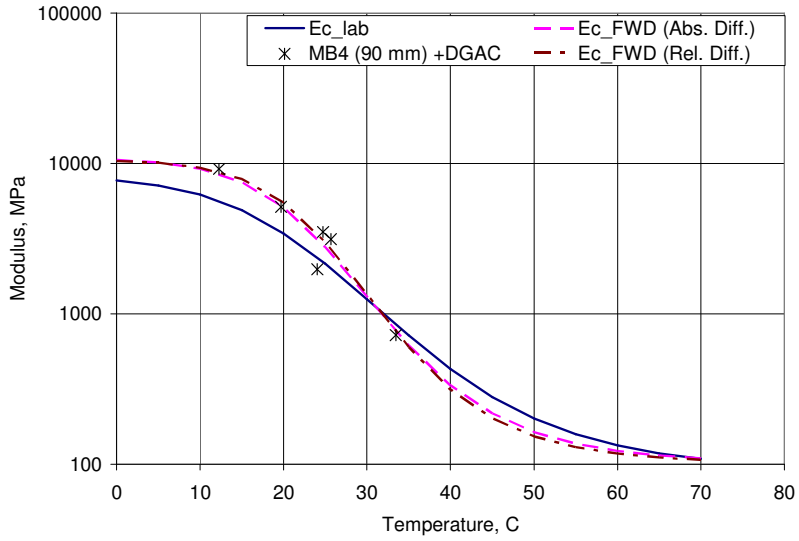

Figure 5.5: Composite AC moduli from laboratory and FWD tests for Section 590RF (MB4-G-90).

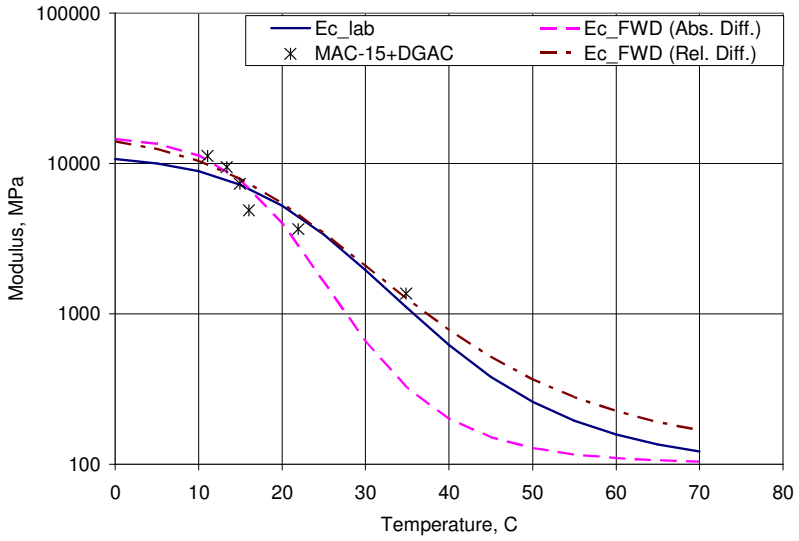

Figure 5.6: Composite AC moduli from laboratory and FWD tests for Section 591RF (MAC15-G).

$$M_r = k_1 p_a \left(\frac{\theta}{p_a} \right)^{k_2} \left(\frac{\tau_{oct}}{p_a} + 1 \right)^{k_3} \quad \textbf{(5.2)}$$

Where: M_r is resilient modulus (MPa)

θ is bulk stress = $\sigma_1 + \sigma_2 + \sigma_3$

σ_1 is major principal stress

σ_2 is intermediate principal stress

σ_3 is minor principal stress (confining pressure);

τ_{oct} is octahedral shear stress = $\frac{1}{3}\sqrt{(\sigma_1-\sigma_2)^2+(\sigma_1-\sigma_3)^2+(\sigma_2-\sigma_3)^2}$

p_a is atmospheric pressure (0.101 MPa)

k_1, k_2, k_3 are parameters to be estimated.

Table 5.1: Parameters Estimated from Laboratory Test Results

Parameter	Moisture Content (%)						
	5.5	6.5	5.9	8.5	8.6	8.1	9.5
k_1	470.5077	81.7698	72.9065	51.3602	41.1698	90.8122	43.5573
k_2	0.3127	0.5441	0.5488	0.5598	0.5752	0.4909	0.4744
k_3	-0.0490	-0.0642	-0.0547	-0.0578	-0.0620	-0.0363	0.0272

The resilient modulus of the base material changed with water content and confining pressure, but was less affected by the peak deviatorial stress (Figure 5.7). The resilient modulus of the base material was in a range of 100 MPa and 600 MPa for a water content between 5.5 percent and 9.5 percent, and a confining pressure between 21 kPa and 138 kPa,

As discussed in previous sections, the effect of water content was not detected in the backcalculated modulus of the base, primarily due to the limited number of data points and conflicting effects of other factors such as aging and recementation. However, the effect of confining pressure was detected from the FWD data, which indicated that the base modulus dropped when the pavement temperatures increased. Higher temperatures resulted in softer asphalt concrete, and therefore, less confining pressure to the underlying aggregate base. Before Phase 2 HVS testing, the values of the backcalculated moduli of the base were significantly higher than the values measured in the laboratory on most sections except Section 590RF, with the highest value reaching 3,700 MPa on Section 586RF. This difference was attributed to anomalies associated with backcalculation of FWD deflection measurements on relatively thin asphalt layers, and to differences in the degree of recementation of the base material after construction. Laboratory specimens were tested shortly after fabrication, with no curing, and therefore recementation was unlikely to have occurred. The base modulus in the trafficked area dropped to between

200 MPa and 300 MPa on most sections after Phase 2 testing, which is in the range of the laboratory measured values, indicating that cemented bonds were broken down during HVS trafficking.

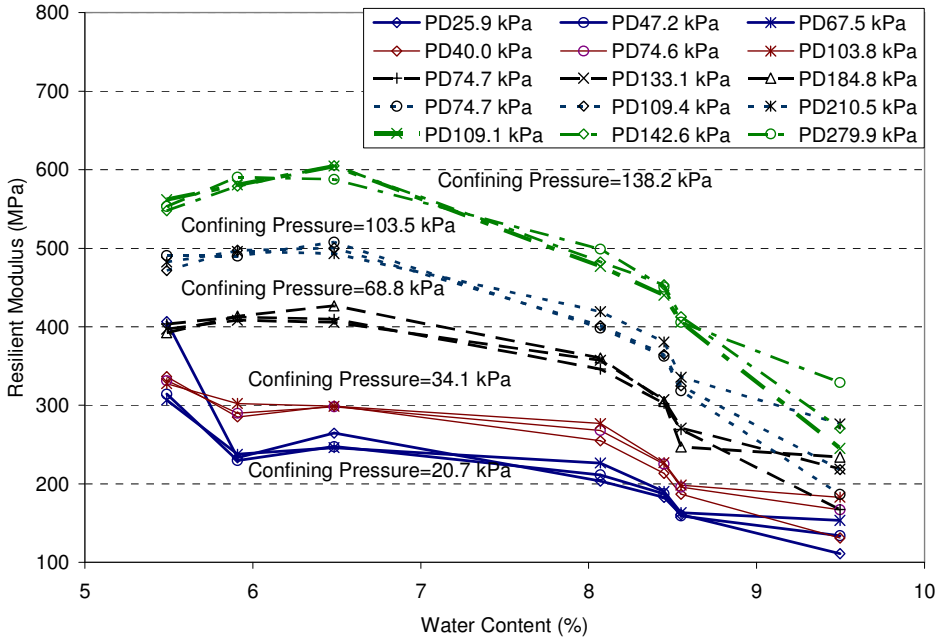

Figure 5.7: Resilient modulus of aggregate base measured in the laboratory.
(PD represents peak deviatory stress)

5.3. Comparison of Stiffness Backcalculated from FWD and RSD

The Road surface deflectometer (RSD) is similar to the Benkelman Beam and is used to measure the surface deflection bowl under HVS loading, with the measuring point positioned between the two tires of a dual tire configuration. Measurement accuracy is approximately 10 microns. In this study, the RSD measurements were taken before, during, and after the HVS testing. Testing was carried out at creep speed, which corresponds to an equivalent loading frequency of about 0.2 Hz. Pavement temperature at 50 mm depth was maintained at either 20°C ± 4°C or at 15°C ± 4°C, depending on the stage of testing (see Chapter 2). The peak deflection results discussed in the first-level reports were very consistent across the various tests, and provided a reliable indication of relative damage over the course of an HVS test.

A Matlab® program, based on layer elastic theory, was developed by UCPRC to backcalculate pavement layer moduli from RSD data. The overlay and underlying asphalt concrete layers were treated as separate layers in this backcalculation. On Sections 589RF and 591RF, it was necessary to fix the overlay modulus at the value from the laboratory frequency sweep test, and to subdivide the underlying DGAC layer into two sub-layers, treated as different materials, in order to obtain rational results. Comparison between the FWD moduli and RSD moduli was therefore not performed on these sections.

The moduli of the overlay and underlying layers from RSD data were converted into the composite modulus using the Odemark method. The composite modulus master curves developed from the FWD data were used to calculate the FWD moduli at 20°C and 0.2 Hz loading frequency. Table 5.2 summarizes the results.

Table 5.2: Comparison of Composite AC Moduli from FWD and RSD Data

Section	Time	Composite AC Modulus Based on RSD (MPa)	Composite AC Modulus Based on FWD (absolute difference) (MPa)	Composite AC Modulus Based on FWD (relative difference) (MPa)
586RF	Before HVS	2,759	898	1,431
586RF	After HVS	1,215	887	871
587RF	Before HVS	689	1,120	1,852
587RF	After HVS	88	754	768
588RF	Before HVS	1,181	2,986	2,700
588RF	After HVS	111	1,175	1,175
590RF	Before HVS	1,427	2,563	2,737
590RF	After HVS	73	1,320	1,369

There was a significant difference between the moduli from the two measuring methods. For Section 586RF, the moduli from the FWD data are smaller than those from the RSD data for both before and after the HVS test. For Sections 587RF, 588RF, and 590RF, the moduli from the FWD data are all larger than those from the RSD data. The reasons for this difference include the different data sets used for backcalculation, and different procedures and assumptions in the two methods of backcalculation, especially with regard to accounting for layer thickness. The RSD data were measured at constant pavement temperatures and an equivalent loading frequency of 0.2 Hz, while the FWD data were measured at varying temperatures and at about a 10 Hz loading frequency. Extrapolating the FWD data to high temperatures or low loading frequencies increases the chance of errors. The development of master curves from FWD backcalculation also requires that the minimum modulus be fixed at 100 MPa, while there is no such constraint in the RSD backcalculation. This requirement could also have influenced the validity of the results.

6. CONCLUSIONS

This report is one in a series of studies detailing the results of HVS testing and associated analyses being performed to validate Caltrans overlay strategies for the rehabilitation of cracked asphalt concrete. It describes the analysis of deflection data measured with a Falling Weight Deflectometer (FWD) after initial construction, before and after each HVS test in the first phase of testing on the original DGAC surface, before and after construction of the overlays, and before and after each HVS test on each overlay. FWD results are compared with Road Surface Deflectometer (RSD) measurements taken during each HVS test.

Findings and observations based on this analysis include:

- Variation of material properties were recorded both between sections and within sections, which was mostly attributed to variation in the degree of recementation of recycled concrete particles in the aggregate base material. Base and subgrade were stiffest on Sections 567RF/586RF (MB15-G), and weakest on Sections 572RF/590RF (90 mm MB4-G).
- The asphalt concrete modulus was significantly affected by the pavement temperature, as expected. In general, lower modulus was obtained at high temperatures, and higher modulus at low temperatures.
- The modulus of the aggregate base was generally positively correlated with the moduli of the asphalt concrete and subgrade. Correlation between the asphalt concrete modulus and the base modulus was weaker in the untrafficked area and/or in the trafficked area before HVS testing, probably because of recementation of particles in the base after construction and subsequent destruction of the bonds during HVS trafficking. No significant correlation was found between the asphalt concrete modulus and the subgrade modulus.
- The load level of the FWD did not have a significant effect on the values of the backcalculated moduli.
- Aging of the asphalt concrete was apparent on all sections except Section 591RF (MAC15-G). A logarithm function appeared to fit the data well.
- The stiffness of the base increased significantly with time after initial construction, primarily due to recementation of the recycled concrete particles. This increase continued after overlay construction in certain areas of the test road (e.g. in the vicinity of Sections 586RF [MB15-G] and 588RF [AR4000-D]), but not in other areas.
- Phase 2 HVS testing generally damaged the asphalt concrete layers in the trafficked area of each section. Minimal damage was measured on Section 586RF (MB15-G).

- In the one to three year period after Phase 2 HVS testing, the modulus of the damaged asphalt concrete generally recovered to some extent except for part of the control section overlaid with AR4000-D, where the asphalt concrete layer was severely cracked. Little change in the moduli of the base and subgrade was recorded on this subsection. The recovery rates of sections overlaid with RAC-G and MB4-G (45 mm) were similar, while that of the MB4-G (90 mm) overlay section was slightly higher.
- Seasonal effects on pavement stiffness were not detected from the limited data collected during this study.
- The asphalt concrete moduli backcalculated from the overlay sections match reasonably well with the moduli determined during laboratory frequency sweep tests on flexural beam specimens. However, the asphalt concrete moduli backcalculated from the underlying DGAC were significantly lower than those measured by the frequency sweep test in the laboratory.
- There was a difference between the moduli backcalculated from FWD data and from the RSD data. Differences in test conditions (temperature, load, and load frequency) and backcalculation assumptions of the two procedures contributed to this difference.

The following recommendations for using backcalculated data in other reflective cracking study analyses are suggested:

- All sections except Sections 573RF/591RF should be subdivided into two equal-length subsections (i.e. Stations 2 to 8, and Stations 8 to 14) to account for non-uniformity of material properties within test sections in pavement modeling and simulation. Sections 573RF/591RF can be treated as one uniform section.
- For pavement modeling and simulations of actual HVS test conditions, the asphalt concrete modulus backcalculated from both FWD and RSD testing should be used. The asphalt concrete modulus determined from laboratory frequency sweep test on flexural beams should be used for modeling and simulation of uniform sections.

No recommendations as to the use of modified binder mixes are made at this time. These recommendations will be included in the second-level analysis report, which will be prepared and submitted on completion of all HVS and laboratory testing and analysis.

7. REFERENCES

1. **Generic experimental design for product/strategy evaluation — crumb rubber modified materials.** 2005. Sacramento, CA: Caltrans.
2. **Reflective Cracking Study: Workplan for the Comparison of MB, RAC-G, and DGAC Mixes Under HVS and Laboratory Testing.** 2003. Davis and Berkeley, CA: University of California Pavement Research Center. (UCPRC-WP-2003-01).
3. BEJARANO, M., Jones, D., Morton, B., and Scheffy, C. 2005. **Reflective Cracking Study: Summary of Construction Activities, Phase 1 HVS Testing, and Overlay Construction**. Davis and Berkeley, CA: University of California Pavement Research Center. (UCPRC-RR-2005-03).
4. TSAI, B.-W., Jones, D., Harvey, J., and Monismith, C. 2006. **Reflective Cracking Study: First-level Report on Laboratory Fatigue Testing.** Davis and Berkeley, CA: University of California Pavement Research Center. (UCPRC-RR-2006-08)
5. GUADA, I., Signore, J., Tsai, B.-W., Jones, D., Harvey, J., and Monismith, C. 2006. **Reflective Cracking Study: First-level Report on Laboratory Shear Testing.** Davis and Berkeley, CA: University of California Pavement Research Center. (UCPRC-RR-2006-11)
6. JONES, D. Tsai, B.W. and Harvey, J. 2006. **Reflective Cracking Study: First-level Report on HVS Testing on Section 590RF — 90 mm MB4-G Overlay.** Davis and Berkeley, CA: University of California Pavement Research Center. (UCPRC-RR-2006-04).
7. JONES, D., Wu, R., Lea, J. and Harvey, J. 2006. **Reflective Cracking Study: First-level Report on HVS Testing on Section 589RF — 45 mm MB4-G Overlay.** Davis and Berkeley, CA: University of California Pavement Research Center. (UCPRC-RR-2006-05).
8. WU, R., Jones, D. and Harvey, J. 2006. **Reflective Cracking Study: First-level Report on HVS Testing on Section 587RF — 45 mm RAC-G Overlay.** Davis and Berkeley, CA: University of California Pavement Research Center. (UCPRC-RR-2006-06).
9. JONES, D., WU, R. and Harvey, J. 2006. **Reflective Cracking Study: First-level Report on HVS Testing on Section 588RF — 90 mm DGAC Overlay.** Davis and Berkeley, CA: University of California Pavement Research Center. (UCPRC-RR-2006-07).
10. JONES, D., WU, R. and Harvey, J. 2006. **Reflective Cracking Study: First-level Report on HVS Testing on Section 586RF — 45 mm MB15-G Overlay.** Davis and Berkeley, CA: University of California Pavement Research Center. (UCPRC-RR-2006-12).

11. JONES, D., WU, R. and Harvey, J. 2007. **Reflective Cracking Study: First-level Report on HVS Testing on Section 591RF — 45 mm MAC15-G Overlay.** Davis and Berkeley, CA: University of California Pavement Research Center. (UCPRC-RR-2007-04).

12. JONES, D., Harvey, J. and Steven, B. 2007. **Reflective Cracking Study: HVS Test Section Forensic Report.** Davis and Berkeley, CA: University of California Pavement Research Center. (UCPRC-RR-2007-05).

13. HARVEY, J., Du Plessis, L., Long, F., Deacon, J., Guada, I., Hung, D. and Scheffy, C. 1997. **CAL/APT Program: Test Results from Accelerated Pavement Test on Pavement Structure Containing Asphalt Treated Permeable Base (ATPB) – Section 500RF**. Davis and Berkeley, CA: University of California Pavement Research Center. (Report Numbers UCPRC-RR-1999-02 and RTA-65W4845-3).